Institute of Fundamental Technological Research
Polish Academy of Sciences

Doctoral Dissertation


Piotr Topolewski

# Sources of the cell-to-cell heterogeneity in interferon gamma and oncostatin M signaling responses

Źródła zmienności międzykomórkowej w odpowiedziach na interferon gamma i onkostatynę M

Supervisor: Dr hab. Michał Komorowski
Institute of Fundamental Technological Research
Polish Academy of Sciences

Warsaw, Poland 2022

I thank:

- my supervisor for teaching me thinking
- my colleagues for being guides in the science world
- my wife for believing in me
- my parents and siblings for being the support whole my life

# Table of Contents

# Summary

Cells of multicellular organisms have to communicate with each other to assure organismal homeostasis and coordinate immune reactions or development. To communicate, cells send signal molecules, such as cytokines, and use a signaling process, a series of biochemical reactions, to sense the signal and trigger specific cellular responses. However, cellular signaling responses of genetically identical cells grown in identical, controlled conditions show substantial cell-to-cell heterogeneity, which is often ascribed to the randomness of biochemical reactions, termed molecular noise. On the other hand, cell-to-cell heterogeneity can also arise from differences in molecular content between cells, i.e., molecular phenotypic variability. However, the exact contribution of these two processes remains unclear, with no answer to a fundamental question of how precise a single cell is in cellular signaling. In addition, it is unknown which factors of phenotypic variability, if any, contribute substantially to the observed cell-to-cell heterogeneity. To fill these knowledge gaps, I used confocal imaging and bi-nuclear, fibroblast-derived syncytia stimulated with cytokines to distinguish molecular noise from phenotypic variability. I showed that molecular phenotypic variability is the main source of cell-to-cell heterogeneity, constituting ~90% of the total variability in the studied cytokine signaling responses. The generated data allowed also for assessing the influence of the measurement error, which was of minor contribution to the total observed signal. In addition, using confocal imaging and flow cytometry in human and mouse fibroblasts cell cultures, I showed that the nuclear state and the level of intracellular cytoplasmic signaling proteins were substantial contributors of observed cell-to cell heterogeneity of the cytokine signaling. Finally, the master process of cellular biology, the cell cycle, did not show substantial influence on the cytokine response, based on the confocal imaging. Taken together, the presented results reveal that cytokine signaling in the used system operates in a reproducible, high-fidelity manner indicating the high precision of a single cell in cellular signaling. The obtained data also gives hope that the cellular response can be at least partially predicted before the stimulation occurs, allowing for a better understanding of cellular biology.

# Summary (in Polish)

Komórki organizmów wielokomórkowych muszą komunikować się ze sobą, aby zapewnić organizmowi homeostazę i m.in, koordynować reakcje immunologiczne lub rozwój. Aby komunikować się, komórki wysyłają cząsteczki sygnałowe, takie jak cytokiny i wykorzystują proces sygnalizacji, czyli serię reakcji biochemicznych, aby wyczuć sygnał i wywołać określone odpowiedzi komórkowe. Jednak takie komórkowe odpowiedzi na sygnał w genetycznie identycznych komórkach hodowanych w identycznych, kontrolowanych warunkach wykazują znaczną heterogeniczność między komórkami, co często przypisuje się losowości reakcji biochemicznych, określanych mianem szumu molekularnego. Z drugiej strony heterogeniczność między komórkami może również wynikać z różnic w molekularnej zawartości między komórkami, tj. molekularnej zmienności fenotypowej. Jednak dokładny udział tych dwóch procesów pozostaje niejasny. Ponadto nie wiadomo, jakie czynniki zmienności fenotypowej, jeśli w ogóle, mają istotny wpływ na obserwowaną heterogeniczność między komórkami. Aby wypełnić te luki w wiedzy, wykorzystałem obrazowanie konfokalne i dwujądrowe, pochodzące z fibroblastów, syncytia stymulowane cytokinami, aby odróżnić szum molekularny od zmienności fenotypowej. Pokazałam, że molekularna zmienność fenotypowa jest głównym źródłem heterogeniczności międzykomórkowej, stanowiąc ~90% całkowitej zmienności w badanych odpowiedziach sygnalizacyjnych cytokin. Wygenerowane dane pozwoliły również na ocenę wpływu błędu pomiaru, który miał niewielki udział w całkowitym obserwowanym sygnale. Ponadto, stosując obrazowanie konfokalne i cytometrię przepływową w hodowlach ludzkich i mysich fibroblastów, wykazałam, że stan jądra komórkowego i poziom wewnątrzkomórkowych cytoplazmatycznych białek sygnałowych były istotnymi czynnikami przyczyniającymi się do obserwowanej między komórkami heterogeniczności sygnalizacji cytokin. Wreszcie, jeden z głównych procesów biologii komórki, cykl komórkowy, nie wykazał istotnego wpływu na odpowiedź cytokinową. Podsumowując, przedstawione wyniki pokazują, że sygnalizacja cytokinami w zastosowanym układzie działa z wysoką wiernością, wskazując na dużą precyzję pojedynczej komórki w sygnalizacji komórkowej. Uzyskane dane dają również nadzieję, że odpowiedź komórkową można przynajmniej częściowo przewidzieć przed wystąpieniem stymulacji, co pozwala na lepsze poznanie biologii komórki.

# Abbreviation list

| | |
|---|---|
| ADP | adenosine diphosphate |
| ATCC | American Type Culture Collection |
| ATP | adenosine triphosphate |
| BD | Becton, Dickinson and Company |
| BJ | human fibroblasts' trade name |
| BSA | bovine serum albumin |
| CFP | cyan fluorescent protein |
| CMCD | chronic mucocutaneous candidiasis disease |
| CO2 | carbon dioxide |
| DAPI | 4,6-diamidino-2-phenylindole |
| DMEM | Dulbecco's Modified Eagle Medium |
| DNA | deoxyribonucleic acid |
| EGF | epidermal growth factor |
| ERK | extracellular signal-regulated kinases |
| FBS | fetal bovine serum |
| FRA | fractional response analysis |
| FRA1 | FOS-related antigen 1 |
| GPCR | G-protein-coupled receptors |
| gp130 | glycoprotein 130 |
| IFN-γ | Interferon gamma |
| IFN-α | Interferon alpha |
| IFN-β | Interferon beta |
| IFNGR | Interferon gamma receptor |
| IFNGR1 | Interferon gamma receptor 1 |
| IFNGR2 | Interferon gamma receptor 2 |
| IGF-1 | insulin-like growth factor-1 |
| JAK1 | Janus kinase 1 |
| JAK2 | Janus kinase 2 |
| JNK | c-Jun N-terminal kinase |
| KO | knock-out |
| LIFR | leukemia inhibitory factor receptor |
| MAPK | mitogen-activated protein kinase |
| MEF | mouse embryonic fibroblast |
| MI | mutual information |
| NLR | NOD-like receptors |
| NOD | nucleotide-binding oligomerization domain |
| OSM | oncostatin M |
| OSMR | oncostatin M receptor |
| PBS | Phosphate-buffered saline |
| qRT-PCR | quantitative Reverse Transcription Polymerase Chain Reaction |
| PE | phycoerythrin |
| PEG | polyethylene glycol |
| PFA | paraformaldehyde |
| RIG-I | retinoic acid-inducible gene I |

| | |
|---|---|
| RLR | RIG-I-like receptors (RLR), |
| RNA | ribonucleic acid |
| SLEMI | Statistical Learning Based Estimation of Mutual Information |
| STAT | signal transducer and activator of transcription |
| TC-PTP | T-cell protein tyrosine phosphatases |
| TF | transcription factor |
| TGF-β | transforming growth factor β |
| TNF-α | tumor necrosis factor alpha |
| TRAIL | TNF related apoptosis-inducing ligand |
| YFP | yellow fluorescent protein |

# 1. Motivation

Multicellular organisms rely on cellular communication: the information about the extracellular environment has to be properly sensed and processed by single cells to trigger the appropriate action, all in the process named cellular signaling. Mutations and dysregulations of signaling components, e.g., receptors or kinases, may lead to severe diseases and organism malfunctions, which include cancers, autoimmune diseases, allergies or uncontrolled inflammation. Despite the importance of cellular signaling, experiments of the last decades show that cellular responses to external stimulation show substantial cell-to-cell heterogeneity. Even if all cells are of the same type, have the same genome and are grown in the same environment, they tend to respond differently, with some cells having strong and other low responses. It is largely unknown, whether the observed cell-to-cell heterogeneity is caused by 1) the stochasticity of biochemical reactions, implying imprecision of signaling of individual cells, or by 2) the differences in molecular content of cells, i.e., phenotypic variability. Resolving the question whether a single cell signaling is more stochastic or deterministic is essential for designing research strategies to understand the functioning of signaling in single cells, as well as functioning of the cell-to-cell communication. Different research directions are needed depending on whether signaling pathways in single cells operate in the stochastic or deterministic regime. For instance, if the cell-to-cell heterogeneity of cellular responses was the result of random processes, then finding the factors that determine the single cell response would not be possible. Noise is a set of impalpable elements, which cannot be pinned down. Therefore, we would need to rely mainly on statistical and probabilistic descriptions. On the other hand, if the cell-to-cell heterogeneity of cellular responses was the result of phenotypic variability, then we would be able to find the components that determine the variability of the responses. Such detrimental components could be then used to predict the response in mutated cells or design new drugs, or to improve the diagnosis. To do all that, first, the question should be answered: how precise the signaling of a single cell actually is?

# 2. Literature review

## 2.1. Single cell measurements

Many biological processes have been traditionally studied with cell population-averaged techniques, like Western blots, quantitative Reverse Transcription Polymerase Chain Reaction (qRT-PCR) or microarrays (Spiller et al., 2010). In this approach, the experimental measurement is derived from a pool of individual cells, implicitly assuming that the population-average value reflects the state of the investigated biological mechanism (Altschuler and Wu, 2010). While these methods are still very valuable, needed, broadly accepted by scientific community and can shed light to a fundamental principle of many biological processes, they also tend to omit the existence of subpopulations of cells which have biologically distinct characteristics and roles (Barteneva and Vorobjev, 2018; Chang et al., 2008; Vilar et al., 2003). In the simplest example, the bulk measurement of DNA content of proliferating diploid cell population will not identify the cells before and after DNA replication, but will indicate the mean DNA content as 3C, where C is the amount of DNA in haploid set of chromosomes (Gregory, 2001). In addition, diseases of each multicellular organism originate from a single cell or a small group of cells which all are averaged in population-oriented methods and therefore cannot be fully investigated (Mazzarello, 1999). Therefore, single cell measurement methods can substantially improve our understanding of cellular processes, including cellular communication, tissue composition or cell development (Raj and Oudenaarden, 2008). So far, single cell measurements have shown that cell-to-cell variability of the genetically identical cells is a common feature that is observed in organism development, gene transcription, cell morphology, drug perturbation, as well as in cellular signaling.

## 2.2. Manifestation of the cell-to-cell variability on the whole-organism scale

One of the earliest investigated examples of the cell-to-cell variability was mosaic X chromosome inactivation in female mice (Lyon, 1961), which were further noticed in other mammals, e.g., calico cats (Harper, 2011). The macro-scaled consequences of the cell-to-cell differences in inactivation of chromosome X is revealed in the existence of irregular color patches on the fur of calico cats. The patches arise in the early stages of the development,

when each cell commits, which of the chromosome X, maternal or parental, will be inactivated. Inactivation of a chromosome X leads to silencing of an allele responsible for a given pigment color located on the same X chromosome (Figure 2.1A). The exact determinants which chromosome will be inactivated have only begun to be understood and more studies are needed for complete explanation (Fang et al., 2019). It is known, however, that chromosome X silencing is an effect of DNA methylation (Nesterova et al., 2008). Similarly to chromosome X inactivation, twins, which at the beginning of their life share identical genomes and develop in the same placenta of the same mother, after the birth they can considerably differ in specific traits, like outer patterning of the armadillo species (Figure 2.1B) (Vogt, 2015). Likewise, an invasive freshwater species originated by the point mutation from the single organism in the pet trade in 1990s, the marbled crayfish, is also an evident example of the cell-to-cell differences due to its asexual type of reproduction (parthenogenesis) (Scholtz et al., 2003). This animal makes clones of itself without egg fertilization, leading to all-female and all-genetically identical offspring and yet, each daughter organism differs slightly by size, color, shape and behavior, even if all are kept in well controlled environmental conditions (Vogt et al., 2008) (Figure 2.1C).

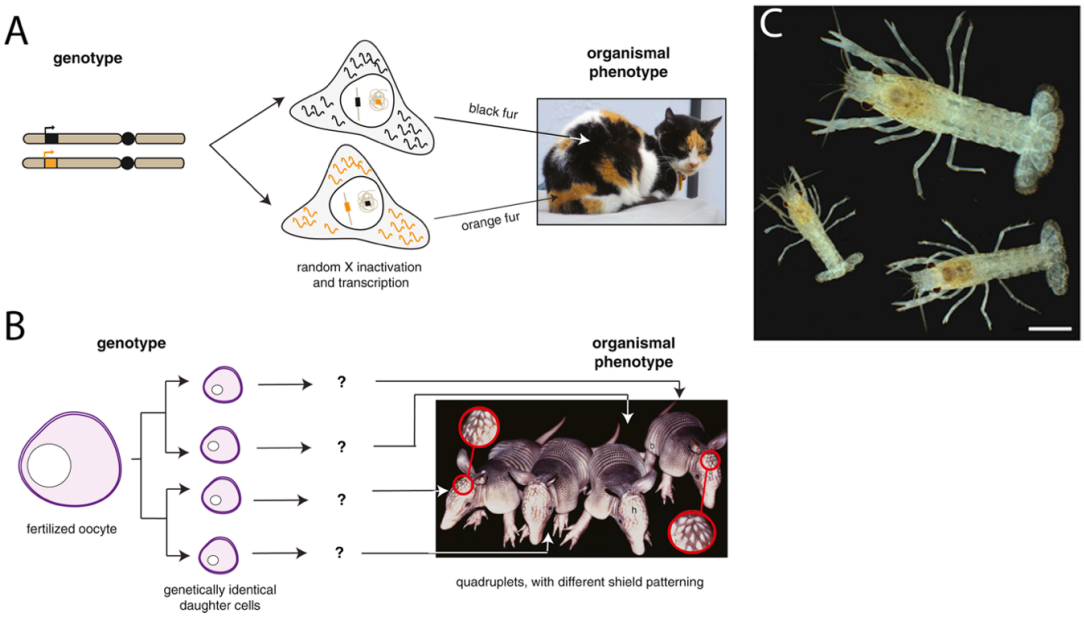


*Figure 2.1. Differences in genetically identical single cells manifest in the whole-organism scale*

(A) Patches on the fur of female calico cats is the manifestation of stochastic X chromosome inactivation in each cell early in the development. (B) Quadruplets of armadillos arise from single fertilized cells, yet have distinct traits, e.g., patterning of heads. (C) Three juvenile clones of marbled crayfish show great size variability, albeit they were size-matched at the early stages of development and then cultured in the controlled conditions for 34 days. Scale bar 4 mm. A and B modified from (Symmons and Raj, 2016), C modified from (Vogt et al., 2008).

All mentioned examples start from single-cell differences, but manifest on the whole-organism scale after an environmental influence, e.g., in placenta, egg or as a mature organism. Therefore, the observed differences can be caused solely by the environment itself, due to the long time between the single cell- and whole-organism stadium. However, there are also many examples showing that characteristics of genetically identical cells grown in homogeneous environments differ substantially from the population-average on the short-time scale.

### 2.2.1. Cell-to-cell variability in cellular processes

It is not surprising nor new, that genetically identical cells of the same organism can perform different actions and have distinct roles, e.g., a human hepatocyte has a completely different phenotype and action profile than a muscle myotube. However, even genetically identical mammalian cells of the same type, originated from the same ancestor cell, grown in a homogeneous, well-controlled environment, can differ substantially in terms of multiple features. For example, the high level of cell-to-cell variability in the mammalian cell culture was shown for endocytosis, viral infections and membrane lipid composition (Snijder et al., 2009), as well as for measurements of protein level (Sigal et al., 2006), shape (Keren et al., 2008), growth rate (Cadart et al., 2018; Vargas–Garcia et al., 2018), time to death after pro-apoptotic treatment (Spencer et al., 2009) and many others. The same applies for single-cell organism such bacteria or yeast, where high cell-to cell variability was observed for cell growth rate (Facchetti et al., 2019), enzyme level (Novick and Weiner, 1957) or chemotaxis (Fuller et al., 2010). Even such a basic biological process as gene expression varies in the intensity substantially from cell-to-cell (Raj and Oudenaarden, 2008). Majority of the above examples at some point utilize the signal sensing – a cell has to sense the signal to grow, to activate the gene transcription, to respond to virus, as well as has to adapt to lack of nutrients or change the proliferation rate based on the signals sent by other cells. Therefore, the signal sensing often occurs prior to the final cellular decision, indicating that maybe the big part of the observed cell-to-cell heterogeneity was due to heterogeneity in signal sensing and processing, in other words in cellular signaling. Indeed, it was shown in many examples, elaborated below, that cellular signaling is also subjected to high cell-to-cell heterogeneity. However the sources of this phenomenon have not been fully resolved. Especially, there is a debate in the literature

on how precise the single cell is and how reliably it can behave after some environmental perturbation. Such knowledge would not only be highly beneficial for our understanding of biology itself, but also could improve the future treatment of the immunological diseases such as cancer or immunodeficiencies.

## 2.3. Cellular signaling

Cells in multicellular organisms are surrounded by the constantly changing extracellular environment. The cellular environment changes because of various reasons, including threats like pathogens or oxygen stress, physical forces exerted during wound creation or cell growth as well as due to complex communication between even very distant cells. To properly perform their actions, like division, death, gene expression or secretion, cells must respond to the changes of the environment. To respond to the changes of the environment, three steps have to take place: sensing the environment state, processing the acquired information and triggering specific actions (Antebi et al., 2017). The biochemical machinery responsible for performing those steps are referred to as signaling pathways and the process itself is considered as cellular signaling.

### 2.3.1. Molecular bases of cellular signaling

Signaling pathways can consist of dozens of chemical species, including proteins and non-peptide hormones, but also small molecules like nucleotides or ions, all ordered in a step-wise activating cascade. Therefore, the signal coming from the environment can be sensed by the cell through the signaling pathway in order to perform specific actions by the cell. Signals can be of mechanical, electrical or chemical nature (Nair et al., 2019). A chemical signal can have a form of lipids (e.g., steroids), proteins (growth factors, peptide hormones, cytokines and chemokines), nucleic acids and many others. In a typical example, a cell detects a chemical environmental signal by binding the signal molecule (ligand) to a specific transmembrane receptor at the cell surface, which results in a biochemical activity on the inside of the cell, e.g., the activation of a receptor-associated kinase. Next, the initial stimuli are processed in a step-wise cascade along intracellular signaling pathways, with one component activating the subsequent one, all finally culminating in effectors like transcription factors (Housden and Perrimon, 2014; Kholodenko, 2006). The effectors carry information about the identity,

intensity, and duration of the stimuli and initiate distinct cellular responses that might involve gene transcription, metabolism, faith commitment, pathogen sensing and many other cellular processes. It is worth noting that such simple representation of cellular signaling does not cover the complexity and inter-relatedness of the signaling process with all its exemptions. For example, there are multiple intracellular receptors which bind lipophilic ligands freely diffusing across the cell membrane and take part, e.g., in steroid signaling (Kumar et al., 2006). There are also internal receptors, including NOD-like receptors (NLR) and RIG-I-like receptors (RLR), recognizing intracellular pathogen associated molecular patterns (PAMPs) derived from pathogen and being a part of the innate immune system (Newton and Dixit, 2012). On the other hand, direct contact between two cells via their membrane proteins (often referred to also as ligands and receptors), with no "bridging" molecule needed, is crucial in developing an adaptive immune response (MacLeod and Anderton, 2015). In addition, the view "one ligand - one receptor - one effector" is convenient and sometimes needed for simplicity, while not showing the full picture of interconnected and cross-linked elements of signaling pathways, with "many ligands - many receptors - many effectors" as a better description (Komorowski and Tawfik, 2019).

The importance of cellular signaling is emphasized by the evidence that its deregulation is connected with severe diseases. The inappropriate sensing of the signal can lead to either too strong or too weak response, which can dysregulate many processes and cause serious diseases and health obstruction ranging from obesity to hypertension, cardiac hypertrophy, drug addiction, aging, hepatitis B and many others, with cancer being one of the most studied in relation with the disrupted signaling pathways (Aggarwal et al., 2009; Berridge, 2014; Clevers and Nusse, 2012; Mora-Garcia and Sakamoto, 1999; Sebolt-Leopold and Herrera, 2004; Taniguchi and Karin, 2018; Zaidi and Merlino, 2011). To develop effective therapies for such diseases we need to understand how the information is transmitted from the external environment through intracellular signaling pathway to the gene expression and cellular decision (Fallahi-Sichani et al., 2013). All the mentioned exemptions and examples, together with the complexity of signaling pathways often presented in enormous, overwhelming schemes (Figure 2.2), all these highlight how difficult to study yet important is the field of cell signaling. Taking into account the complexity of mammalian organisms, often involving dozens of signaling molecules and cell types, it appears natural to think that each information sent to

a cell is precisely sensed and the cell responds to it accordingly. In other words, activation of a specific signaling pathway should lead to reproducible outcomes in all receiver cells. There are examples when different cell fates like death, senescence, proliferation or morphological changes are governed by the action of one signaling pathway, indicating that specificity and precision of the information processing is of ultimate importance for the single cell (Purvis and Lahav, 2013; Spencer et al., 2009). In addition, the complex organism-level processes like immunity, circadian rhythms, muscle contraction, or wound healing seems to be well regulated and controlled, with not much space for imprecision. All these show that the reliable, high fidelity signaling appears to be essential for functioning of single cells as well for the multicellular organisms as a whole. However, experiments of recent decades cast a shadow of doubt at such thinking, indicating that the signaling responses to a stimulus of a given intensity can differ substantially between isogenic and outwardly identical cells.

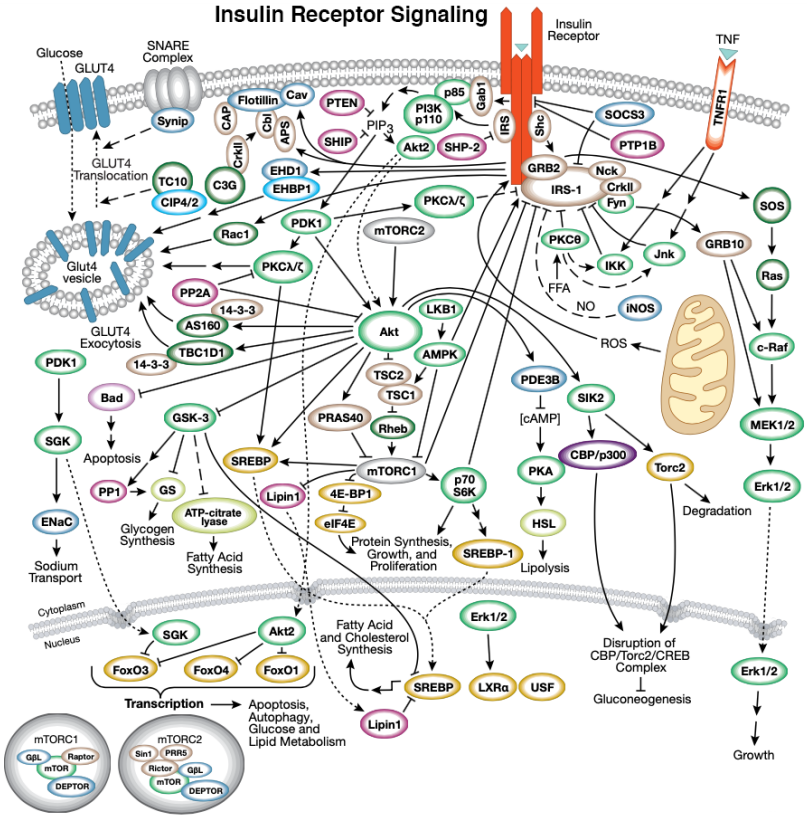


*Figure 2.2 Insulin Receptor Signaling*

Insulin, an important hormone of metabolism, acts via a complex network of regulators, signal processors and effectors, indicating the difficulties in studying the signaling pathways. Illustration reproduced courtesy of Cell Signaling Technology, Inc. (www.cellsignal.com).

## 2.4. Cell-to-cell variability in cellular signaling

Pioneering studies regarding single-cell responses to the uniform, environmental signals were performed on mammalian cells using glucocorticoid hormones signaling (Ko et al., 1990). They revealed that individual cells exhibit very heterogeneous expression levels of hormone-inducible genes after hormone stimulation. More recent experiments aiming to examine cell-to-cell variability in cellular signaling used single-cell high-throughput techniques such as confocal imaging, microfluidics, flow cytometry, live imaging, single molecule fluorescence in situ hybridization (smFISH) or combination of them (see reviews(Topolewski and Komorowski, 2021; Wollman, 2018). These investigated a variety of signaling molecules, including cytokines, chemokines (cytokines that promote the movement of a cell or organism) and growth factors in bacteria (Ruiz et al., 2018), yeast (Colman-Lerner et al., 2005), protista (Fuller et al., 2010) and mammalian cells (Cheong et al., 2011; Jetka et al., 2019; Selimkhanov et al., 2014). The conclusions were always similar: the response to a given dose of a stimulant was of great variability among single cells, sometimes spanning orders of magnitude. In addition, some fraction of cells stimulated with a saturating dose of the stimulus was observed to have responses similar to cells stimulated with a low dose or even to the unstimulated population (Lee et al., 2014). In other words, strongly responding cells after low stimulation showed similar levels of responses as weakly responding cells after high stimulation. From a perspective of an individual cell, it can be interpreted that sensing of the existing signal can be done only with inaccurate approximation, or imprecisely, as some cells give a very similar response to either high or low dosage of the signal. However, despite this variability of responses to the same stimulus, the majority of the outcomes seems to be correct: the homeostasis of an organism is being sustained, the pathogens are being defeated, the tissues are being regenerated and the cancer cells in majority are being killed. To explain this paradox and to efficiently study the signal transfer from environment to a cell, the method of quantifying cellular signaling fidelity was needed. The formalism which gives such ability is the information theory, traditionally used in computer science for quantifying the fidelity of electric signal receiving.

## 2.5. Information theory in cellular signaling

Information theory, a formalism initially used in electronic communication and quantification of statistical accuracy (Cover and Thomas, 2012; Shannon, 1948), gained much broader applicability than originally anticipated. Recently, these concepts have been used in the research of many biological systems, including transcription regulation, development, neuroscience, or cellular signaling, allowing for the assessment of cell-to-cell variability on the accuracy of signal sensing (Uda, 2020). Adopting the information theory formalism, a cellular signaling pathway can be considered as a communication channel, which senses the given stimulus (input, or X) and converts it to the specific response (output, or Y) (Uda, 2020). It is thought that each biochemical reaction relayed in a signaling pathway introduces some noise or uncontrolled variability (Garner et al., 2016). Therefore, the input-output relationship of the biochemical signaling can be represented as a probability distribution, $P(Y|X=x)$, instead of a deterministic dependency (Figure 2.3A). A high amount of information about values of x present in a variable Y would indicate the high probability of accurate estimation of x after observing Y. Such information transfer between the two variables, e.g., cytokine concentration and transcription factor nuclear level can be quantified as Mutual Information (MI), which measures the reliability of signal prediction based on the given response. MI is expressed in bits, where $2^{MI}$ can be interpreted as the maximum number of inputs that can be encoded from the observed output, assuming that the input follows a given probability distribution. In other words, a channel having 1 bit of MI can resolve 2 states of input (binary response), while when MI equals 2, then the number of input values increases to 4 and so on. Unfortunately, the input distribution is often unknown, limiting the confidence about the true information transfer. Therefore, to account for this and to represent the upper bound of the information transfer in the signaling channel, the channel capacity (C*) term has been introduced, representing the maximum of MI over all possible input distribution. C* also takes the values in bits and, similarly to MI, is a $\log_2$ of the maximum number of distinguishable input values, based on the output distribution.

Heading to more intuitive representation of information transfer quantification, the amount of information that can be transmitted through a signaling pathway depends on the overlap between response distributions corresponding to different inputs. Assuming the four different

input values used, the completely distinct output distributions would imply the maximum, that is four resolvable input values and two bits of transferred information (Figure 2.3B). Similarly, when the output distributions fully overlap, then the channel can distinguish only one resolvable input value, with zero bits of information transferred. In the intermediate scenarios, that is when the output distributions are only partially overlapped, the information can vary between zero and two bits, with the bigger overlaps, the lower information transfer value.

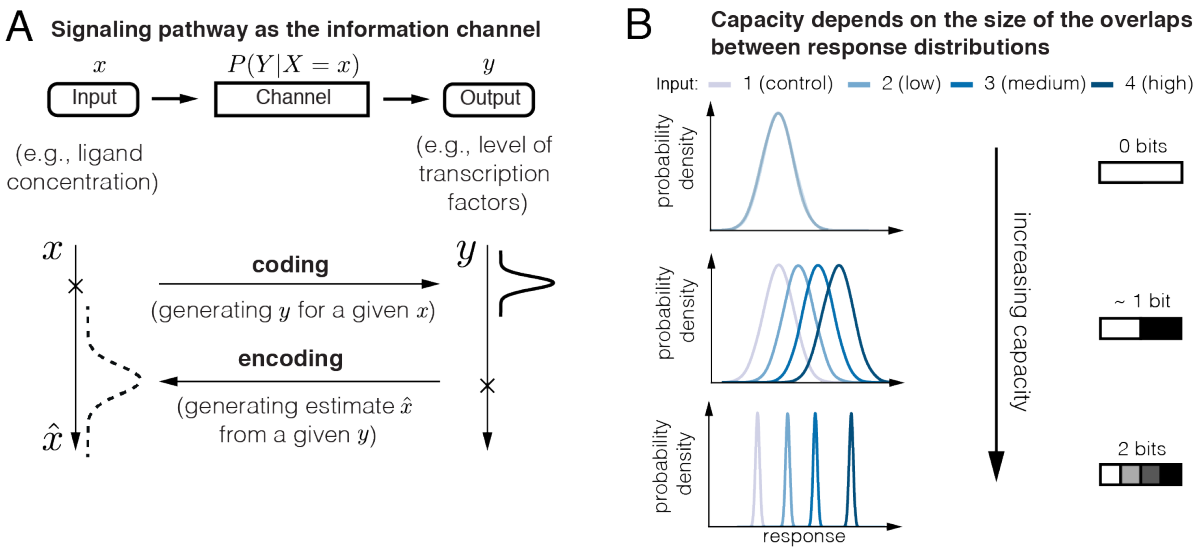


*Figure 2.3. Information theory and its application in cellular signaling*

(A) A biochemical signaling pathway can be represented as a probabilistic input-output relationship, P(Y|X=x), which encodes input, x, using output, y. Due to stochastic factors decoding is possible only with a limited precision. (B) Channel capacity is a suitable way of measuring the amount of information processed. Hypothetical responses distributions to four inputs (e.g., ligand concentrations) in three scenarios with a different degree of overlaps. Completely overlapping distributions do not allow for information transfer and imply the capacity of 0 bits. Information capacity increases for more distinct distributions and reaches 2 bits for completely distinct distributions to four considered inputs. Modified from (Topolewski and Komorowski, 2021)

## 2.6. Cellular strategies for high signaling capacity

The first quantification of signaling fidelity based on information theory was performed on mouse embryonic fibroblasts stimulated with a range of doses of tumor necrosis factor α (TNF-α) (Cheong et al., 2011). The stimulation doses were considered as input, or X (Figure 2.4A). The response, or the output, Y, was measured in individual cells with immunostaining as the nuclear level of the transcription factor, nuclear factor κB (NF-κB). The obtained single cell response distributions were then used to calculate the channel capacity, reaching ~ 1 bit of information transferred in the investigated signaling pathway (Figure 2.4B). The result can be

interpreted as cells being able to distinguish only between presence or absence of a stimulant, with limited sensitivity to other stimulation levels.

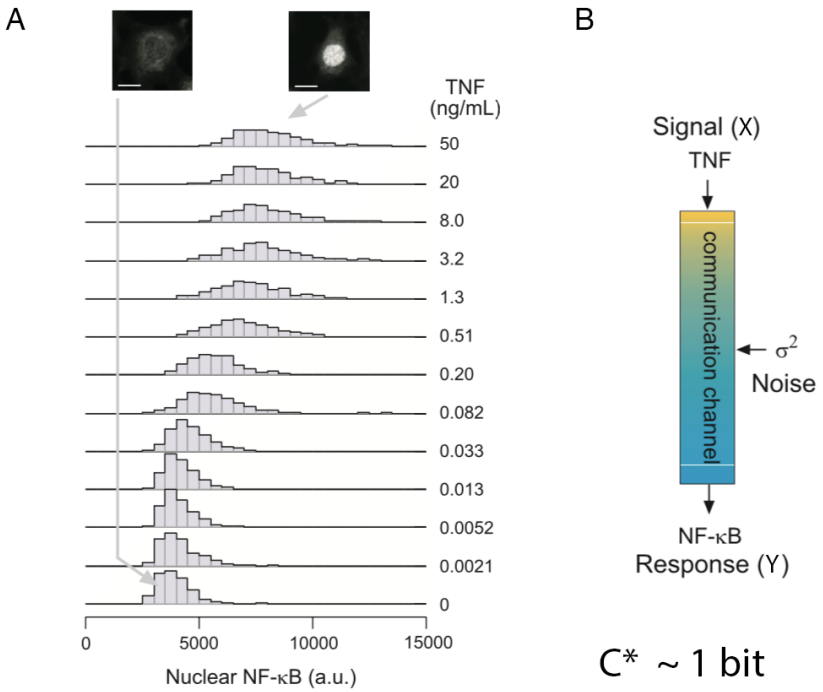


*Figure 2.4 Channel capacity of NF-κB signaling pathway*

(A) Single cell response distributions to 30-min TNF-α stimulations based on microscopic images (exemplary cells are shown above the distribution, scale bars = 20 μm). Please note the big overlaps of distributions in 0 ng/mL and 50 ng/mL responses. (B) The noisy communication channel with channel capacity of ~ 1 bit calculated based on results in A. Modified from (Cheong et al., 2011).

Similar quantity of mutual information or information capacity reaching at most ~ 1 bits was obtained using other signaling models, including ATP (adenosine triphosphate) (Selimkhanov et al., 2014), hormone- (Garner et al., 2016) or growth factor- signaling (Benary et al., 2020). Motivated by these results, researchers started to investigate the roles of different cellular mechanisms that ensure reliable signal sensing, processing and translating into a specific action. Researchers also started to explore the various ways of thinking about the fidelity of cellular signaling, e.g., by considering a group of individual cells as a signaling unit. Therefore, a number of mechanisms have been postulated to reconcile the apparent lack of signaling fidelity (two state recognition: presence or absence of the stimulant; Figure 2.5A) with the reliable functioning of individual cells during physiological processes (Topolewski and Komorowski, 2021).

### 2.6.1. Time averaging

In electronic communication systems the average of multiple measurements taken over time has lower variability than a single measurement (Balaguer and Ibeas, 2021). In biological systems, the information about the ligand identity can be encoded in the dynamics of the response instead of a steady state- or maximum-response time point (Purvis and Lahav, 2013; Santos et al., 2007). Combining those observations and taking into account time trajectories of cellular response provided additional information over single time-point measurements in case of multiple signaling pathways, including those stimulated by growth factor, ATP, or a synthetic equivalent of bacteria (lipopolysaccharide) (Selimkhanov et al., 2014), as well as in cytokine-stimulated mammalian cells (Jetka et al., 2019) and yeast under stress conditions (Granados et al., 2018). The information gain was up to 0.5 bits of information, what can be translated as the ability of cells to resolve one additional dose of a stimulant (Figure 2.5B).

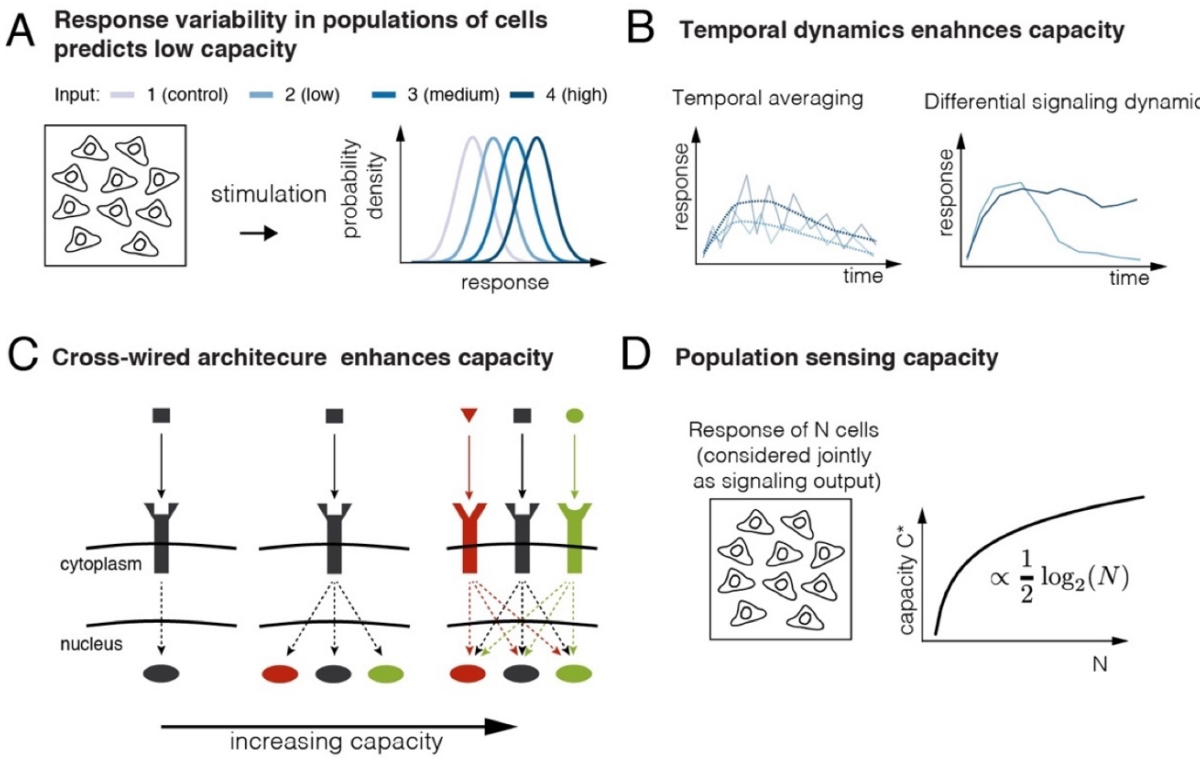


*Figure 2.5. Schemes of cellular strategies for high signaling capacity*

(A) Population of cells stimulated with different levels of inputs often show high overlaps of response distributions, implying low information capacity. (B) Temporal averaging (left panel): intertwined responses to two inputs (solid lines) can be reliably distinguished when their averages (dashed lines) are inspected, which increases information capacity. Differential signaling dynamics (right panel): two inputs may induce responses that are similar over one time-window but differ over another, which increases information capacity. (C) Activation of several distinct signaling effectors by a single ligand enhances information transfer. (D) Responses of N cells can be jointly considered as an output of a signaling system, leading to increased information capacity compared to cells analyzed individually. Information capacity was shown to scales with ½ $\log_2$(N).

### 2.6.2. Differential signaling dynamics

In a similar line to time averaging strategy and exploiting measurements of cellular responses over time, the differential signaling dynamics can also enable the cells to increase the acquired information about identities and quantities of ambient ligands (Figure 2.5B). This concept has been elegantly shown on Notch signaling, which is a model of neighbor cell-to-cell communication (Guruharsha et al., 2012). In mammals, the Notch1 receptor can be activated by multiple transmembrane ligands placed in signal-sender cells, however each ligand bears different information and can promote different cell fates, e.g., during mice embryonic development (Preuße et al., 2015). After binding the ligand, the Notch1 receptor activity was either pulsatile or sustained, depending on the ligand used, which in turn induced different effects on the embryonic myogenesis (Nandagopal et al., 2018). Similarly, different growth factors elicit distinct nuclear-cytosolic translocation of transcription factor over time, providing the proof, that the transcription factor dynamics (the output) can encode the identity and concentration of the stimulant (the input) (Sampattavanich et al., 2018).

### 2.6.3. Cross-wiring

The research on the cellular precision of signal sensing often focuses only on one specific signaling pathway, single receptor type or one transcription factor to simplify the methodology and to make conclusions more straightforward. However, the nature of cellular signaling in biology is much more complicated, with multiple inputs possessing ability to bind to multiple receptors, which in turn can activate number of effectors leading to highly cross-wired system (Figure 2.5C) (Rowland and Deeds, 2014; Rowland et al., 2017). Such interconnected architecture of signaling pathways was shown in theoretical models to be evolutionarily favorable, with higher signaling precision compared to simple signaling pathways with no cross-reactivity (Komorowski and Tawfik, 2019). Similarly, in experimental works measuring two outputs (two-dimentional response) after stimulation with insulin, epidermal growth factor (EGF) and specific inhibitors (Pope et al., 2020) or TNF-α (Cheong et al., 2011), the information capacity was significantly higher than when only one output was taken into account.

### 2.6.4. Combination of time averaging, differential dynamics and cross- wiring

All the mentioned cellular approaches for increasing information capacity, that is time averaging, differential signaling dynamics and cross-wiring, can all be utilized in the same cell to increase the information capacity of the same signaling pathway, giving a more in-depth understanding of cell biology complexity and evolution. It was shown, that a yeast cell can distinguish with high precision the type and severity of environmental stress (including oxidative, osmotic and carbon stress) by integrating information from multiple TF dynamics, indicating that knowledge about combination of specific effectors can give almost optimal decoding, reaching up to 2.5 bits of information (Granados et al., 2018). Another study reveals that macrophage cells can detect and distinguish different types of bacterial infections (with varying pathogenicity, location and replication), by integrating dynamical activation of both NF-κB and mitogen-activated protein kinase (MAPK) signaling (Lane et al., 2019). Therefore, cells presumably use a complex biochemical circuit to precisely distinguish between multiple abiotic (environmental stress) and biotic (bacterial infections) stresses.

### 2.6.5. Population response

In many biological processes the response of a cell to stimulation is binary, that is yes or no responses, e.g., proliferation vs death or the contraction of a muscle fiber (Suderman et al., 2017; Wada et al., 2020). Yet all of them are well regulated and can be triggered by specific stimuli. In case of such signaling processes, instead of considering single cells individually, the group of cells can be used as an information channel, because what can matter at the whole organism level is the percentage of cells which have undergone apoptosis or a combined contraction effect of a population of muscle fibers in a muscle. Therefore, examining the information capacity of several cells considered jointly can potentially lead to more efficient information flow (Figure 2.5D). This hypothesis was first tested in cells stimulated with TNF-α, when responses of a group of cells (multi-cell channels) were averaged, plugged into the formula to calculate the mutual information and compared to mutual information of single-cell channels (Cheong et al., 2011). Such an approach led to the conclusion that the mutual information increases with the increase in the number of cells in the multi-cell channel. The further investigations using pro-apoptotic agent TNF-related apoptosis-inducing ligand (TRAIL) showed, that cellular populations with higher heterogeneity respond to a broader

range of the stimulant doses compared to populations of small heterogeneity (Suderman et al., 2017). To explain it more intuitively, one can imagine a hypothetical situation of a population of perfectly identical cells (Figure 2.6, blue dots). Each cell in such a population will die after the exactly same dosage of pro-apoptotic TRAIL, leading to the population of cells being able to recognize only two levels of a stimulation: lower than causing the death and higher than this threshold level, so bearing only 1 bit of information. In contrary, the population of higher levels of cell-to-cell heterogeneity will consist of cells with distinct threshold level of death, therefore a given small dose of stimulation will cause the death of some, but not all cells, with more cell deaths with increasing level of stimulation (Figure 2.6, red and blue dots). These findings indicate that the cell-to-cell heterogeneity can increase the information capacity of multiple-cell channels and indeed be beneficial, as such variable population is more robust to various death signals.

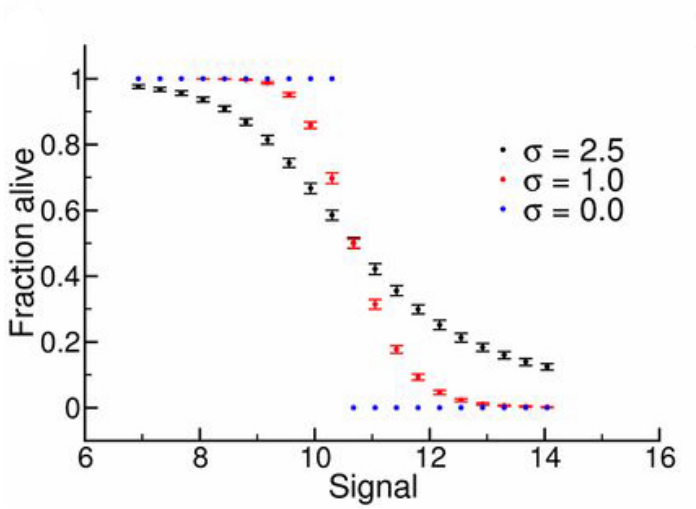


*Figure 2.6. The simulation of population responses.*

The population death as responses to increasing doses of signal with 3 levels of noise. The higher the noise, the population is more sensitive to signal doses. Modified from (Suderman et al., 2017).

The insight that multicellular organisms favor high cell-to-cell heterogeneity were extended in the recent work on myotubes and muscle tissue (Wada et al., 2020). Single muscle cells were stimulated repetitively with 10 levels of electric pulses showing the binary response of $Ca^{2+}$ with the great cell-to-cell variability in intensity of the electric pulse needed for the cell activation. In other words, each cell had a specific threshold level required for the on/off response. The ability to discriminate stimulation levels based on the one-cell channel response reached the ~2.7 unique levels of stimulation (~1.4 bits). However, when the cells were grouped into multi-cell channels of up to 128 cells in one channel with summing up all the responses, the number of stimulation levels that could be discriminated increased up to almost 10 levels (~3.3 bits), indicating the perfect decoding. All these findings confirm that

cell-to-cell heterogeneity can indeed be highly beneficial in specific biological processes. This advantageous nature of the heterogeneity raises the question of the origin of cell-to-cell variability in cellular signaling, its regulation and robustness (Wollman, 2018). If we knew the sources of cell-to-cell heterogeneity, we would better understand the overall signaling precision and maybe adjust the research accordingly, for example focusing on the cellular characteristics influencing the observed heterogeneity the most.

## 2.7. Origins of cell-to-cell heterogeneity in biology

The origins of cell-to-cell heterogeneity of many cellular processes have been extensively investigated but a comprehensive understanding is missing. The initial work on decomposition of variability sources was done in the context of gene expression (Elowitz et al., 2002; Swain et al., 2002), but conceptually similar approach has been applied in development processes (Tkačik et al., 2014), cell fate decisions (Spencer et al., 2009) as well as in cellular signaling (Selimkhanov et al., 2014; Wada et al., 2020).

### 2.7.1. Categories of sources of cell-to-cell heterogeneity

The observed differences between cellular responses or behaviors and traits are canonically thought to be of two, non-exclusive sources: extrinsic (sometimes referred to as deterministic, cellular phenotype or cellular state) and intrinsic (sometimes referred to as probabilistic, molecular noise, random, stochastic). The extrinsic sources are of intercellular origin and cover all differences among cells in terms of protein concentration, cell size, cell cycle state, metabolic state, number of past mitosis processes, but also the small differences of microenvironment, different DNA methylation, mutations and many others (Figure 2.7A). The intrinsic sources are of intracellular origin and include fluctuations in biochemical reactions or unpredictability of microscopic collision of individual atoms and molecules, especially in systems of low copy-number of molecules (Figure 2.7B). In other words, the influence of extrinsic sources on the cell-to-cell variability is minimized in a population of perfectly identical cells, all having the same cellular morphology and concentration of all proteins. On the other hand, the influence of intrinsic noise on the cell-to-cell variability is maximized, e.g., in systems with low number of molecules.

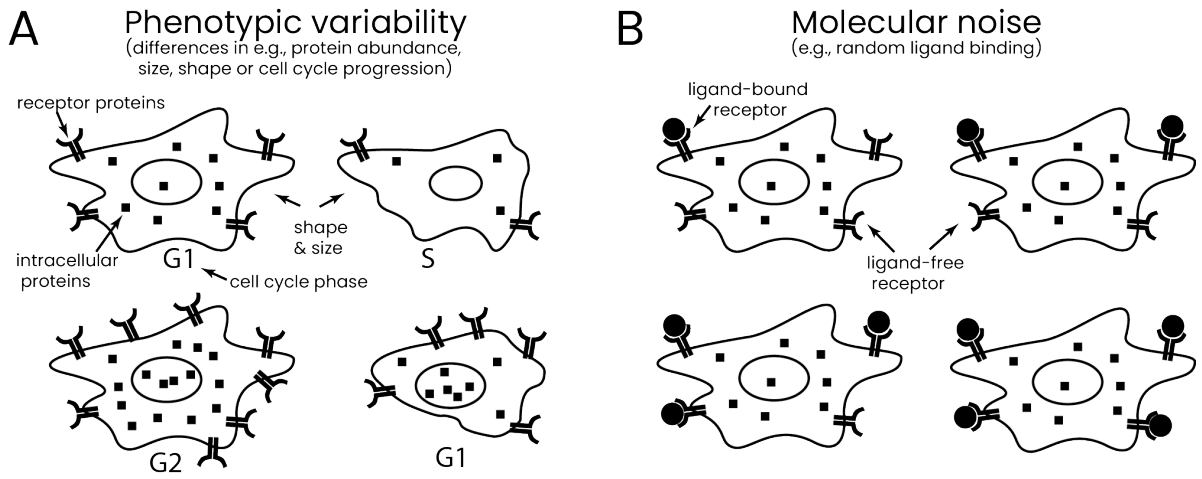


*Figure 2.7. Sources of cell-to-cell heterogeneity*

(A) Phenotypic variability, so differences of cellular features including protein abundance, cell size and shape as well as cell cycle phase and others all can influence the final cell behavior. (B) Molecular noise, e.g., random ligand binding of cells with identical phenotypes, is an inevitable characteristic of all biochemical reactions, influencing the final cellular behavior.

To put the proposed categories into perspective of the already mentioned variable activation of chromosome X in female calico cats, the extrinsic source could be differences in the methylotransferases level between cells, the enzymes responsible for DNA methylation, with certain threshold level required for silencing of one pigment allele, while intrinsic source could be unpredictable number of methylation reactions, with the certain level of needed methyl-residues needed for inactivation of the pigment allele. Traditionally, both intrinsic and extrinsic sources of cell-to-cell variability have been considered as noise that reduces the precision of cells in their action (Elowitz et al., 2002). However, the term “noise” implicitly assumes the loss of information between the signal and a cell action or implies unpredictability of a single cell in its behavior caused by both intrinsic and extrinsic sources of noise. Therefore, from the perspective of a single cell, the true uncertainty in a cellular action can be caused solely by stochastic biochemical effects, or in other words by the intrinsic noise (Eling et al., 2019). The extrinsic source of the cell-to-cell variability on the other hand does not necessarily cause the information loss, but only be the joint effect of the previous stochastic and deterministic factors influencing the current cellular phenotype. Therefore, the noise, or molecular noise, should be termed only in regards to intrinsic noise, while extrinsic noise should be rather termed as phenotypic variability. The existence of both variability sources was demonstrated in simple, yet potent dual-color fluorescent protein experiments on bacteria (Elowitz et al., 2002), which were further extended to both yeast (Bar-Even et al.,

2006; Raser and O'Shea, 2004) and mammalian cells (Raj et al., 2006; Sigal et al., 2006), all related to gene expression. In addition, similar noise source decomposition into intrinsic and extrinsic sources has also been applied for cellular signaling research.

### 2.7.2. Sources of heterogeneity in cellular signaling

In terms of cellular signaling, the heterogeneity could result from a combination of the two opposing scenarios. In one extreme, signaling responses could be fully determined by the molecular content of the cell, i.e., cellular phenotype. Then, the cell-to-cell heterogeneity of responses would result solely from differences in cellular phenotypes, or phenotypic variability. Towards the other extreme, signaling processes could be subjected to the strong inherent randomness of cellular biochemistry, i.e., molecular noise. Then, the cell-to-cell heterogeneity of signaling responses would result mainly from random effects inside the cell, i.e., be dependent on the intrinsic sources of variability. Most probably, neither of the above two extreme scenarios is true for any signaling pathway and the truth lies somewhere in between. At this point, multiple questions may arise. What is the contribution of phenotypic variability and molecular noise in the cell-to-cell heterogeneity of cellular signaling? How much is it signaling pathway-dependent? What are the main cellular features of molecular phenotype that drive the observed heterogeneity? To answer these questions, we would need only one, simple, biological model: a group of cells perfectly identical in terms of any cellular characteristics and intracellular protein concentrations. In such a model the phenotype of each cell would be exactly the same, while the molecular noise would affect each cell independently. We could then stimulate such a group of cells and all the observed heterogeneity would result only from intrinsic sources. However, such an approach is extremely hard, if at all possible, to execute in practice. Even the natural process of cell division, which would of course replicate the single cell creating two daughter cells, is not a perfect solution, as the newborn cells are not perfectly identical neither. The natural process of cell division often causes stochastic differences in cell size of daughter cells (Cadart et al., 2018) as well as uneven segregation of organelles (Chang and Marshall, 2017), proteins (Cohen et al., 2009; Fuentealba et al., 2008) and mRNAs (Shlyakhtina et al., 2019), especially influencing the low copy-number molecules (Huh and Paulsson, 2011). Therefore, researchers proposed a number of approaches, elaborated below, which were meant to mimic such an

ideal model of identical cells. These approaches limit the contribution of cellular phenotype variability in the overall cell-to-cell heterogeneity of cellular responses and therefore are great methods to investigate the true molecular noise, or stochasticity of cellular signaling.

## 2.8. Experimental strategies for limiting the contribution of molecular phenotype

To minimize the influence of a molecular phenotype the following methods were utilized: considering fold-change response instead of absolute response; correlating the cellular response with the cellular characteristics or cellular state; considering the sibling cells as the approximation of cellular clones; repetitive stimulation of the same cell with the same or increasing dosage of a stimulant; decomposition of extrinsic vs intrinsic noise by dual-color reporters.

### 2.8.1. Fold-change response

Traditionally, the cellular response after stimulation was considered as the absolute value of the effector signal, often measured as the arbitrary unit of fluorescence intensity with some flat-field correction applied. Such an approach does not take into account the differences of the effector level prior to the stimulation, a component of the molecular content of the cell. Such basal level of the effector before stimulation could be considered as the approximation of the cellular potential to be responsive- in other words, cells with high basal level of the effector before stimulation could be more prepared to respond strongly after stimulation. Indeed, when the dynamics of the nuclear levels of the signaling effector, NF-κB, was measured after stimulation with TNF-α, cells exhibited the usual level of cell-to-cell heterogeneity of responses (Lee et al., 2014). Nevertheless, when responses were redefined in terms of fold-changes, i.e., as the ratio between nuclear NF-κB level at a given time of after stimulation and before stimulation, the cell-to-cell heterogeneity decreased considerably. Besides, fold-change in the response of individual cells exhibited significantly higher correlation with downstream gene expression than the absolute level, indicating that indeed the fold-change is a better representation of the response value instead of the absolute level of the effector. Such an approach removes one component of the phenotypic variability- the basal level of the effector, making the whole population more unified. Similar results were

also obtained in the transforming growth factor beta (TGF-β) pathway, with the transcription factor Smad3 as the effector (Figure 2.8) (Frick et al., 2017) as well as in the EGF pathway with the modified version of the FOS-related antigen 1 (FRA1) transcription factor as the effector (Benary et al., 2020). Fold change responses were also considered to bear more information about the dosage used, that is to have higher information capacity than absolute values in these studies (Benary et al., 2020; Frick et al., 2017; Zhang et al., 2017).

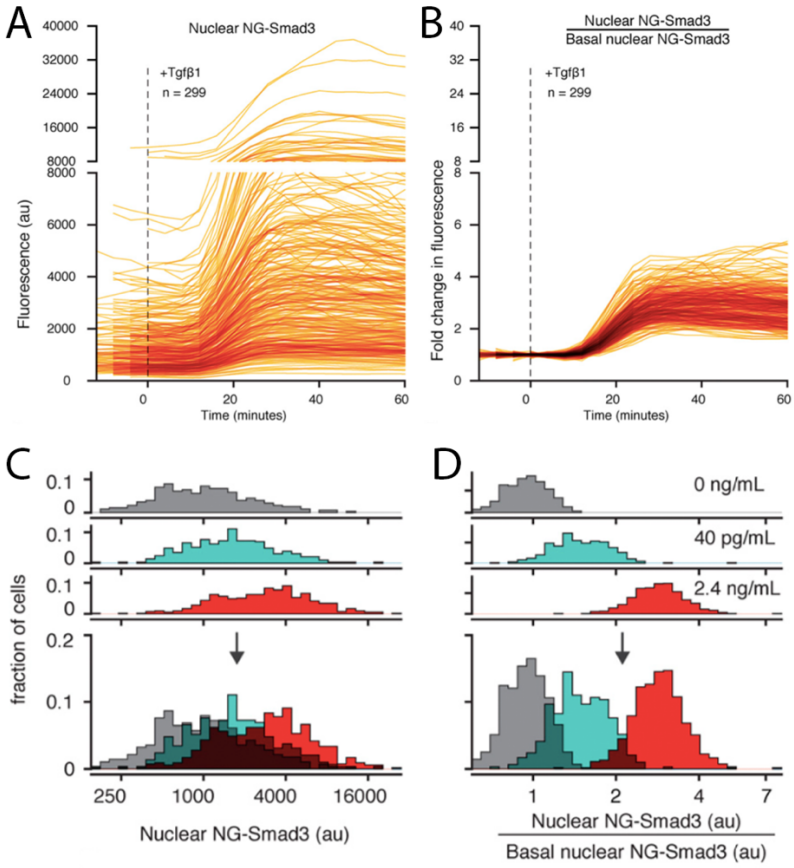


*Figure 2.8. Fold change values allow for better signal discrimination*

(A) Absolute nuclear level of Smad3 protein after TGF-β treatment. (B) Values of A normalized by the basal level of Smad3, leading to fold-change values. (C) Histograms of absolute nuclear level of Smad3 after low, medium and high dose of TGF-β stimulation show high overlaps. **(D)** Histograms of fold change values of Smad3 after low, medium and high dose of TGF-β stimulation show small overlaps, indicating the fold change as better information-bearing unit. Modified from (Frick et al., 2017).

### 2.8.2. Cellular state as a determinant of the response

Considering the cellular characteristics or cellular state as a determinant of the response is very similar to the fold-change response, but focuses on cellular features not directly related to the response effectors, e.g., on levels of certain proteins that could pre-determine response of a cell. With such determinants, the observed cell-to-cell heterogeneity of cellular responses could not be attributed to noise, but rather to differences in cellular states. Indeed, based on mathematical modeling, it was predicted and next experimentally confirmed (Yao et al., 2016) that the majority ($R^2$ ~ 70%) of variance of ATP-stimulated $Ca^{2+}$ response can be explained by variability in intracellular receptor activity, indicating that an individual cell itself could be very

precise and that the cell population is very heterogeneous in terms of cellular states. Similarly, the work on the response to heat, based on the modeling and microscopy, showed, that the basal levels of heat shock proteins (specifically, chaperone HSD72 and heat shock factor 1) explain 56% of the observed heterogeneity in heat-caused response (Guilbert et al., 2020). In the massive work connecting the gene expression variability with multiple cellular features, the authors measured the RNA level of 150 genes together with $Ca^{2+}$ responses in live microscopy as well as with measurements of cell size, cell cycle and differentiation potential. They showed that the expression variability of the majority of genes can be significantly reduced (up to theoretical limit related to pure stochasticity of gene transcription reactions), when all cellular state features were considered (Foreman and Wollman, 2020). These findings indicate that the cellular state explains the majority of variance in the gene expression. Also, all these studies showed that our understanding of cell identity and uniformity of environmental signals is not complete. Cells can differ in their molecular states and therefore respond to stimuli in different ways. The cell cycle is one of the cellular processes, which divide cells into subgroups and could be potential factors changing the sensitivity of cells to external signals. It broadly changes the intracellular state of many proteins and biochemical reactions (Uzbekov, 2004). The cell cycle leads to the cell division and can be divided into 4 main phases: G1, when the cell is preparing for the DNA synthesis, S, when the DNA is synthesized, G2, when the cell is preparing for the division and M, that is mitosis, when the exact cell division occurs (Tyson and Novak, 2008). After that, the cycle starts from the beginning. During the cell cycle, the DNA content is doubled in S phase and changes from 2c in G1 phase, to 4c in G2 and mitosis (Figure 2.9). What is important, the cell cycle shows a high level of desynchronization in the single cells, bearing the potential of inducing the variability of e.g., cytokine or growth factor responses (Roukos et al., 2015). Unfortunately, the impact of the cell cycle on the signal processing in the single cells has not been studied in the literature so far.

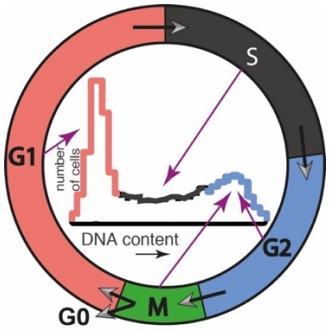


*Figure 2.9 Cell cycle progression*

The cell cycle consists of successive phases: in G1 (gap 1), a cell prepares for the DNA duplication; in S (synthesis) phase the DNA duplication occurs; in G2 (gap 2) a cell prepares for mitosis; in mitosis the cell divides. After the mitosis, cell can stop in the cycle and go to G0 phase. Each phase can be characterized by analysis of DNA content histogram- cells after the DNA duplication have around twice as much DNA as cells before DNA duplication.

### 2.8.3. Responses of sibling cells

Mammalian cell division leads to division of a mother cell into two daughter cells (Tyson and Novak, 2008). Each of the daughter cells is very similar to the other, however with some differences (Huh and Paulsson, 2011), which further accumulate along the progression of the cell cycle (Huang, 2009; Spencer et al., 2009). However, accepting these limitations, one can assume that daughter cells just after the division have higher similarity between each other than similarity between two random chosen cells from a population. Then, such two cells would serve as a non-perfect model of two identical cells, which scientists are looking for so extensively. Such assumption has been done in terms of cell fate decision-making (Spencer et al., 2009). Cells were tracked using time-lapse microscopy and treated with the TRAIL, which causes the cell apoptosis some time after the treatment. Such time was observed to be very variable among single cells – some cells died soon after treatment, some long after treatment. However, when the information about the cellular lineage was retrieved from the time lapse microscopic images, the death time of sibling cells turned out to be very similar ($R^2$ between sisters up to 0.93, while for cells chosen at random only $R^2$= 0.04). Lower $R^2$ values were obtained in terms of responses to insulin-like growth factor-1 (IGF-1), while still much higher than for random sampled newly born cells (Gross et al., 2019). In addition, we know from the gene expression research, that the transcriptional activity dynamics was similar in daughter cells and transcriptional dynamics is synchronized (Phillips et al., 2019). Taking together, the cellular features inherited by both daughter cells are enough to make those cells comparable responsive, indicating that the cellular state can be passed from mother to daughter and that it at least partially governs the cellular behavior to stimulation.

### 2.8.4. Repetitive stimulation

Instead of looking for identical cells, one could think of stimulating the same cell multiple times and treating each single outcome of the perturbation as coming from a perfectly identical, but separate cell. Such an approach bears, however, some disadvantages. Mainly, it can be adopted only to a situation of rapid signaling, when the period of activation-relaxation cycle is relatively fast, in the order of seconds or minutes rather than hours, as many of the cellular characteristics can be naturally changing throughout such long time, due to e.g., progression in the cell cycle, stochasticity of gene expression, nonlinearity of cell growth or,

maybe the most potent, the gene expression activation caused by the stimulation (Shamir et al., 2016). Such changes in cellular phenotype can affect the response to subsequent stimulation, abolishing the assumption of cell identity. Therefore, the best choice of signaling pathways to utilize such a strategy is related to ion-responses, e.g., influx to the cytoplasm of $Ca^{2+}$. Nevertheless, the repeated stimulation can be also adopted to signaling pathways operating on the regimes of hours, however with weaker cellular identity assumptions. Utilizing the workhorse of cellular signaling, TNF-α cytokine, the cells were stimulated twice: first by the reference concentration and second by the increased concentration, with the 3 h recovery period between both stimulations (Zhang et al., 2017). The response of the second stimulation turned out to be highly proportional to the response of the first stimulation for each of the doses used, indicating that a cell can respond to increasing dosage of a stimulant with higher precision than predicted by the studies with only single stimulation. Similar research of repetitive stimulation with ~2-3 h washout between doses of a stimulant was done on gonadotropin-releasing hormone (GnRH) (Voliotis et al., 2018) and IGF-1 (Gross et al., 2019), with similar conclusions: cells respond to the second dose proportionally to the first dose, indicating that cells can distinguish multiple doses of a stimulant with high precision. The studies using cellular responses triggered in a very short time scale also showed similar phenomena. Repeated stimulation of acetylcholine (Keshelava et al., 2018) or electric pulses (Wada et al., 2020) both considered a response as the fast $Ca^{2+}$ influx-efflux cycle counted in seconds. Such a signaling model not only limited the changes in the cellular state caused by the stimulation, but also allowed the use of more doses (up to 10, compared to 4 in the cases of long-lasting signaling responses). Overall, these studies enabled reconstitution of a dose response curve, with response level vs dose for each individual cell (Figure 2.10). Such curves elegantly show that depending on the signaling pathway used, the response is either mainly binary or mainly graded, but for both scenarios, the individual cell reliably responds to the used dose and each cell does it in a unique way. In other words, the phenotypic variability exceeds the molecular noise in cellular response.

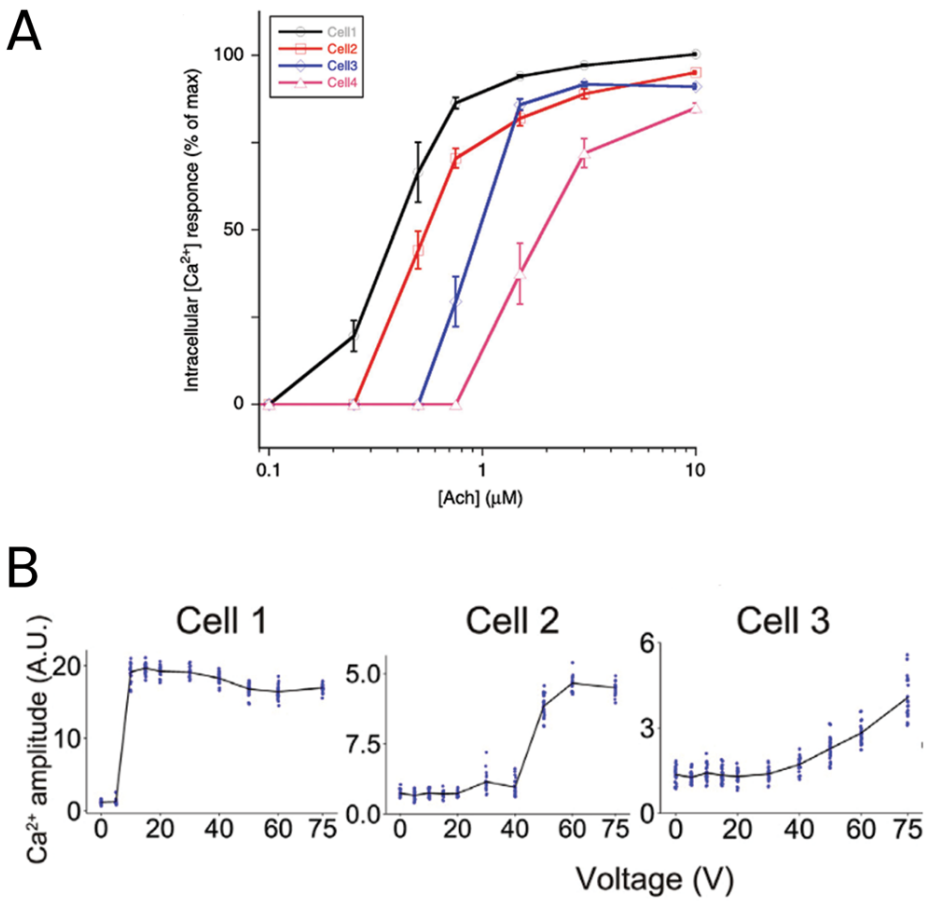


*Figure 2.10. Single cell-dose curves*

(A) Single **c**ells were treated with indicated doses of acetylcholine (Ach, X axis) and the response as $Ca^{2+}$ was measured (Y axis). Data for 4 cells presented, with error bars as standard deviation of repetitive measurements. Response curves for each cell are graded. Modified from (Keshelava et al., 2018) (B) Single cells were treated by electric pulse and $Ca^{2+}$ influx was measured. Each cell has a unique response curve. Response curves are binary for two first cells, and graded for the third cell. Modified from (Wada et al., 2020)

From the above examples it can be concluded that not all of the observed cell-to-cell heterogeneity in cellular signaling is the result of biochemical noise, but rather arises from the differences in cellular states. Prior to the stimulation, cells can be already predetermined to have the given response to the given dose of stimulation. In that way, single cell stimulated multiple times with increasing dosage will have much lower variability and therefore very high channel capacity, contrary to the observable low channel capacity population of single cell population (Figure 2.11). The decomposition of the sources of cell-to-cell heterogeneity into molecular noise and cellular phenotype of some cellular behaviors was also elegantly done for the first time in dual-color experiments.

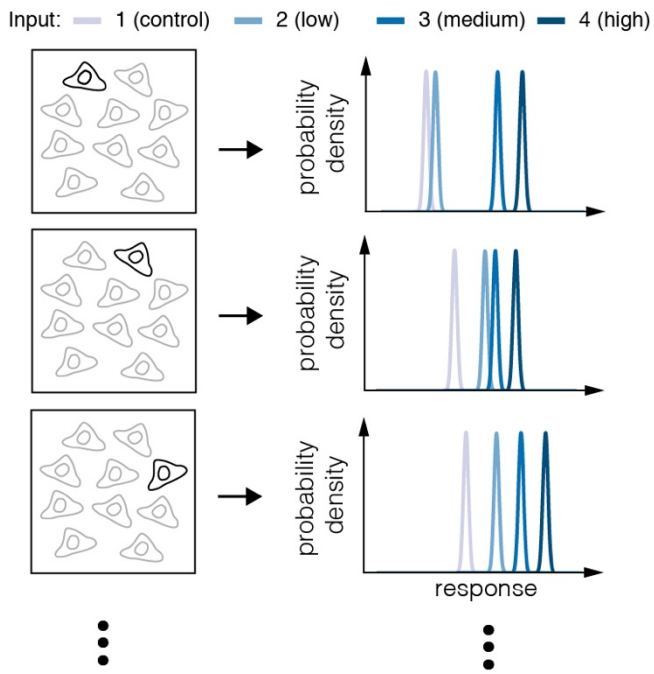


*Figure 2.11. Response variability of individual cells stimulated repeatedly.*

Each row represents a hypothetical single cell and its response to repetitive stimulation. Each cell has a unique cellular state and response characteristics to increasing doses of a stimulation. Low distribution overlaps indicate, that cell-to-cell response heterogeneity in a population of single cells is not necessarily equivalent to signaling noise. Modified from (Topolewski and Komorowski, 2021).

### 2.8.5. Dual-color decomposition

Instead of creating a perfect copy of the whole cell, which is difficult, one could imagine creating a perfect copy only of the cellular subsystem of interest inside the cell, e.g., in a gene expression study it would be introducing the two identical gene constructs into the genome of a cell. In this way, for each of the constructs, the majority of the cellular machinery is the same, i.e., the global level of polymerases, transcription factors, cell cycle stage, cell size and many others. The major difference would be then the stochasticity of biochemical reactions, so the molecular noise. Such an idea was applied first in bacteria (Elowitz et al., 2002). Two identical promoters were introduced into *E. coli* cells, each promoter regulating the production of either YFP or CFP (Yellow or Cyan Fluorescent Protein) (Figure 2.12A), which stands for the "dual-color" in the experiment description. Next, cell fluorescence of both channels was visualized and measured, producing the two-dimensional data that can be presented as a scatter (Figure 2.12C-E). Each dot on the scatter corresponds to a single cell with fluorescence of CFP on X axis and YFP on y axis. If there was no molecular noise at all, both fluorescence values would be equal, with all dots lying on the diagonal. The more the dot is off-diagonal, the higher the contribution of molecular noise. On the other hand, the higher influence of phenotypic variability, the more points are spread along the diagonal direction, which accounts for the between-cell differences in the fluorescence signal. Such

decomposition of: diagonal = phenotypic variability; off-diagonal = molecular noise, can be quantified and presented as the ratio of each component in the total variance of the data set. The decomposition idea can be presented more intuitively at microscopic images colored that red signal corresponds to YFP and green to CFP fluorescence (Figure 2.12C-D).

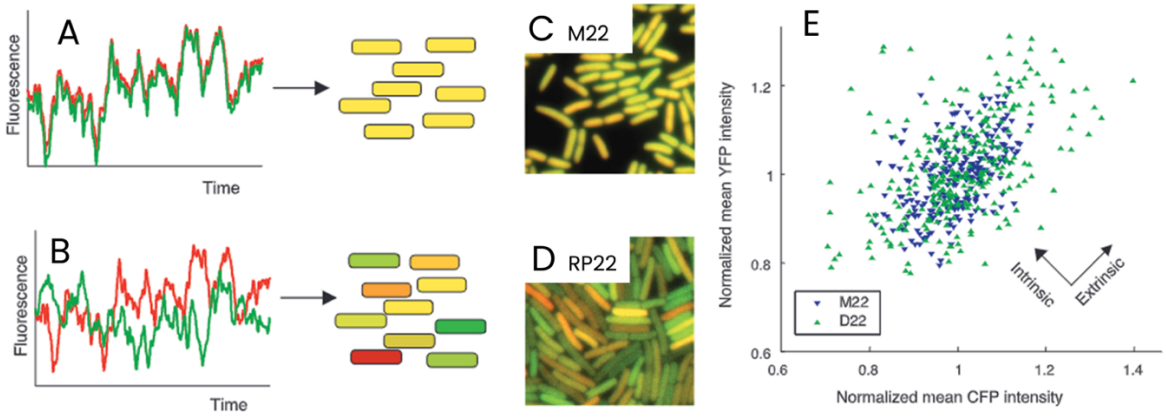


*Figure 2.12. Dual color experiment in gene expression study*

Two identical promoters were introduced into *E. coli* cells. Each promoter regulated the expression of one fluorescent protein, either CFP or YFP. The fluorescence of both proteins (green or red pseudo colors presented) was measured over time on the single cell level. Two scenarios are possible: (I) each protein is produced synchronously with the other, leading to equal yfp and cfp signals (red + green = yellow cell), implying low contribution of noise; (II) the protein production is asynchronous, with mosaic color of single cells, implying high contribution of noise. (C) and (D) microscopic images of cells with low noise (C) and high noise (D). (E) Decomposition of noise vs phenotype sources to total cell-to-cell heterogeneity. Each axis corresponds to the fluorescence signal of one fluorescence protein. Diagonal variability corresponds to phenotype differences. Variability perpendicular to the diagonal corresponds to noise. Each point represents a single cell: blue ones correspond to highly noisy bacterial strain; green one corresponds to strain of low noise.

On such images, the perfectly identical signals of CFP and YFP would give the yellow color in total (low molecular noise), while more green or red cells would indicate the higher differences between two fluorescent signals (higher molecular noise). In the *E. coli* cells, the contribution of molecular noise increased with the decrease in the gene transcription level (Elowitz et al., 2002). Similar dual-color experiments were done regarding gene transcription in yeast (Bar-Even et al., 2006; Raser and O'Shea, 2004) and mammalian cells (Raj et al., 2006; Sigal et al., 2006), leading to similar conclusions. However, such dual-color experiments have not been performed in relation to signaling processes, which would give great insight into the nature of stochasticity of signaling-related biochemical reactions. The cellular signaling of the immune system is of great need to be understood, as the global rate of autoimmune diseases

affects up to 5% of the worldwide population, not accounting for cancer and immune-deficiency diseases (Abbas et al., 2017; Wang et al., 2015).

## 2.9. The importance of studying cellular signaling in immune system

One of areas with the greatest complexity and requirements for information processing is the immune system. Mammalian immune responses involves cooperation of a great orchestra of tissues and immune cells, including B-cells, T-cells, granulocytes, macrophages, dendritic cells, as well as dozens of cytokines- signal proteins regulating the immune system and modulating the immune response (Abbas et al., 2017). The threat has to be precisely recognized, the information about its existence and nature has to be precisely passed to other cells, which in turn has to detect the signal sent, prepare for the threat spread, inform the other cells about the threat as so on. Specifically, thousands and millions of cells, signal molecules and biochemical reactions have to coordinately act with each other to successfully fight against bacteria and viruses, to specifically locate the cancer cells, to ensure homeostasis or to regulate the developing processes of a growing organism. Since signaling pathway disfunctions were characterized in cancers as well as in diabetes, drug addiction, ageing, neurodegeneration and immunodeficiencies (Berridge, 2014; Mora-Garcia and Sakamoto, 1999), the responses to immune signals must be robust to molecular noise and have to reliably correspond to given immune signal. Therefore, the communication in immune responses is crucial. Revealing the sources of cell-to-cell heterogeneity would not only broaden our understanding of immune responses in general, but it will also shed light on the evolution reason behind high cell-to-cell heterogeneity of cellular response to immune stimuli, specifically, explaining whether this variability is actually beneficial and, e.g., by ensuring increased response diversity (Wollman, 2018). On the other hand, new therapeutic strategies can be developed. For example, let assume that a specific signaling pathway is up-regulated in cancer cells of a given type. Once we know which element of this pathway contributes the most to the overall cell-to-cell variability of cancer cells, let's make other assumptions that it is an internal kinase, we can focus on blocking this specific protein from the activity, instead of blindly looking for the best molecular target. Such a strategy would decrease the survival rate of a small population of cells after cancer treatment, the phenomena called fractional killing, which is often the reason behind further re-growth and metastasis of cancers(Fallahi-

Sichani et al., 2013; Roux et al., 2015). But first, to establish the methodology of studying the sources of cell-to-cell heterogeneity, a proper biological model of signaling pathway has to be chosen.

## 2.10. Signaling pathways to study the sources of cell-to-cell heterogeneity of cytokine responses

Although multiple signaling pathways have been already mentioned here and used throughout the research, not all of them constitute good models for studying the cell-to-cell heterogeneity of signaling responses in the context of the immune system. In principle, such suitable signaling pathway should fulfill the following criteria:

- First, be strictly related to immune responses, with cytokine-signaling pathways as one of the best candidates, which govern a great majority of all immune-related communication processes.

- Second, be widely studied in the literature and for which the molecular bases have been established. This is needed, as the research will not focus on discovering the new molecular species of this pathway, or the new negative feedback loops existed, but on measuring the precision of the pathway. Also, depending on the methodology, reliable antibodies should be available, for obvious reasons.

- Third, has the easily measured outcome of the stimulation, or the output, with preference to signaling pathways of one main “effector” protein, which level being considered as the output. This excludes the pathways with existence of multiple outputs, which measuring all would be experimentally hard in each cell.

- Fourth, be selectively responsive to only external stimulation, and not to, e.g., heat, culture medium or autocrine/paracrine signaling, which influence could compromise the further conclusions.

Such suitable candidates which meet the above requirements are signaling pathways of interferon gamma (IFN-γ) and oncostatin M (OSM).

### 2.10.1.Interferon gamma pathway

Interferons are pleiotropic cytokine proteins, involved in both innate and adaptive immune systems (Rauch et al., 2014). They are canonically divided into three groups, with IFN-γ as the only member of the interferons II type. In mammals, IFN-γ was proven to regulate the anti-microbial immunity (Shtrichman and Samuel, 2001) and pregnancy (Murphy et al., 2009) as well as to have the impact on the developing of autoimmune diseases (Lees, 2015), obesity (Rocha et al., 2008), allergies (Teixeira et al., 2005), schizophrenia (Sharma et al., 2017) and cancers (Zaidi, 2019) in mammals. In addition, mice with impaired IFN-γ signaling showed deficiencies in resistance to both bacterial, viral and parasite infections as well as have higher spontaneous rate of tumorigenesis (Tannenbaum and Hamilton, 2000). The biological activity of IFN-γ pointed it to the use in therapy, with multiple clinical trials designed and started up, mainly in the anti-cancer treatment (Ni and Lu, 2018). Unfortunately, hopes for IFN-γ as the potential anti-tumor treatment factor had to be dismissed, as some studies showed that IFN-γ has a very complex and dual role in anti-tumor treatment, with adverse outcomes in cancer patients and development of autoimmune responses (Mojic et al., 2018; Zaidi, 2019).

All these indicate the need for a better understanding of the IFN-γ action. The knowledge about the heterogeneity of the dynamics of IFN-γ response can shed light on the mechanisms behind the variable and complex functions of IFN-γ. This, in turn, can lead to more effective use of its potential in biomedical applications.

### 2.10.2.Molecular mechanism of Interferon gamma pathway

Canonically, after IFN-γ binds to its receptor (formed as a complex of two heterodimers – IFNGR1 and IFNGR2), the signal is processed in the cytoplasmic JAK-STAT signaling pathway, composed of the Janus kinase1 and 2 (JAK1 and JAK2) and transcription factor signal transducer and activator of transcription 1 (STAT1). Briefly, STAT1 molecules are phosphorylated at the Tyrosine 701 (Y701) residue by JAK kinases and after dimerization, Tyrosine701-phosphorylated STAT1 (pSTAT1) dimers are translocated to the nucleus, where they induce the transcription of specific genes (Murray, 2007) (Figure 2.13). Therefore, the easy-to-measure output of IFN-γ stimulation can be assumed as a pSTAT1 level in the nucleus. After some time, ranging from minutes to hours, the activated pSTAT1 is dephosphorylated,

mainly by the TC45 phosphatase enzyme, a nuclear isoform of the T-cell protein tyrosine phosphatases (TC-PTP). Dephosphorylation enables the binding of exportins to nuclear STAT1, which further causes the export of STAT1 to cytoplasm, where it is ready for the next round of the activation (Haspel and Darnell, 1999; Hoeve et al., 2002; Meyer et al., 2003).

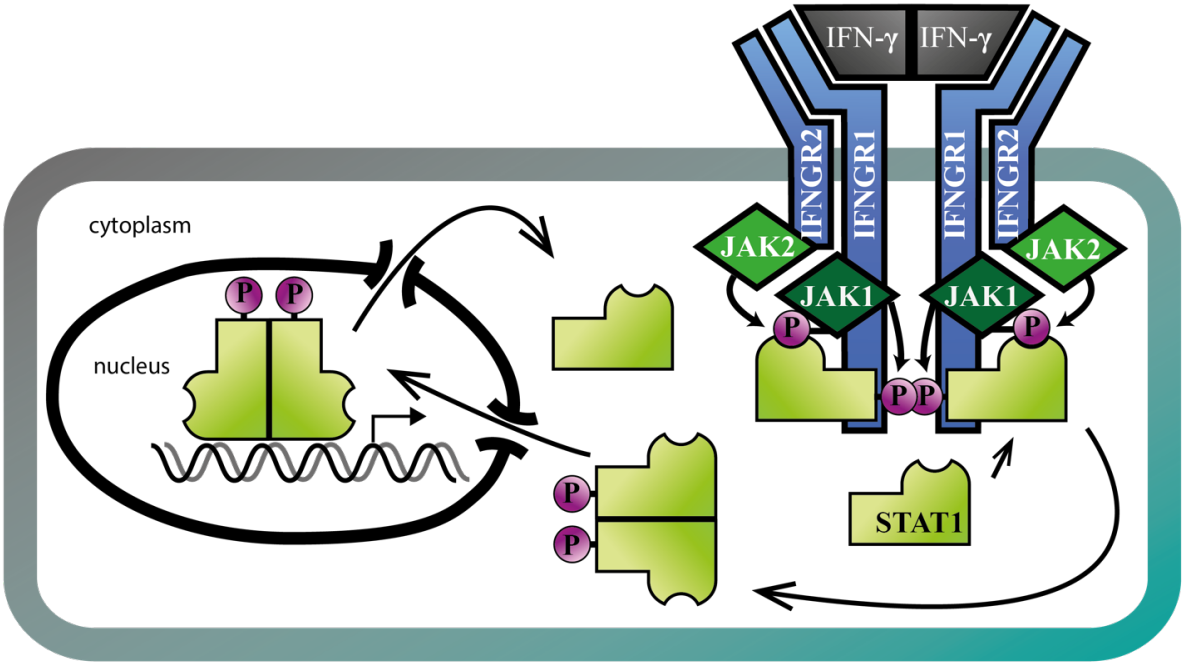


*Figure 2.13. IFN-γ signaling*

When IFN-γ molecules bind the IFNGR1 - IFNGR2 double heterodimer receptors, a cascade of phosphorylation occurs, involving JAK1 and JAK2 kinases, leading to phosphorylation and dimerization of transcription factor called STAT1. Such activated STAT1 molecules translocate to the nucleus where they can activate the gene transcription. After the dephosphorylation, STAT1 exits the nucleus and can be re-activated.

However, not surprisingly for those who study biology (as biology always has some exemptions to the rules), there are known other, non-canonical ways of the signal flow after IFN-γ stimulation. Among them, there can be listed pSTAT3 nuclear translocation instead of pSTAT1 or activation of phosphorylation of STAT1 Serine 727 residue by phosphatidylinositol 3-kinase (PI3K), mitogen-activated protein kinase (MAPK) or protein kinase Cδ (PKCδ) (Deb et al., 2003; Nguyen et al., 2001; Takaoka et al., 2013). Activated STAT3 protein is considered as an anti-inflammatory factor, whose elevated level can lead to oncogenesis and therefore acts in an opposing way to STAT1 protein (Ho and Ivashkiv, 2006). However, in normal cell lines pSTAT1 is the most dominant and abundant effector protein in the nucleus after IFN-γ stimulation, while STAT3 is activated very weakly (Majoros et al., 2017). On the other hand, the alternative phosphorylation of STAT1 (on Serine 727), leading to the creation of pS727-

STAT1, causes an increase in the transcriptional activity of STAT1 molecules (Qing and Stark, 2004). This modification, however, does not influence the DNA binding or nuclear translocation processes (Decker and Kovarik, 2000). This data suggests that Serine 727 phosphorylation is important, but not crucial for the proper functioning of activated STAT1 molecules. Studying both modifications (that is, phosphorylation of Tyrosine 701 and Serine 727) simultaneously in the same cell would be of a great asset when focusing on gene transcription activation after IFN-γ stimulation. However, when focusing on the phosphorylated protein nuclear translocation, Tyrosine 701 phosphorylated STAT1 (pSTAT1) protein molecules is a main indicator of IFN-γ caused modification of STAT1 protein. It is worth noticing, that STAT1 can be subjected to many other posttranslational modifications, like acetylation, sumoylation, or ADP-ribosylation (adenosine diphosphate ribosylation), which are likely to change the conformation, functions and kinetics of STAT1 molecules (Begitt et al., 2018; Iwata et al., 2016; Krämer et al., 2006; Zimnik et al., 2008) All these changes probably contribute to the final outcome of IFN-γ signaling and therefore also contribute to some extent to the observed heterogeneity. However, all listed changes, as of now, are considered less frequent and less crucial than the phosphorylation of Tyrosine 701.

The molecular details of the IFN-γ signaling pathway show the amount of research done on that biological model, indicating that the basic molecular mechanisms have been at least partially established. At the same time, IFN-γ receptor (IFNGR) can be found in the membrane of a broad range of different cell types including immune system cells as well as epithelial and fibroblast cells of human and mouse tissues (Lee et al., 2013; Valente et al., 1992), justifying the use of easy-to-handle cell lines in the study. Moreover, IFN-γ is secreted exclusively by the immune cells like antigen-presenting cells, T-cells, or Natural Killers cells. These exclude the potential of the unwanted paracrine or autocrine signaling, when, e.g., fibroblast cells are used.

All the above make the IFN-γ signaling pathway suitable for studying the sources of heterogeneity in immune responses.

### 2.10.3. Oncostatin M pathway

Similarly to IFN-γ, oncostatin M (OSM) is a cytokine involved in many immune-related processes. OSM was originally named after its ability to inhibit the proliferation of cancer cells (Zarling et al., 1986), but nowadays was shown to be involved in multiple biological processes like hematopoiesis, lipid metabolism, tissue remodeling, neuroprotection, inflammation and cancer development (Tanaka and Miyahima, 2003). Enhanced responsiveness to OSM was shown for some cancer types (Caffarel and Coleman, 2014; West et al., 2012), while others showed the decrease of OSM signaling strength (Kim et al., 2009; Lacreusette et al., 2007), proving the need for further research, especially in cancers (Masjedi et al., 2020).

### 2.10.4.Molecular mechanism of the oncostatin M pathway

OSM signaling occurs through two types of receptors: type I, composed of glycoprotein 130 (gp130) and leukemia inhibitory factor receptor (LIFR) units, and type II, composed of gp130 and OSM receptor (OSMR) units. In humans both receptor complexes are active and can downstream process the signal of OSM, while in mouse OSM binds with high affinity only to type II receptors (Hermanns, 2015) (Figure 2.14). After OSM binding, the JAK kinases (JAK1 and JAK2), associated with cytoplasmic domains of the receptors (Hermanns et al., 1999), start to phosphorylate STAT proteins, mainly STAT3 at Tyosine 705 (pSTAT3) which in turn homo- or heterodimerize and translocate to the nucleus for regulation of transcription (Morris et al., 2018; Okada et al., 2018). Similarly to IFN-γ, the level of pSTAT3 molecules can be considered as the simple output after the OSM stimulation. pSTAT3 in the nucleus is a substrate of dephosphorylation by the nuclear TC45, what in turn leads to STAT3 export to the cytoplasm, where it can be re-activated (Herrmann et al., 2007; Hoeve et al., 2002).

However, the overall cross-wiring and inter-relatedness of OSM signaling is more complex compared to IFN-γ, which has to be taken into account during analysis of the results. In particular, OSM stimulation can also activate STAT5 and STAT1 transcription factors, depending on the receptor type engaged and cell type investigated (Auguste et al., 1997; Hintzen et al., 2008a). Moreover, OSM stimulation can activate not only JAK-STAT signaling pathways, but also extracellular signal-regulated kinases (ERK), c-Jun N-terminal kinase (JNK), MAPK, PKCδ and PI3K pathways, depending on the cell type and OSM concentration

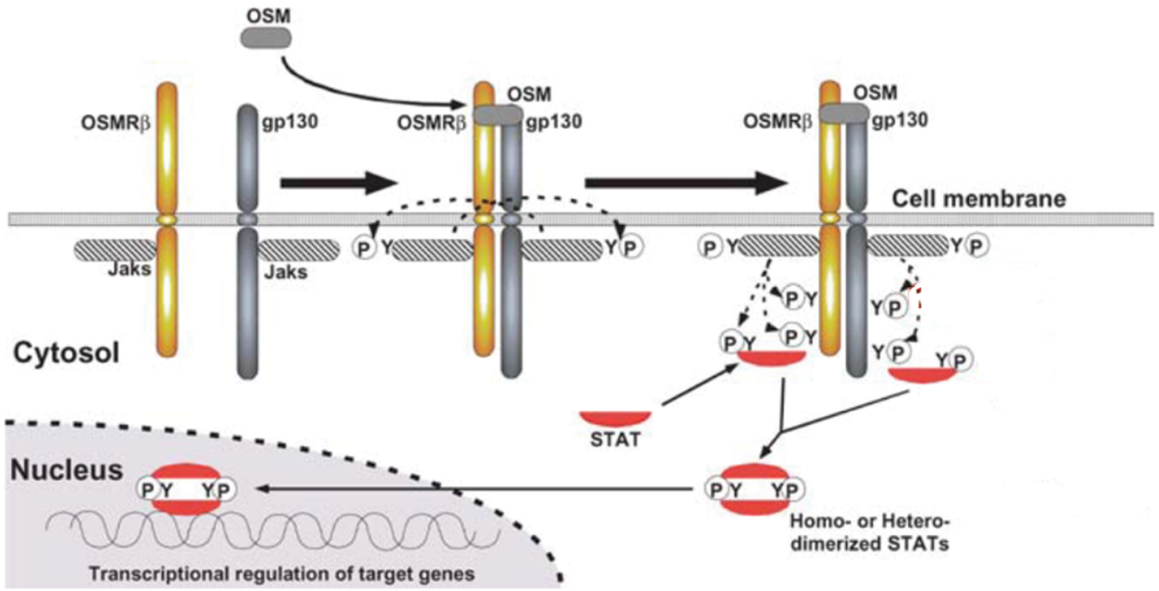


*Figure 2.14 OSM signaling pathway via the OSMR receptor*

When OSM molecules bind the OSMR and gp130 receptors, a cascade of phosphorylation occurs, involving various JAKs kinases, leading to phosphorylation and dimerization of transcription factors, mainly STAT3. Such activated STAT3 molecules translocate to the nucleus where they can activate the gene transcription. After the dephosphorylation, STAT3 exits the nucleus and can be re-activated. Modified from (Tanaka and Miyahima, 2003)

(Hermanns, 2015). However, JAK-STAT signaling pathways is considered as one of the most potent and canonical way of OSM signaling, with STAT3 as the main effector (Hermanns, 2015; Tanaka and Miyahima, 2003; Walker et al., 2016), especially in fibroblasts (Nagahama et al., 2013; Scaffidi et al., 2002).

The human type I and II receptors as well as mouse type II receptors, so all the active receptor types, are expressed in a broad range of human and mouse cell types, including fibroblasts (Consortium et al., 2014; Hermanns, 2015; Uhlén et al., 2015), justifying the use of common fibroblast cell lines in the research. Expression and secretion of OSM occurs exclusively in immune cells, including T cells, dendritic cells, neutrophils, with macrophages and monocytes as the primary source (Richards, 2013), excluding the paracrine or autocrine signaling of fibroblast cells, if used in the research (O'Hara et al., 2003; Scaffidi et al., 2002).

Taken together, both IFN-γ and OSM signaling pathways need more understanding of its dual-role, e.g., in cancer development and treatment as well as they constitute a suitable model for studying the cellular heterogeneity as they are experimentally easily controlled with single

input-single output. They also represent two distinct biological activities, with pSTAT1 acting as a pro-inflammatory and pSTAT3 as an anti-inflammatory agent, all important in, e.g., anti-cancer immune responses, making the research broader and more universal.

# 3. Aim and hypotheses

## 3.1. Aim

The aim of this dissertation is to identify sources of the cell-to-cell heterogeneity of cellular responses to cytokine stimulation in murine and human fibroblasts, with IFN-γ and OSM as model cytokines, both inducing JAK-STAT signaling pathway.

## 3.2. Hypotheses:

I. Phenotypic variability and not molecular noise accounts for most of the cell-to-cell heterogeneity in IFN-γ and OSM signaling responses.
II. Measurement error has a minor contribution to the observed level of immunofluorescence signals.
III. Nuclear state contributes to the cell-to-cell heterogeneity of the IFN-γ and OSM signaling responses.
IV. Intracellular levels of cytoplasmic and membrane signaling proteins partially predict the IFN-γ and OSM signaling responses.
V. Cells before and after DNA replication show a different level of responses in IFN-γ and OSM signaling

# 4. Materials and methods

## 4.1. Cell culture

Mouse embryonic fibroblasts were kindly provided by Prof. Alan Brasier (Brasier et al., 2011). These cells were previously used in several studies including (Brasier et al., 2011) and (Czerkies et al., 2018). Normal human fibroblasts, or BJ cells, were purchased from the American Type Culture Collection (ATCC, CRL-2522). MEF S1 KO (MEF S1 -/-) cells, being genetically depleted of STAT1 genes were kindly gifted by Prof. Max F. Perutz Laboratories, University of Vienna, Vienna, Austria. PC3 cells, being naturally depleted of STAT3 gene were kindly gifted by Małgorzata Milczarek, National Medicines Institute, Warsaw, Poland. All cells were cultured in full medium: Dulbecco's Modified Eagles Medium with 4.5 g/L D-glucose (#41965, Gibco), supplemented with 10% fetal bovine serum (FBS, #10500064, Gibco), 1% penicillin-streptomycin (#15140122, Gibco). BJ cells were additionally supplemented with 1% non-essential amino acids (#11140, Gibco). Cells were grown in a humidified incubator at 37$^{o}$C with 5% $CO_2$.

## 4.2. Cytokine stimulation and immunofluorescence for microscopy imaging

For cytokine stimulation and immunofluorescence cells were plated in 96-well microplates with $\mu$Clear® flat bottom (Greiner, #655090) at densities 7500 and 3000 cells per well for MEF and BJ, respectively. After 24 h, cells were subjected to 5 min pulse stimulation of either recombinant mouse interferon gamma (IFN-*γ,* #PHC4034, ThermoFisher) or recombinant human oncostatin M (OSM, #300-10T, PeproTech). Each of the cytokines was diluted down to indicated concentrations in full medium collected from cell cultures grown for 24h (conditioned medium). After 5 min, cytokine solutions were replaced with the same volume of conditioned medium. Cells were fixed by 10 min incubation with 3.7% paraformaldehyde (PFA, #P6148, Sigma Aldrich) at indicated time points after stimulation, permeabilized in 100% methanol at -20$^{o}$C for 20 min, blocked for 1.5 h in 5% bovine serum albumin (BSA, #821006, Merck) solution containing 0.3% Triton X-100 (#T9284, Sigma Aldrich) at the room temperature and incubated overnight at 4$^{o}$C with primary antibodies: phospho-STAT1 (Tyr701) (p-STAT1, #9167, Cell Signaling) diluted 1:100, phospho-STAT3 (Tyr705) (p-STAT3, #9131, Cell Signaling) diluted 1:200, STAT1 (#610115, BD, or Becton, Dickinson and Company)

diluted 1:200 or STAT3 (#9139, Cell Signaling) diluted 1:200. The next day, cells were incubated with the secondary anti-rabbit IgG antibody conjugated with Alexa Fluor 488 (#A-21202; ThermoFisher) diluted 1:500 or anti-mouse IgG antibody conjugated with Alexa Fluor 555 (#A-21422; ThermoFisher). Both primary and secondary antibodies were diluted in 1% BSA 0.3% Triton X-100. Nuclei were counterstained using 2 $\mu$g/mL 4,6-diamidino-2-phenylindole (DAPI, #D9542, Sigma Aldrich).

## 4.3. Microscopy imaging and image analysis

Cells were visualized using the automated confocal microscope (Pathway 435, BD) with the UAPO/340 20x objective (0.75 NA; Olympus). Obtained images were flat-field corrected to compensate for unequal illumination. Further, background fluorescence was subtracted. CellProfiler (Carpenter et al., 2006), custom scripts written in R and ImageJ as well as the automated platform for image analysis IPIQA, developed by Karol Nienałtowski and Agnieszka Gromadka in our Team were used for image segmentation and quantification. To quantify responses of individual nuclei, the average fluorescence of nuclear pixels was measured first. Then, the background-corrected nuclear fluorescence of each nucleus was divided by the average of non-stimulated cells' nuclei fluorescence to obtain relative fluorescence reported in the figures.

## 4.4. Fusion of cells

### 4.4.1. Preparation of syncytia

Both MEF and BJ cells were subjected to the same polyethylene glycol (PEG)-mediated fusion to create double-stained syncytia composed of one cytoplasm and two nuclei. To accurately identify fused cells, cells were subjected to the whole-cell staining using two types of CellTrace (ThermoFisher) fluorescent dye: either CellTrace Yellow (#C34573; 555/580 excitation/emission maxima) or CellTrace Far Red (#C34572; 630/661 excitation/emmision maxima). After the fusion, only cells fluorescent in both CellTrace channels were considered as fused. In detail, cells were first trypsinized, counted, divided into two equal populations, and stained with one of the CellTrace dyes according to the manufacturer's instructions. Two single-color populations of cells were then mixed 1:1 and 7.5 mln were seeded onto the 10 cm dish plate and kept in the culture incubator. After one hour, cells were washed with pure

DMEM (Dulbecco's Modified Eagle Medium) and fused by slowly adding 1.5 ml of 50 % (m/v) polyethylene glycol (PEG 1500, #86101-250G-F, Sigma Aldrich) resuspended in fresh FBS-free DMEM. Cells were kept in PEG for 2 min in total. The PEG solution was then aspirated and 10 ml of fresh DMEM was slowly added and the dish plate with the cells was then placed in the incubator for the 30 min since the beginning of PEG adding and the fusion procedure was repeated up to 2 times in total. After that, DMEM was replaced by the full medium and cells were kept in the incubator for the next two hours. Finally, cells were seeded onto the 96-well imaging plate (Greiner) and kept 18 h until the stimulation and immunofluorescence procedure began. The fraction of fused cells reached around 4% of the whole population. Immunofluorescence procedure was the same as with single cells, but additional images related to whole-cell staining dyes were captured during image acquisition.

### 4.4.2. Identification of properly fused bi-nuclear syncytia

To properly assign two nuclei to one cytoplasm of a syncytium based on microscopy images, the whole-cell dye was needed in addition to nuclei dye. Unfortunately, fibroblasts often create dense cellular colonies, which hinders the segmentation of individual cells due to close proximity of cell boundaries. This can lead to the error of assigning two nuclei from separate cells as coming from the two unfused single cells. Therefore, to correctly identify cells which have undergone a fusion, two dyes for whole cell identification were used. In this way, only cells with cytoplasm stained with both dyes were considered as properly fused. Such syncytia were automatically identified in microscopic images, based on the signal in both images of whole-cell staining dyes. Next, such automatically marked syncytia were manually inspected, syncytia only with two nuclei were kept and those two nuclei were manually segmented. Finally, the manually marked nuclei together with parent cytoplasm were automatically quantified in terms of fluorescence intensity in all fluorescent channels. CellProfiler and custom scripts written in R and ImageJ were used for image segmentation and quantification (Carpenter et al., 2006). Data analysis, background subtraction and signal normalization were done the same way as for single cells. In addition, bi-nuclear syncytia with merged nuclei were excluded from analysis based on the manually adjusted threshold (see Figure 5.7).

## 4.5. Flow cytometry measurements

For flow cytometry experiments, MEF cells were plated in 6-well plates (353046, Becton Dickinson, BD) at density 1 mln/well, whereas BJ cells in 10 cm dish (#353003, Falcon) at density 1 mln/dish. After 24h MEF and BJ cells were exposed to a 5-minute pulse of the indicated dose of IFN-γ and OSM, respectively, similarly as for microscopy imaging. Cells were then trypsinized, centrifuged (150 x g for 5 min) and fixed by 10 min incubation with 3.7% PFA (#P6148, Sigma Aldrich) after 15 minutes of IFN-γ stimulation or 30 minutes after OSM stimulation. Next, the samples were washed in 2% FBS in PBS, permeabilized in 100% methanol at -20$^{o}$C for 20 min, washed in 2% FBS in PBS and blocked for 0.5 h in 2% FBS in PBS in room temperature. Cells were then incubated with a mixture of primary antibodies against 3 antigens in the following way. MEF cells were incubated for 1h in room temperature with antibodies against: phospho-STAT1 (Tyr701) (pY-STAT1, #9167, Cell Signaling) diluted 1:100, STAT1 (#610115, BD) diluted 1:200 and for 15 min with primary antibodies against IFNGR1-PE (PE-Phycoerythrin; 12-1191-82, eBioscience) diluted 1:200. BJ cells were incubated for 1 h in room temperature with antibodies against: phospho-STAT3 (Tyr705) (pYSTAT3, #9131, Cell Signaling) diluted 1:200, STAT3 (#9139, Cell Signaling) diluted 1:200 and OSMR-PE (#12-1303-42-PE, ThermoFisher) diluted 1:500. To show specificness of receptor antibodies, I used isotype control antibodies in the same concentration as antigen antibodies: for IFNGR1: normal mouse IgG-PE (#12-4888-81, eBioscience); for OSMR-PE: Mouse IgG1 kappa Isotype Control (#12-4714-81, ThermoFisher). To show specificness of anti-STAT1 and anti-pSTAT1 antibodies, I used MEF S1 KO cells, while to show specificness of anti-STAT3 antibody and anti-pSTAT3 antibody I used PC3 cells. Then, cells were centrifuged and incubated for 30 min in room temperature with the secondary antibodies conjugated either with Alexa Fluor 488 (anti-rabbit, #A-21202; ThermoFisher) diluted 1:500 or Alexa Fluor 647 (anti-mouse, #A-21235; ThermoFisher) diluted 1:500. Both primary and secondary antibodies were diluted in 2% FBS in PBS. Therefore, the pSTAT levels were measured in Alexa Fluor 488 fluorescent channel, receptors in the PE channel and STAT levels in Alexa Fluor 647 channel. Finally, cellular fluorescence was measured at the Laboratory of Cytometry, Nencki Institute of Experimental Biology, Polish Academy of Sciences using the BD FACSAriaII flow cytometer with each sample suspended in a PBS buffer supplemented with 2% FBS. Debris exclusion,

compensation on single-stained samples and cell doublet discrimination were done in FlowJo 10.7.1.

## 4.6. Phosphatase inhibition

Sodium orthovanadate $Na_2VO_4$ (#450243, Sigma Aldrich) was dissolved in $H_2O$ up to 100 mM, filter sterilized, aliquoted and kept in +4°C until used. Cells were incubated 1 h with 1 mM vanadate before cytokine stimulation. Cytokine stimulation was performed similar to previous experiments, but in the medium with 1 mM vanadate to assure constant block of the phosphatases.

*Table 1. List of primary and secondary antibodies used during the studies*

| Antigen | host | dilution | manufacturer | cat. number |
|---|---|---|---|---|
| primary antibodies | | | | |
| pSTAT1 | rabbit | 1:100 | Cell Signaling | 9167 |
| pSTAT3 | rabbit | 1:200 | Cell Signaling | 9131 |
| STAT1 | mouse | 1:200 | BD | 610115 |
| STAT3 | mouse | 1:200 | Cell Signaling | 9139 |
| IFNGR1 | hamster | 1:200 | eBioscience | 12-1191-82 |
| OSMR | mouse | 1:500 | ThermoFisher | 12-1303-42-PE |
| isotype | hamster | 1:200 | eBioscience | 12-4888-81 |
| isotype | mouse | 1:250 | ThermoFisher | 12-4714-81 |
| cyclin B | mouse | 1:200 | Cell Signaling | 4138 |
| β-actin | rat | 1:200 | BioLegend | 664802 |
| secondary antibodies | | | | |
| rabbit IgG (Alexa Fluor 488) | donkey | 1:500 | ThermoFisher | A-21202 |
| mouse IgG (Alexa Fluor 555) | donkey | 1:500 | ThermoFisher | A-21422 |
| mouse IgG (Alexa Fluor 647) | donkey | 1:500 | ThermoFisher | A-21235 |

## 4.7. DNA microscopic measurements

To measure the DNA content in individual cells during the microscopy measurements, I adopted the methodology from (Roukos et al., 2015). In detail, I used similar nuclei staining as in Methods 4.2, but during image acquisition, in addition to confocal mode, I imaged the cells in the DAPI channel in epi-fluorescence mode. Then, during image analysis in CellProfiler I adopt the analysis accordingly to obtain the information of both the cell cycle phase and the level of protein of interest in each individual cell. For cellular measurement of STAT1 and cyclin B (#4138, Cell Signaling, 1:200), I immunostained the whole cell with β-actin antibody (664802, BioLegend, 1:200), to outline the cellular boundaries. Images of quantized protein (pSTATs and cyclin B) as well as β-actin were acquired in a confocal mode.

## 4.8. Calculation of the overlaps between response distributions

For calculation of the overlaps between distributions corresponding to different doses of a given cytokine (e.g., in Figure 5.4) the following strategy was used. For each dose a kernel density estimation was performed. Then the range of all observed responses was divided into four intervals such that responses in one interval are most likely for one specific dose according to estimated densities of. Subsequently, for each estimated distribution, its fraction of probability in each interval was calculated by numerical integration and presented as pie-charts. For calculation of the overlaps in Figure 5.11E, F, a similar strategy was used. However, instead of density estimates, Gamma density with mean given by response curves corresponding to different percentiles and standard deviation equal to 11% of the mean was used.

## 4.9. Simulation of response distributions with the assumed noise strength

For simulation of response distributions with the assumed noise strength the following strategy was used. I considered response curves corresponding to every percentile from 0.05 to 0.95, similarly to the curves shown for 0.05, 0.5, 0.95 percentiles in Figure 5.11C, D. For every curve, I calculated response distributions corresponding to every dose. The mean was assumed to be equal to the value of the dose-response curve. The standard deviation was assumed to be equal to ~0.11 of the mean, for both IFN-*γ* and OSM responses. Also, I assumed

the responses to have gamma distribution. The use of normal or log-normal distributions gives nearly identical results. Next, I calculated overlaps between these distributions according to maximum likelihood decoding. Quantified overlaps were averaged over all percentiles.

## 4.10. Statistical hypothesis testing, statistical analysis and data presentation

All statistics, statistical hypothesis testing, data processing and data presentation were done using custom scripts in R. The details of statistical tests for hypothesis testing are provided for each use. The percent of variance explained was calculated as the coefficient of determination ($R^2$) of linear regression. Linear regression was done by least squares.

## 4.11. Technical and biological replicates

All experiments were performed in at least two technical replicates per experiment and presented as one representative of at least three biological replicates, unless stated otherwise.

## 4.12. Linguistic disclaimer

In the presented dissertation, the majority of results are described in the first-person perspective, predominantly in the active voice structure, e.g., “I performed the staining…” etc. In the opinion of the author, or in my opinion, such an approach is clearer, makes it easy to follow the story as well as engage the reader more, compared to the passive voice description. This opinion is shared worldwide in the scientific journal editorial boards (Nature). At the same time, I am aware of the disadvantages of such an approach, mainly the false belief that the whole study was planned, performed, discussed, improved and re-performed on my own, without any help from my teammates. Therefore, I would like to admit that the study presented in the dissertation was indeed planned and performed by me, but with great help of my supervisors, teammates, colleagues, students, scientists met throughout the studies as well as reviewers and editors of the published articles and alumni of the Systems Biology of Signaling group, which all not only improved my research, but often made it possible to perform.

# 5. Results

## 5.1.IFN-γ pathway in MEF cells and OSM pathway in BJ cells

To analyze precision of single-cell signaling and what contributes to the cell-to-cell heterogeneity of cellular signaling I used two signaling pathways: IFN-γ and OSM. To provide more general conclusions I utilized cell lines from two mammalian species: mouse embryonic fibroblasts (MEF cells) and human BJ fibroblasts (BJ cells). However, to limit the experimental complexity, the IFN-γ pathway was investigated in MEF cells while the OSM pathway in BJ cells. Firstly, before proceeding with the exact investigation of sources of cell-to-cell heterogeneity of cellular signaling, I verified the usefulness of the biological model, so I investigated the responsiveness of the cells to given stimulation.

### 5.1.1. MEF and BJ cells are responsive to cytokine stimulation

One of the main molecular effects of IFN-γ stimulation is the nuclear accumulation of STAT1, while for OSM stimulation it is the nuclear accumulation of STAT3. Therefore, to confirm the responsiveness of investigated cell lines to given cytokine stimulation I performed the fixed-cell immunofluorescence of the nuclear levels of STAT1 or STAT3 proteins together with confocal imaging. Cells were pulse-stimulated for 5 min with the high dose of the cytokine (10 ng/mL of IFN-γ and OSM, (Gough et al., 2014; Meyer et al., 2002)) and nuclear levels of total STAT1 after 30 min (Figure 5.1A) or total STAT3 after 30 min (Figure 5.1B) were visualized and quantified as the mean fluorescence of the nuclear area (Figure 5.1C, D, upper panels). To account for experiment-to-experiment differences, the STAT nuclear levels were normalized to the mean level of the control cells (relative nuclear STAT). The cells stimulated with the cytokine showed the increased level of STATs in the nuclei. The similar analysis performed on cells lacking the STAT1 (MEF S1 KO cells, Figure 5.1 C) or STAT3 (PC3 cells, Figure 5.1 D) showed no increase in STATs level after stimulation. All these confirm that the cytokine stimulation indeed causes the nuclear translocation of STATs and that this effect can be measured by the used methodology. However, the heterogeneity of cellular responses was very high, with distributions of control and stimulated cellular responses overlapping substantially, covering more than 20% of the range of stimulated cells.

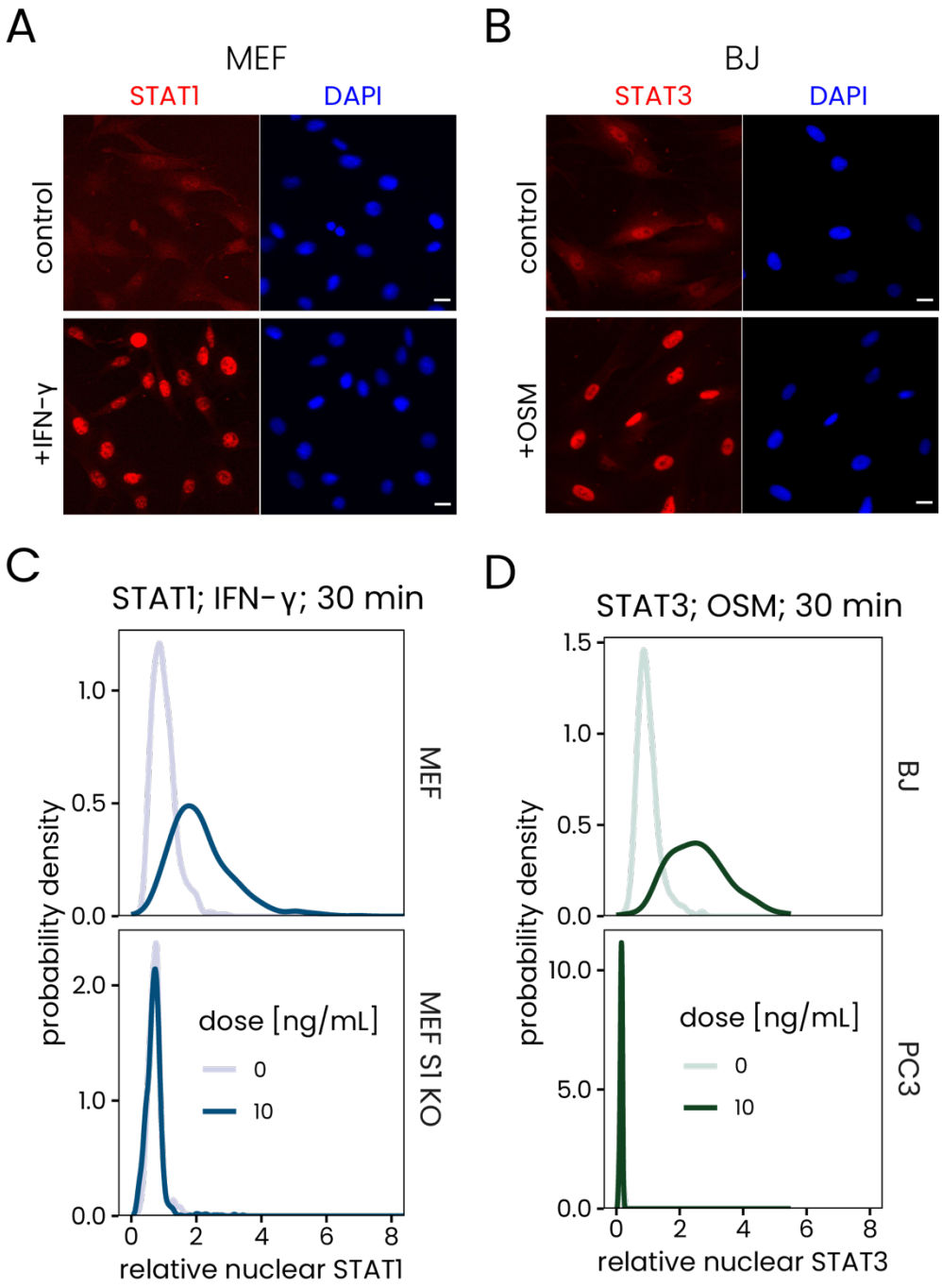


*Figure 5.1. Stimulation of MEF and BJ with cytokines caused the increase of nuclear STAT levels*

(A) MEF cells untreated (upper panel) or stimulated for 5 min with 10 ng/mL of IFN and immunostained against STAT1 (in red) after 30 min since the beginning of stimulation. Nuclei were counterstained by DAPI (in blue). Scale bars 20 um. (B) Same as A but for BJ cells stimulated with 10 ng/mL OSM and STAT3 immunostained after 30 min. (C) The quantification of mean nuclear STAT1 level in nuclei of MEF cells (upper panel) or MEF S1 KO cells (bottom panel) stimulated with indicated doses of IFN-γ for 5 min and immunostained after 30 since the beginning of stimulation. The STAT1 value was normalized to the mean level of the untreated cells ("related"). (D) Same as C, but for BJ (upper panel) or PC3 (bottom panel, a STAT3 KO model) cells stimulated with OSM and immunostained after 30 min since the beginning of stimulation. Please note the big overlaps between non-stimulated cells and 10 ng/mL-stimulated cells of bottom panels in C and D. For each condition at least 600 cells for C and 300 cells for D were analyzed.

To quantify the observed overlaps, the information theory can be used, with the R-package SLEMI facilitating the calculation of Shannon information based on experimental data (Jetka et al., 2019). The channel capacity in both IFN-γ and OSM cases were below 0.65 bits, indicating that the single cells cannot reliably distinguish even between absence of any dose and presence of the high dose of a cytokine. Therefore, the total level of STATs cannot be considered as the perfect information carrier, probably due to the already high basal level of STATs in the nucleus before stimulation (Figure 5.1A, B, upper panels), which was shown to reduce the dose discriminability in other signaling pathways (Frick et al., 2017; Lee et al., 2014). Fortunately, STAT molecules are abundantly tyrosine-phosphorylated (pSTATs) after cytokine stimulation, with little basal level of phospho-form before stimulation (Bachmann et al., 2014; Gough et al., 2014; Nagel et al., 2014). Therefore, instead of considering the total STAT levels in the nucleus as the response measure, pSTAT nuclear level can be used to more precisely represent the cellular response. In addition, it is considered that the tyrosine-phosphorylation of STATs regulate the DNA binding and nuclear translocation (Decker and Kovarik, 2000; Qing and Stark, 2004), justifying the choice of pSTAT levels as a more biologically relevant measure of the cellular response.

### 5.1.1. pSTATs are better outputs to cytokine stimulation than STATs

After confirming that the cells can properly react to the cytokine stimulation, I investigated whether the measurements of pSTAT nuclear levels instead of STAT levels would allow for better dose discrimination. Indeed, cells stimulated with high doses of the cytokines showed much higher responses compared to control cells (Figure 5.2A, B), allowing for almost perfect dose discrimination (0.87 bits for IFN-γ and 1bit for OSM). Therefore, the pSTAT1 nuclear level for IFN-γ and pSTAT3 for OSM are the outputs bearing more information about the stimulation than STAT levels. From now on in this dissertation, unless clearly stated, the cellular response to cytokine stimulation will be considered as either pSTAT1 (for IFN-γ) or pSTAT3 (for OSM) mean nuclear level (see material and methods for more details regarding quantification of the signal).

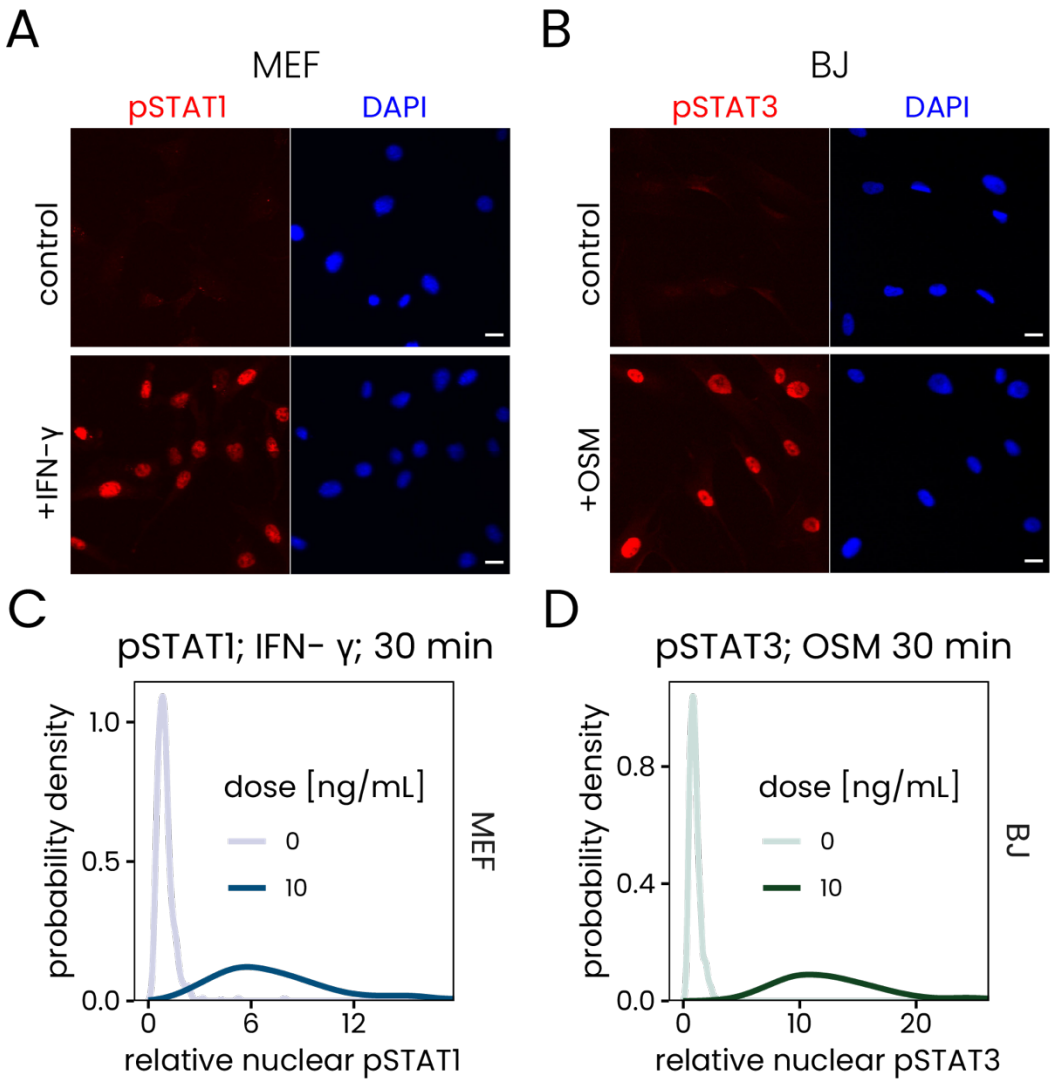


*Figure 5.2. pSTAT nuclear levels precisely discriminate between presence and absence of cytokine stimulation*

(A) MEF cells untreated (upper panel) or stimulated for 5 min with 10 ng/mL of IFN and immunostained against pSTAT1 (in red) after 30 min since the beginning of stimulation. Nuclei were counterstained by DAPI (in blue). Scale bars 20 um. (B) Same as A but for BJ cells stimulated with 10 ng/mL OSM and pSTAT3 immunostained after 30 min. (C) The quantification of nuclear pSTAT1 level in nuclei of MEF cells stimulated with indicated doses of IFN-γ for 5 min and immunostained after 15 since the beginning of stimulation. The pSTAT1 value was normalized to the mean level of the untreated cells ("relative"). At least 500 cells per dose are shown (N≥500). (D) Same as C, but for BJ cells stimulated with OSM and immunostained after 30 min since the beginning of stimulation. At least 150 cells per dose are shown (N≥150)

The heterogeneity of such cellular responses was high, with some cells responding dozen times stronger than others, questioning the possibility of further dose discrimination. Therefore, more detailed studies with more doses were needed. However, to apply the multiple dose analysis and proceed with quantification of dose discrimination, the optimal time of stimulation should be chosen for each of the cytokine. This would assure the most prominent differences between control and stimulated cells and therefore more reliable conclusions of the limits of information flow in the investigated signaling pathway.

### 5.1.2. Temporal dynamics of cytokine responses

Nuclear accumulation of pSTATs after IFN-γ and OSM stimulation usually start to decline after minutes to hours in a population of single cells (Hintzen et al., 2008b; Majoros et al., 2016; Miyawaki et al., 2019; Sarközi et al., 2011), indicating that there must be the time point with the maximum level of pSTAT in the nucleus after which the level only decreases. To find such a time point of the maximum response I performed the cytokine response measurements over multiple time points ranging from 0 to 90 min, for both IFN- γ (Figure 5.3A) and OSM (Figure 5.3B). The time point of maximum response for IFN-γ stimulation was 15 min since the beginning of stimulation. For OSM the responses at 15 min and 30 min were similarly high, with slightly higher values at 30 min. Therefore, for further analyses and experiments, the time of maximum responses for IFN-γ were considered as 15 min and for OSM- 30 min. Therefore, the established method of cellular response measurement together with properly responding cells allowed to start the investigation on the signaling pathway precision on the single cell level.

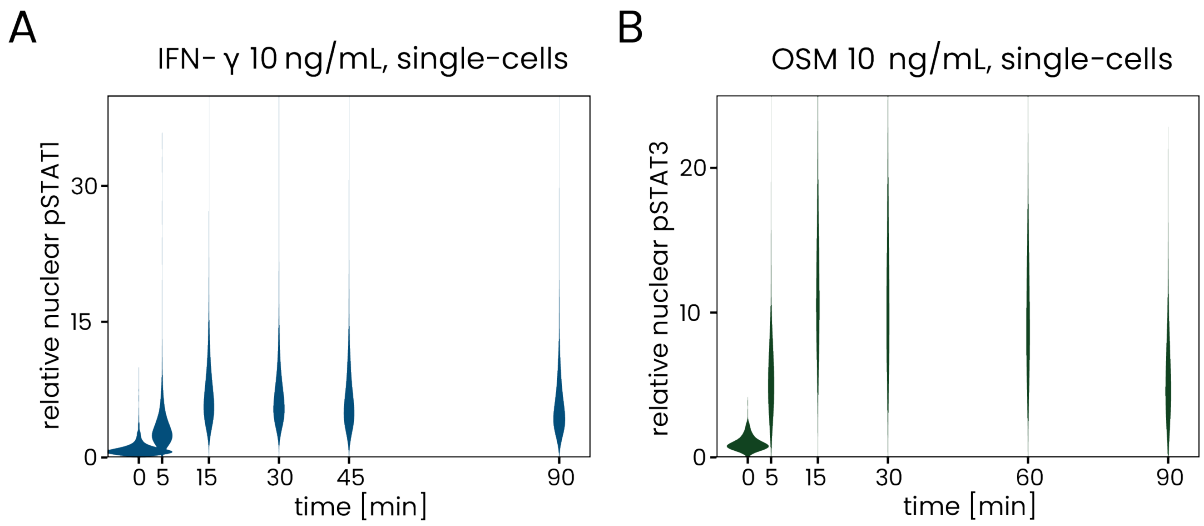


*Figure 5.3. Distributions of responses to IFN-γ or OSM over time.*

(A) Distributions of MEF single-cell responses (γ-axis) to 10 ng/mL of IFN-γ over time (x-axis) presented in the form of the violin plots. The width of the "violin" corresponds to the probability of the given response level to arise in the population of single-cells. Each violin has the same area. The plot jointly presents two technical replicates of one, out of two, biological replicates. At least 2000 cells per dose are shown (N≥2000). (B) As in A but for BJ cells stimulated with 10 ng/mL of OSM. At least 150 cells per dose are shown (N≥150)

## 5.2. Phenotypic variability vs molecular noise

The decomposition of the phenotypic variability vs molecular noise of cellular signaling is challenging and no universal approach for it has been established. I used bi-nuclear syncytia model to quantify the contribution of both phenotypic variability and molecular noise in total cell-to-cell variability of the JAK-STAT signaling after cytokine stimulation. First, I quantified the level of cell-to-cell heterogeneity of signaling pathway responses. Next, I established and prepared the bi-nuclear syncytia which I used to decompose the two main sources of heterogeneity. Finally, I approximated the single-cell responses with the neglected influence of the molecular phenotype allowing for the assessment of the true single cell precision to dose discrimination.

### 5.2.1. Distributions of single-cell dose responses to IFN-γ and OSM exhibit substantial overlaps

The single cell response distributions of cells stimulated with one dose showed almost perfect discrimination between absence and presence of the cytokine (Figure 5.2). To perform more comprehensive analysis allowing for more precise assessment of information flow, I measured the responses to multiple doses at the time of maximal response for both cytokines. Specifically, I stimulated the cells with 5 min pulses of three doses, 0.1, 1, and 10 ng/mL, of either of the two cytokines and measured the responses after 15 min for IFN-γ (Figure 5.4A) or after 30 min for OSM (Figure 5.4B). The responses are marked with substantial cell-to-cell heterogeneity, with significant overlaps between responses to different doses, which is in line with previous studies on cytokine signaling (see Literature review 2.4). In other words, the same response can be evoked by multiple doses of the stimulant. On the other hand, it could be expected that a coordinated immune response requires high fidelity signaling at the single-cell level. If the cell-to-cell heterogeneity was the result of molecular noise, the two above statements would be difficult to reconcile. Before addressing this seeming contradiction in more detail, I inspected the overlaps between response distributions qualitatively, using the methodology called fractional response analysis, FRA (Nienałtowski et al., 2021).

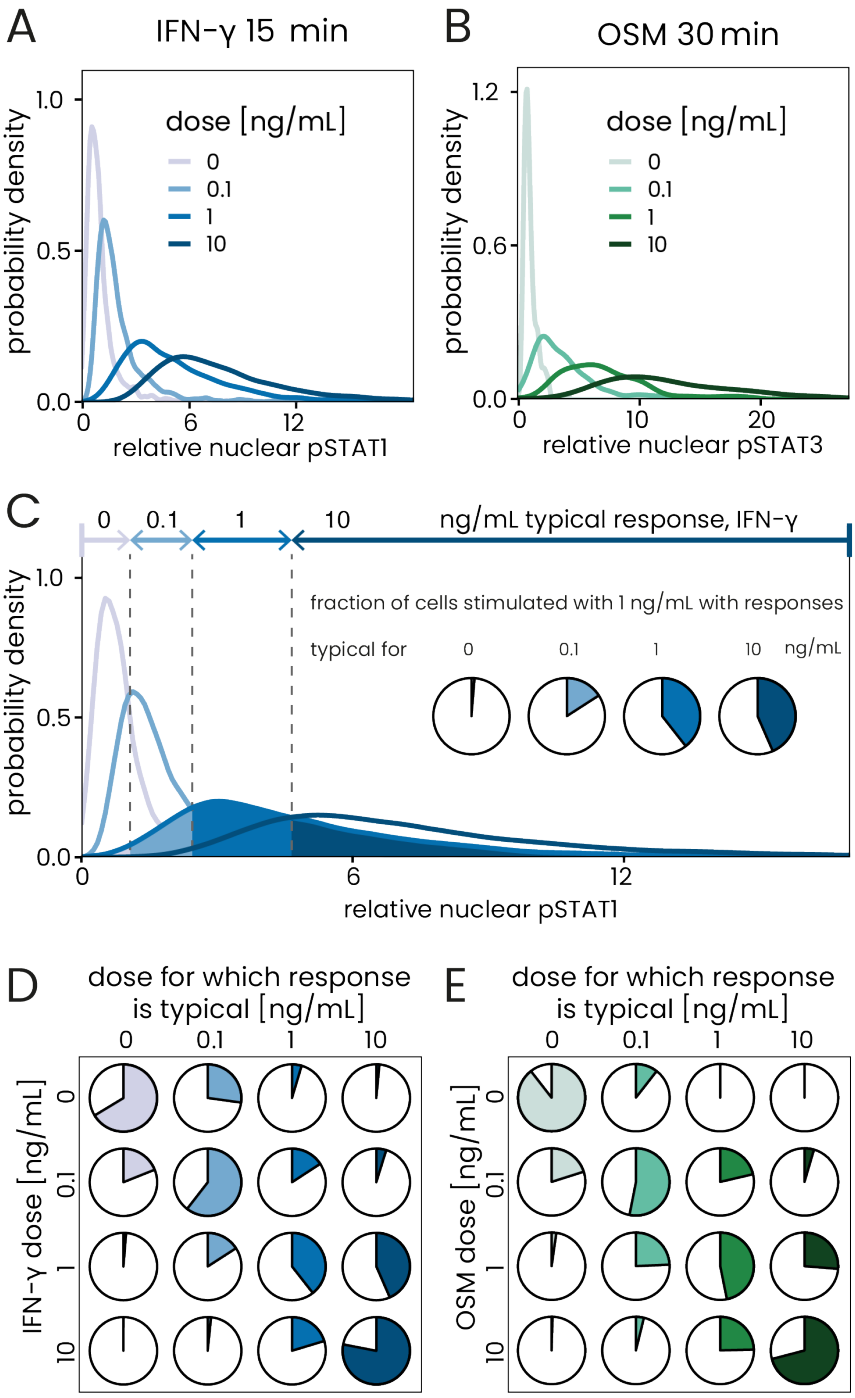


*Figure 5.4. Cell-to-cell heterogeneity of single-cell dose-responses to IFN-γ and OSM.*

(A) Distributions of responses (phosphorylated STAT1) at 15 minutes after different doses of IFN-γ in MEF cells. Probability density (γ-axis) is proportional to the frequency of cells with a given response. (B) Same as in A but for OSM responses (pSTAT3) at 30 minutes after stimulation of BJ cells. (C) Quantification of the overlaps between distributions corresponding to different doses of IFN-γ. Responses to 1 ng/mL are dissected into fractions typical to any of the doses and represented as pie-charts. (D) Quantification of the overlaps between IFN-γ response distributions presented in A. (E) Quantification of the overlaps between OSM response distributions presented in B.
Distributions consisting of the sum of two technical replicates are shown in A and B. In A, between 2217 and 2485 cells were used to estimate each response distribution, whereas in B it was between 208 and 220 cells. Differences in cell counts result from cell-specific growth characteristics required for sub-confluency and reliable microscopy imaging. Responses at other time- points are shown in Figure 5.5.

Suppose one divides a range of all responses into smaller parts in which responses to one dose are more likely than for other doses (IFN-γ response distribution, Figure 5.4C). The responses that are most likely to a given dose can be called typical for this dose. Further, the fraction of cells responding typically for the same dose and typically for the other doses can be calculated for each stimulated dose. Upon stimulation with 1 ng/mL IFN-γ, 16% of cells have responses typical for 0.1 ng/mL, 39% typical for 1 ng/mL, and 43% typical for 10 ng/mL (Figure 5.4C). This dissection can be presented in the form of the matrix, known as confusion matrix in statistics, which then can be transformed into the pie-charts (Figure 5.4D, E). The matrix quantifies the overlaps between response distributions. It shows what fraction of cells stimulated with a given dose (rows) has responses most likely to arise for either of the doses (columns). In particular, the diagonal shows what fractions of cells have responses most likely, or typical, for the dose they were exposed to. Off-diagonal elements show what fractions of cells have responses typical for the dose other than the administered one. Compared to channel capacity, this approach gives a more comprehensive view on the cell-to-cell heterogeneity in cellular responses to multiple doses of the stimulant and is not dependent on the input distribution (Nienałtowski et al., 2021). Furthermore, the FRA does not implicitly assume, contrary to channel capacity, that the whole cell-to-cell heterogeneity results from noise, either intrinsic or extrinsic, both leading to the information loss. The pie charts can help to assess the probability of a single cell to decode the dose correctly. Specifically, if we assume that the cellular response depends only on the molecular noise, then the pie charts show the probabilities that a cell stimulated with one dose (rows) will decode the signal as another dose (columns). The diagonal elements show the probabilities of correct decoding. Off-diagonal elements show probabilities of confusing one concentration (rows) with another (columns). Therefore, using this interpretation, the probability of correct decoding is at best 78%, for 10 ng/mL IFN-γ, and 89% for 0 ng/mL OSM. Besides, due to stochasticity of cellular processes, $\sim$20% of cells confuse 0.1 ng/mL of the cytokine with its absence. In addition, the similar approach gave similar results at not-optimal time after stimulations (Figure 5.5). Even though it appears rather unlikely that cells could function reliably with such noisy sensing apparatus, the knowledge about the contribution of molecular noise and cellular phenotype is still limited (see Literature review 2.8).

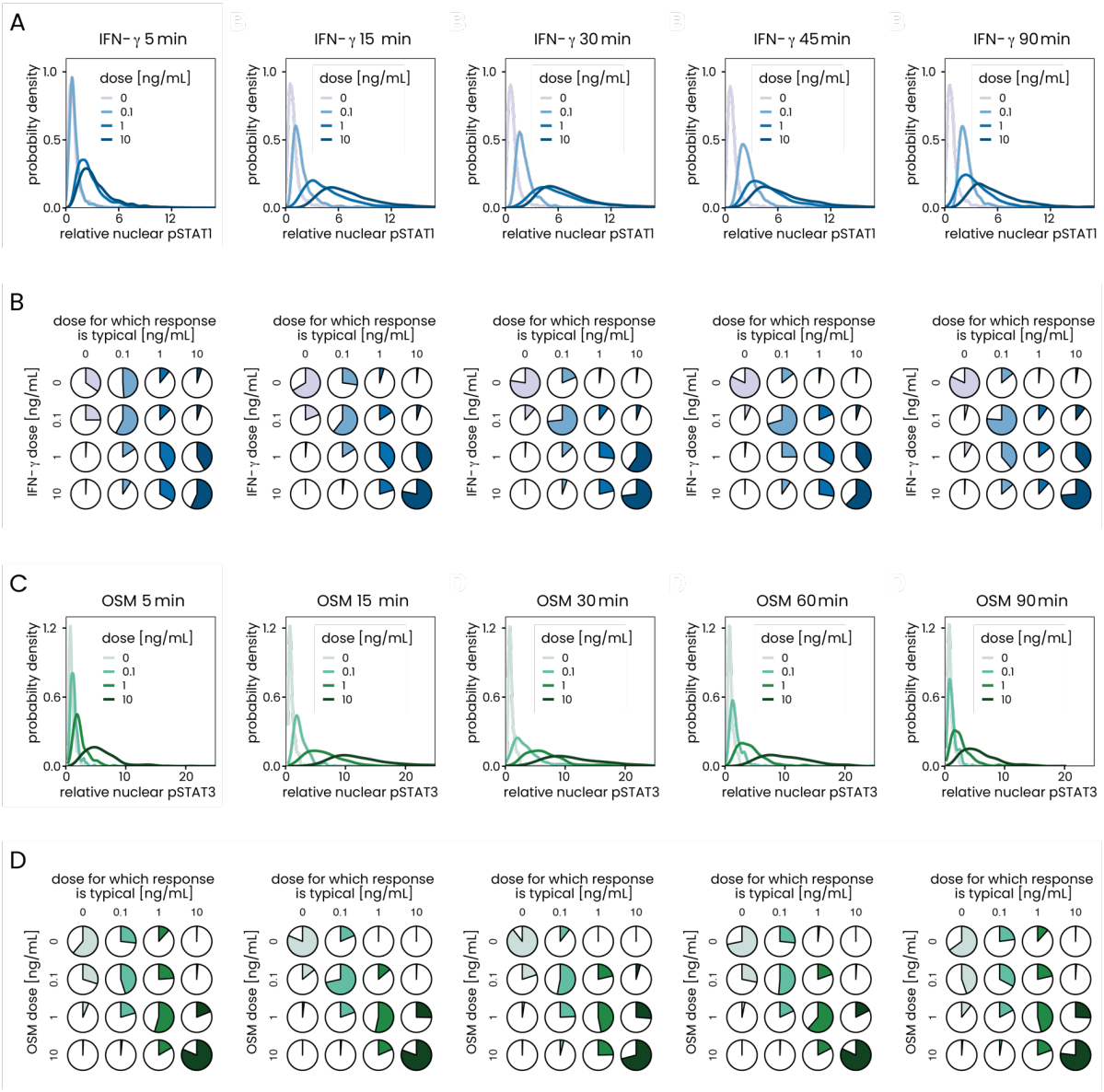


*Figure 5.5. Cell-to-cell heterogeneity of single-cell dose-responses to IFN-γ and OSM at optimal and sub-optimal time-points.*

(A) Distributions of responses at indicated time-points (from 5 to 90 minutes) after stimulation with different doses of IFN-γ, similarly to Figure 5.4A. At least 1100 cells per dose per time- point are shown (N≥1100). Panel of 15 min is repeated from Figure 5.4A (B) Quantification of the overlaps between IFN-γ responses at different time-points shown in A. Quantification was performed as shown in Fig. 1C. (C) Same as in A but for OSM responses. At least 150 cells per dose per time-point are shown (N≥150). Panel of 30 min is repeated from Figure 5.4B. (D) Same as B but for OSM stimulation. At least 150 cells per dose per time-point are shown (N≥150).

In addition to the above heterogeneity quantification, the calculation of channel capacity can be made, as it is the broadly accepted measure of signaling pathway ability to resolve stimulation doses (see Literature review 2.5). Specifically, I used SLEMI R-package (Jetka et al., 2019) to estimate the channel capacity for both IFN-γ and OSM data presented in the Figure 5.4A, B. For IFN-γ, the channel capacity reached 0.78 bits, while 1.02 bits for OSM, allowing

for discrimination of only around 2 doses out of 4 possible. Both results, that is the low probability of correct decoding of doses presented in the pie-charts as well as low channel capacity of each signaling pathway confirm high cell-to-cell heterogeneity of cellular responses to both IFN-γ and OSM. In order to validate to what extent, the cell-to-cell heterogeneity results from molecular noise vs. from cellular phenotype, I used the bi-nuclear syncytia, with two nuclei and one shared cytoplasm, which imitate the two identical cells.

### 5.2.2. Bi-nuclear syncytia as a model approximating the two cells with identical molecular phenotype

The sources of the observed heterogeneity are not fully understood and need further investigation. Especially, it is to be confirmed, to what extent the response of a single cell is governed by the cellular phenotype and to what extent by the molecular noise. Multiple studies have postulated that the potential to discriminate signal doses by single cells is very limited (see Literature review 2.4), which is hard to reconcile with the well-regulated functioning of the whole organism, especially in immune response. Whether the low dose discriminability comes from stochasticity of biochemical reactions or from differences between cellular phenotypes has been estimated only for specific, fast-acting signaling pathways or via indirect methods (see Literature review 2.8). In other words, more universal and direct methods of quantification of how precise a single cell is in signal sensing is of special interest. To do that, I utilized the bi-nuclear syncytia system, resembling in the basics the dual-color experiments as well as imitating the two-identical-cells set up. I fused two cells of the same type, creating a syncytium with two nuclei and one, shared cytoplasm (Figure 5.6A). For proper cell identification I used two non-specific protein dyes which stain the whole cell. After the fusion, only cells with signals of both dyes were considered as fused (Figure 5.6B, C). The two nuclei shared the cellular membrane and cytoplasmic content, so the signaling outcome in each of nucleus can be approximated as the outcome of the two cells with the same molecular phenotype. Therefore, after the cytokine stimulation, any differences between responses of the both nuclei can be attributed to molecular noise and not differences in cellular phenotypes. The principle of the proposed approach is analogous to the two-color experiment used to dissect gene expression noise into intrinsic and extrinsic components (see Literature review 2.8.5). Here, however, as opposed to the expression level of two genes in

the same cell, the signaling responses in two nuclei of the syncytium are measured. It is to be determined in the future, to what extent the assumed biological model of bi-nuclear syncytia represents reality and reflects the two-identical cells setup. The technical details of bi-nuclear formation and identification are described in Methods 4.4. However, as the obtained syncytia would next be used for comparing the responses in two nuclei, one can argue that process like establishment of a physical connection could lead to sharing of nuclear content between nuclei in a syncytium and, in turn, averaging of signaling responses between nuclei. Therefore, it had to be accounted for.

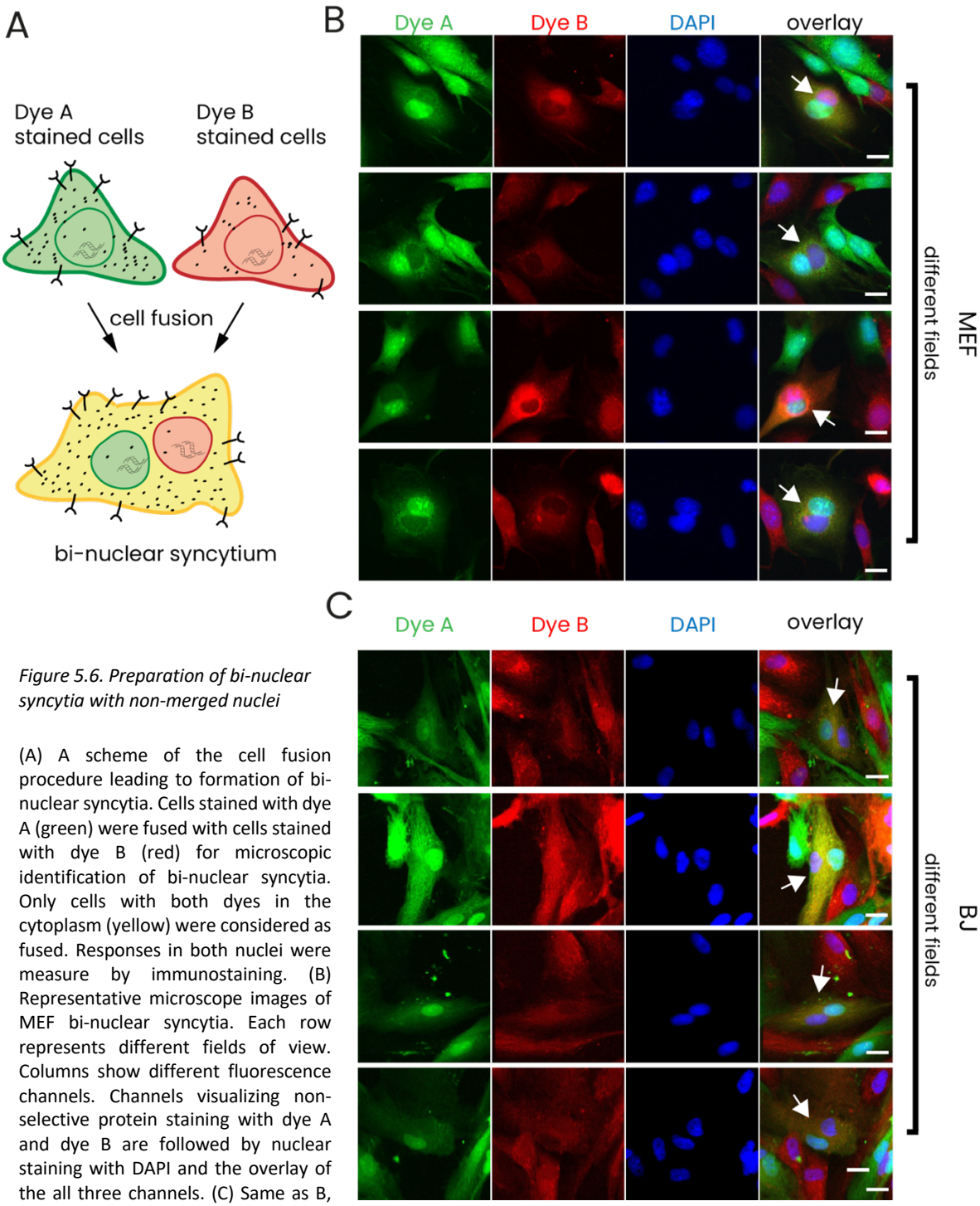


*Figure 5.6. Preparation of bi-nuclear syncytia with non-merged nuclei*

(A) A scheme of the cell fusion procedure leading to formation of bi-nuclear syncytia. Cells stained with dye A (green) were fused with cells stained with dye B (red) for microscopic identification of bi-nuclear syncytia. Only cells with both dyes in the cytoplasm (yellow) were considered as fused. Responses in both nuclei were measure by immunostaining. (B) Representative microscope images of MEF bi-nuclear syncytia. Each row represents different fields of view. Columns show different fluorescence channels. Channels visualizing non-selective protein staining with dye A and dye B are followed by nuclear staining with DAPI and the overlay of the all three channels. (C) Same as B, but for BJ syncytia.
The arrows indicate bi-nuclear syncytia. For the clarity, only syncytia with clearly distinct and separate nuclei were presented. The scale bar: 20 µm.

### 5.2.3. Nuclei of bi-nuclear syncytia do not share nuclear content as indicated by the non-specific protein staining

To investigate whether two nuclei in a syncytium share the molecular content I utilized the non-specific protein staining, the same as for fused cells identification. Precisely, I quantified the fluorescence intensity of both dyes (A and B) for both nuclei of all syncytia. In properly fused syncytia, one nucleus comes from the cell stained with the dye A ("red nucleus") and the second nucleus comes from the cell stained with the dye B ("green nucleus"). Therefore, if any physical connection or fast exchange occurs in a tangible degree after the fusion, the proteins from the "green nucleus" would be equilibrated with the "red nucleus" and vice versa- proteins from "red nucleus" would be equilibrated with the "green nucleus". A comparison of fluorescence of both dyes in each nucleus would give us information about the level of presumably equilibration. To do that, I quantified the inter-nuclear ratio for each dye and plotted individual syncytia points as the scatter: on the X-axis the ratio for the dye A and on the Y-axis the ratio for the dye B (Figure 5.7A). The plot revealed two distinct groups:

1) those of very similar nuclear ratios (on the diagonal), and therefore shared nucleoplasm
2) those of dissimilar nuclear ratios (off the diagonal), and therefore separate nucleoplasm for each nucleus

Points of group 1 were also accumulated around the point (1; 1), while those of group 2 had one of coordinates smaller than 1 with the second of coordinates much larger than 1. The groups were very distinct, indicating that the process of nucleoplasm mixing was largely binary: the nucleoplasm is either shared (group 1) or separate (group 2) with very little syncytia between. Presumably the physical connection could cause such equilibration, although I did not directly nor experimentally confirm that. However, to eliminate the effect of shared nucleoplasm in some syncytia, those with ratios similar for both dyes (merged nuclei, violet dots close to the diagonal) were excluded from the analysis, whereas syncytia with dissimilar ratios in either dye (non-merged nuclei, yellow dots, off-diagonal) were retained. The threshold for rejection was selected manually based on visual inspection, as shown by the dashed lines. Further visual analysis of microscopic images indicated that syncytia which were categorized as having "merged nuclei" indeed possessed two nuclei which had boundaries, but at the same time had very similar levels of non-specific dyes

(Figure 5.7B). In contrast, syncytia with non-merged nuclei had clearly different levels of fluorescence in each nucleus (Figure 5.6 B, C). All these indicate that full equilibration of all proteins of both nuclei is possible, but such nuclei can be excluded using non-specific, whole cell staining.

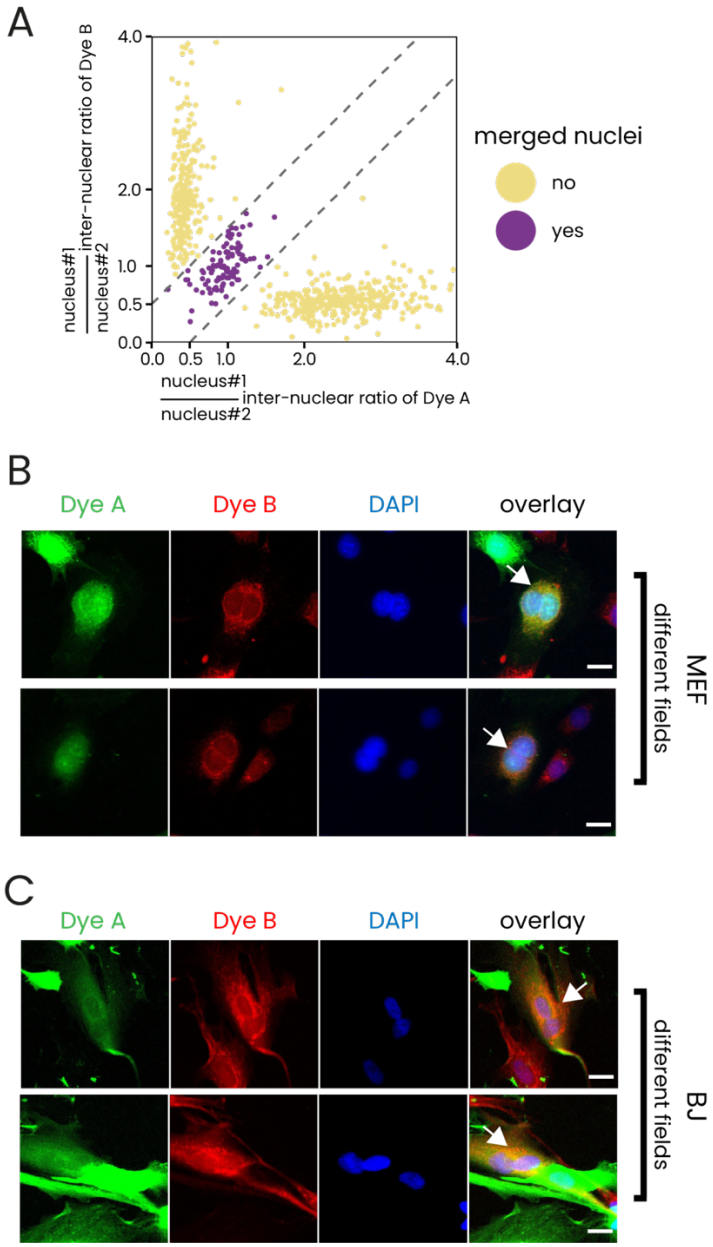


*Figure 5.7. Discrimination between merged and non-merged nuclei in bi-nuclear syncytia based on non-specific protein staining.*

(A) The ratio of both nuclei in dye A (X axis) and dye B (Y-axis) is plotted for each MEF- and BJ-derived bi-nuclear syncytia identified. Two distinct groups were identified: those of similar ratios (violet dots, with merged nuclei) and those of dissimilar ratio, with one ratio greatly different than the other (yellow dots, non-merged nuclei). Syncytia with merged nuclei were excluded from the analysis based on the manually adjusted threshold. (B) Representative microscope images of MEF bi-nuclear syncytia with merged nucleoplasm. Each row represents different fields of view. Columns show different fluorescence channels. Channels visualizing non- selective protein staining with dye A and dye B are followed by nuclear staining with DAPI and the overlay of the all three channels. (C) Same as B, but for BJ syncytia with merged nucleoplasm. The arrows indicate bi-nuclear syncytia with merged nucleoplasm. The scale bar: 20 µm.

### 5.2.4. Bi-nuclear syncytia respond similarly to single cells

After preparing the bi-nuclear syncytia, I stimulated those of MEF origin with IFN-γ and those of BJ-origin with OSM of the high dosage (10 ng/mL) and measured the response in each nucleus with multiple time points after stimulation to compare the response dynamics to the dynamics of single cells. Again, the maximum response was noted at the time of 15 min for IFN-γ and 30 min for OSM, which indicates the similar temporal response characteristics for both syncytia and single cells (Figure 5.3 and Figure 5.8). However, the responses of syncytia were slightly higher for IFN-γ compared to single cells (compare Figure 5.3 and Figure 5.8), which does not exclude the use of bi-nuclear syncytia set-up, as this set-up focuses on the signals of two nuclei of the same syncytia and does not directly compare the response characteristics to the normal, single cells.

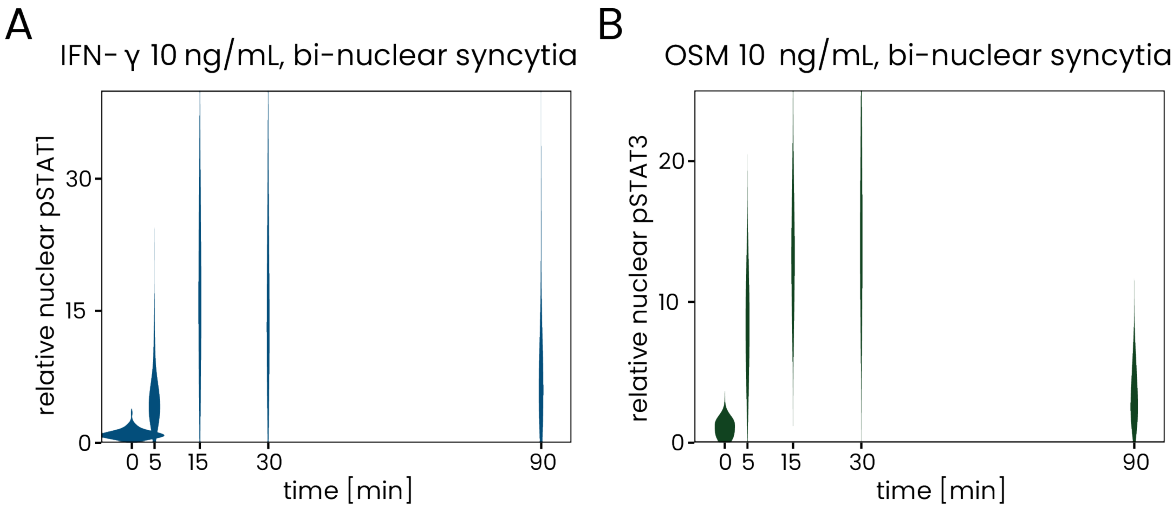


*Figure 5.8. Distributions of responses to IFN-γ or OSM in nuclei of bi-nuclear syncytia over time.*

*(A)* Distributions of single-nuclei responses (y-axis) of MEF-derived bi-nuclear syncytia to 10 ng/mL of IFN-γ over time (x-axis) presented in the form of the violin plots. The width of the "violin" corresponds to the probability of the given response level to arise in the population of single-cells. Each violin has the same area. The plot jointly presents two technical replicates of one, out of two, biological replicates. At least 60 nuclei per time are shown (N≥60). (B) As in A but for 10 ng/mL of OSM in BJ cells. N≥120 for each time.

### 5.2.5. Contribution of molecular noise and cellular phenotype to the cell-to-cell heterogeneity of cytokine responses as approximated by bi-nuclear syncytia

In addition to temporal dynamics of the response to cytokine stimulation, I quantified the response in each nucleus of the bi-nuclear syncytia, allowing for the assessment whether

molecular noise has a tangible effect in the final cellular outcome. I stimulated the cells with a 5-minute pulse of 4 doses of each cytokine: 0, 0.1, 1 and 10 ng/mL to see whether the noise contribution is dose-dependent. I chose the optimal time for the analysis, that is 15 min for MEF-derived, IFN-γ- stimulated bi-nuclear syncytia and 30 min for BJ-derived, OSM-stimulated bi-nuclear syncytia (Figure 5.9 A). Based on the visual inspection of microscopic images, the responses to the highest dose were very similar for both nuclei (Figure 5.9 B, C), giving a clue that the molecular noise can have only a minor contribution into the total cell-to-cell heterogeneity of cellular responses to cytokines. However, to better assess it, I plotted the value of response in one nucleus vs the value of response in the other nucleus in the form of a scatter plot for IFN-γ (Figure 5.9D) and OSM (Figure 5.9E), presented also with discriminability between replicates (Figure 5.10). In such a plot, the total variance of all responses can be decomposed to the diagonal direction and to direction perpendicular to the diagonal (Figure 5.9D, E, first panel). As discussed before, any difference between two nuclei responses can be approximately attributed to molecular noise, therefore the variability along the direction perpendicular to diagonal corresponds to the contribution of stochasticity of biochemical reactions. Similarly, any variability occurring in the diagonal direction can be attributed to cellular phenotype contribution, as this direction represents the variability among averaged responses of two nuclei in individual syncytia. Therefore, the level of spread of points in each of two directions can help in decomposing the sources of total cell-to-cell heterogeneity of cellular responses to cytokine stimulation. In case of stimulation with IFN-γ (Figure 5.9D) and OSM (Figure 5.9E), majority of points of all non-zero stimulations are spread diagonally, indicating similar responses in both nuclei, which confirms the initial visual inspection of microscopic images and indicates the main contribution of phenotypic variability and not molecular noise in total observed variance. However, to draw more robust conclusions, a more quantitative analysis of variance decomposition should be performed.

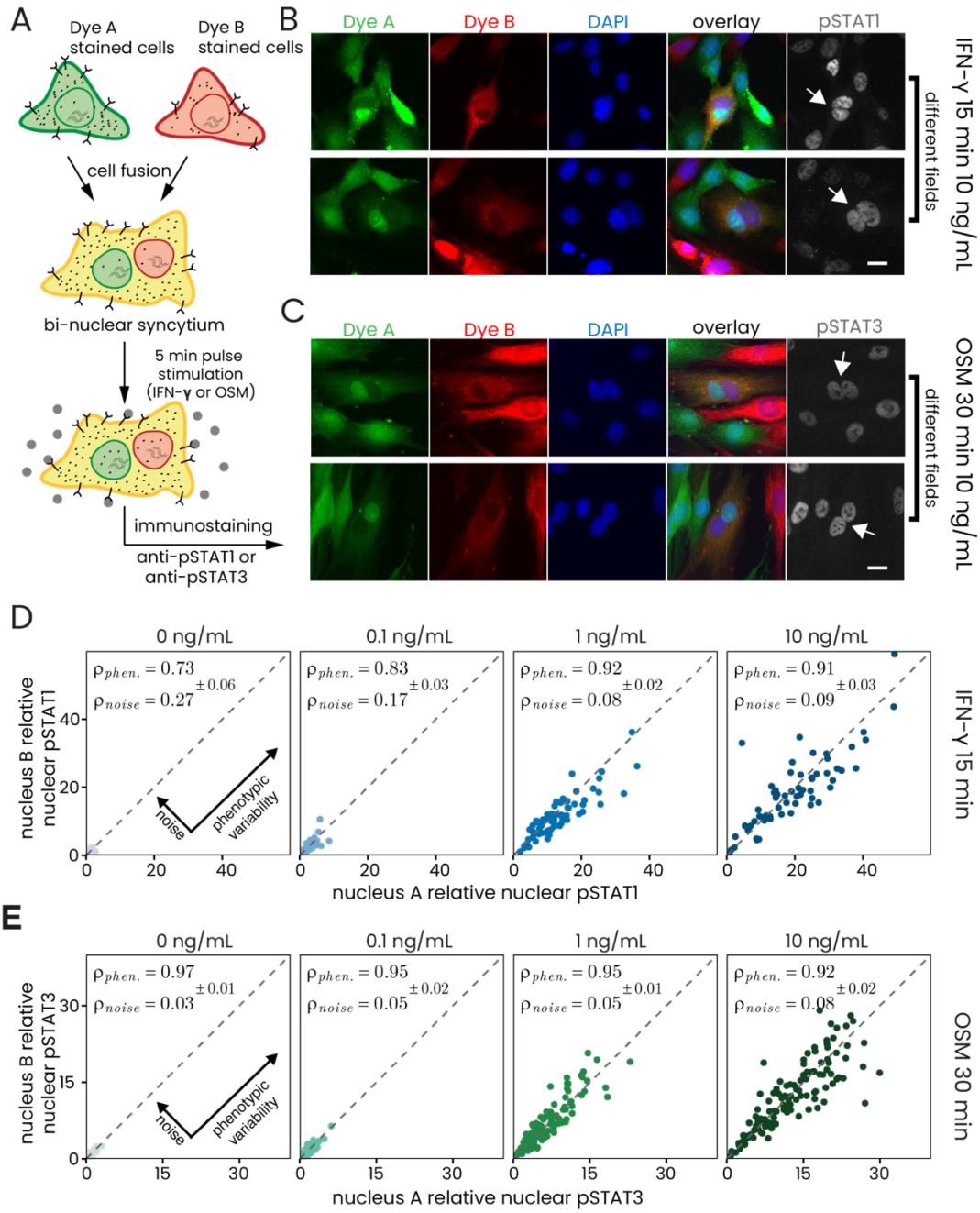


*Figure 5.9. Molecular noise contributes marginally to the cell-to-cell heterogeneity of responses to IFN-γ and OSM.*

(A) A scheme of the cell fusion procedure leading to formation of bi-nuclear syncytia, similar to Figure 5.6A, but followed by stimulation with IFN-γ or OSM and immunostaining against pSTAT1 or pSTAT3, respectively (B) Representative microscope images of MEF-derived bi-nuclear syncytia 15 minutes after stimulation with 10 ng/mL IFN-γ. Each row represents different fields of view. Columns show different fluorescence channels. Channels visualizing non- selective protein staining with dye A and dye B are followed by nuclear staining with DAPI, the overlay of the three channels and finally the pSTAT1 image in grey-scale. The scale bar: 20 µm. (C) Same as B, but for BJ-derived bi-nuclear syncytia 30 minutes after stimulation with 10 ng/mL OSM and pSTAT3 image in grey-scale. The scale bar: 20 µm. (D) FN-γ responses in bi-nuclear syncytia at 15 minutes post-stimulation with indicated doses (columns). Responses of the two nuclei, A and B, determine the coordinates of the corresponding point in the scatter. Variability along the diagonal, dashed line, corresponds to phenotypic variability. Variability in the perpendicular direction corresponds to variability due to molecular noise. Standard deviation of fractional contributions was estimated with bootstrap resampling. (E) The same as in A but for OSM responses at 30 minutes post-stimulation. Sum of two biological replicates is shown in D and E presenting between 41 and 126 syncytia for each dose. See Figure 5.10 for the exact number of syncytia used.

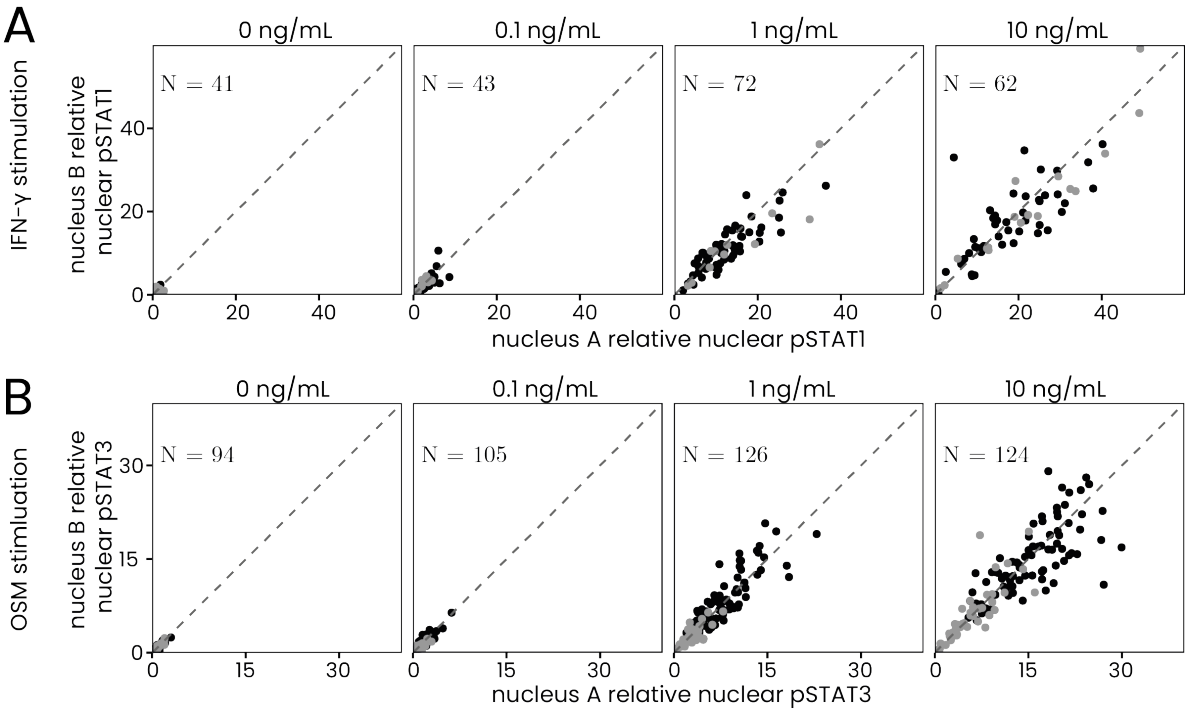


*Figure 5.10. Two replicates of bi-nuclear syncytia measurements show similar phenomena*

Two biological replicates of data shown in Figure 5.9. Replicate 1 is plotted in black whereas replicate 2 in grey. The number of cells measured, N, is printed each plot. Panel (A) shows responses to IFN-γ in MEF-derived bi-nuclear syncytia, and Panel (B) shows responses to OSM in BJ-derived bi-nuclear syncytia.

### 5.2.6. Total response variability can be decomposed to molecular noise and cellular phenotype components

The decomposition proposed below resembles in basics the decomposition of intrinsic and extrinsic noise used in bi-color gene expression experiments (Elowitz et al., 2002; Swain et al., 2002). However, such decomposition, based on bi-color experiment principle, is here used for the first time for the signaling responses. According to the variance decomposition formula, the total variance of the cytokine responses, $\sigma^2_{tot.}$, can be decomposed to cellular phenotype variability, $\sigma^2_{phen.}$, and molecular noise, $\sigma^2_{noise}$:

$$\sigma^2_{tot.} = \sigma^2_{phen.} + \sigma^2_{noise} \qquad (5\text{-}1)$$

Neither $\sigma^2_{phen.}$ nor $\sigma^2_{noise}$ can be approximated from one dimensional data presented, e.g., in Figure 5.4A, B. Therefore, I used inter-nuclear variance of bi-nuclear syncytium as a measure

of $\sigma^2_{noise}$. If $y_i^A$ and $y_i^B$ are the signaling outcomes of the two nuclei in the i-th out of n measured syncytia, then $\sigma^2_{noise}$ can be approximated as:

$$\sigma^2_{noise} = \frac{1}{2n}\sum_{i=1}^{n}((y_i^A - \bar{y}_i)^2 + (y_i^B - \bar{y}_i)^2) , \quad (5\text{-}2)$$

where $\bar{y}_i = \frac{1}{2}(y_i^A + y_i^B)$ is the average of the two nuclei in the i-th syncytium. In the presented scatter plot of bi-nuclear syncytia (Figure 5.9D, E), $\sigma^2_{noise}$ corresponds to variability perpendicular to the diagonal $y_i^A = y_i^B$. Indeed, the variability in this direction represents the variability around the inter-nuclear mean, i.e., around the point with coordinates $(\bar{y}_i; \bar{y}_i)$, Eq. 1. Further, the variability of the responses resulting from the differences in the molecular content of the syncytia is the variability of responses between syncytia themself. Therefore, the variability of inter-nuclear mean can be approximated as variability of the different cellular phenotypes, $\sigma^2_{phen.}$ in the following way:

$$\sigma^2_{phen.} = \sum_{i=1}^{n}(\bar{y}_i - \bar{y})^2 , \quad (5\text{-}3)$$

where $\bar{y}$ is the average response of the all measured nuclei in all bi-nuclear syncytia. Again, on the scatter plot (Figure 5.9D, E), the variability resulting from differences in cellular phenotype is the variability of the average of the both nuclei of all bi-nuclear syncytia. These assumptions allow to interpret the variability of cellular phenotypes as the variability along the diagonal line, i.e., $y_i^A = y_i^B$. In other words, if no molecular noise exists, then both nuclei inside one syncytium would respond exactly the same, $y_i^A = y_i^B$, but each syncytium would respond in a different way, spreading along the diagonal line, indicating the cellular phenotype-caused variability. Finally, the total variability of signaling responses of all nuclei is given as:

$$\sigma^2_{tot.} = \frac{1}{2n}\sum_{i=1}^{n}((y_i^A - \bar{y})^2 + (y_i^B - \bar{y})^2) \quad (5\text{-}4)$$

Now we have formulated all components of the decomposition formula $\sigma^2_{tot.} = \sigma^2_{phen.} + \sigma^2_{noise}$ in regards to bi-nuclear syncytia measurements. To assess the contribution of each component to the total variance, the fractional contribution of both the molecular noise, $\rho_{noise}$, and cellular phenotype, $\rho_{phen.}$, to the total variability of signaling responses are introduced as:

$$\rho_{noise} = \frac{\sigma^2_{noise}}{\sigma^2_{tot.}}, \quad (5\text{-}5)$$

$$\rho_{phen.} = \frac{\sigma^2_{phen.}}{\sigma^2_{tot.}}, \quad (5\text{-}6)$$

Both $\rho_{noise}$ and $\rho_{phen.}$ vary between 0 and 1, with their sum being 1. In summary, the comparison of the signaling responses of the two nuclei with the cell-to-cell heterogeneity allows for decomposing the origin of the cell-to-cell heterogeneity into differences resulting from molecular noise and cellular phenotypes.

### 5.2.7. Phenotypic variability and not noise accounts for most of the cell-to-cell heterogeneity in cytokine signaling

Having established the quantitative analysis of the decomposition of cell-to-cell heterogeneity, I applied it to the results of bi-nuclear syncytia. Fractional contribution of both molecular noise, $\rho_{noise}$, and cellular phenotype, $\rho_{phen.}$, is provided for each stimulation set-up (Figure 5.9D, E), with standard deviation calculated using the bootstrap method. For all non-zero doses, the fractional contribution of molecular noise $\rho_{phen.}$ is greater than 0.83. Furthermore, for doses 1 and 10 ng/mL, where cells respond the strongest and decrease the influence of the basal response levels, $\rho_{phen.} \geq 0.91$. On average, for both cytokines and all non-zero doses, 91.3% of the variance results from the differences in the cellular phenotype, with the remaining 8.7% resulting from molecular noise. In summary, the results indicate that indeed the cellular phenotype accounts for most of the cell-to-cell heterogeneity in IFN-γ and OSM signaling, with molecular noise having only a limited impact on the total variability.

### 5.2.8. Doses can be discriminated with high accuracy

The data from bi-nuclear syncytia demonstrate that cellular biochemistry controls signaling responses with very good precision when compared to the overall cell-to-cell heterogeneity. If so, then the conventional interpretation of dose discriminability in terms of information theory is far from being perfect. Specifically, the overlaps of response distributions to multiple doses of a stimulant (e.g., in Figure 5.4) cannot be considered as an effect of the erroneous signal transmission. Instead, such overlaps should be interpreted only in terms of fractions of a cellular population that responded typically for a given dose. For instance, let us consider the responses to stimulation with 10 ng/mL of IFN-γ (bottom row of Figure 5.4D). Then, it is

correct to say that ~25% of cells stimulated with 10 ng/mL of IFN-γ have responses typical for stimulation with 1 ng/mL. Nevertheless, this does not mean that, due to noise, in 25% of cells the output signal incorrectly encodes 1 ng/ml as opposed to correct 10 ng/mL. It does not mean neither, that a single cell can correctly recognize only the presence and absence of a stimulant. Then, the question arises: to what extent does the noise compromise the potential of a single-cell to discriminate between different doses? Or, in other words, how precise is an individual cell in sensing the external signal? To provide further insight into these questions, a more detailed analysis should be done. For example, we would want to investigate the real precision of a single cell by simulating the cell-to-cell heterogeneity coming exclusively from the molecular noise. To simulate or approximate the heterogeneity caused exclusively by the molecular noise, we would need two measures. First, (a), we would need a measure of the noise strength in a single cell, depending on the response level. Second, (b) we would need a single cell dose-response curve, indicating how the same single cell would respond when stimulated with different doses of a stimulant. Fortunately, the data obtained during single cell analysis (Figure 5.4A, B) and from bi-nuclear syncytia (Figure 5.9D, E) jointly allow for estimation of the true precision of a single cell.

Firstly, to obtain a measure of a noise strength in a single cell (a), we cannot use the variance of inter-nuclear responses, $\sigma^2_{noise}$, itself, as it is only a summary statistic of the noise strength from the whole population. Having only this value, we would be not sure whether the noise strength in low responding cells is the same or much different than in highly responding cells. Instead, I utilized the relation between the noise strength of syncytia and their response level. To do that, I related the inter-nuclear standard deviation for each syncytium, $\sigma^{(i)}_{noise}$:

$$\sigma^{(i)}_{noise} = \sqrt{\frac{1}{2n}\sum_{i=1}^{n}((y_i^A - \bar{y}_i)^2 + (y_i^B - \bar{y}_i)^2)}, \qquad (5\text{-}7)$$

with inter-nuclear mean, $\bar{y}_i$ of each measured syncytium, $i$, by plotting them as a scatter for both IFN-γ (Figure 5.11A) and OSM (Figure 5.11B). For both cytokines, the trend was linear $\sigma^{(i)}_{noise} = \alpha\bar{y}_i$. Linear regression quantified that for both cytokines $\alpha \sim 0.11$ indicating that the molecular noise constitutes 11% of the response level. Therefore, for both cytokines, I considered the 11% of the response level as a measure of the noise in a single cell (a). Secondly, to obtain the single cell dose-curve (b), the best approach would be to stimulate the

cell repetitively, with increasing doses of a stimulant. This, however, cannot be done as I utilized long-lasting responses, up to 90 min (Figure 5.3A and Figure 5.3B) and measured the signal via immunofluorescence, which kills the cells. Unfortunately, the obtained data do not provide any direct measurement of such dose-responses and how these differ between individual cells. To overcome this shortcoming, I employed a simple model of a single-cell response. I supposed that the dose-response curves of individual cells can be represented by percentiles of the response distributions. The assumption is that the low responding cells for the low dose will also be the low responding cells for the high dose of a stimulant. In other words, I divided response distributions for each dose into percentiles and created, for example, $5^{th}$, $50^{th}$ and $95^{th}$ percentile cells, representing weakly, moderately and strongly responding cells for IFN-γ responses (Figure 5.11C) and OSM responses (Figure 5.11D). In this way, I constructed the response curves (b) corresponding to every percentile from 0.05 to 0.95. Although this procedure does not reconstruct the exact response curves of single cells it seems to be suitable for the considered context. Having constructed the two measures, that is (a) the level of noise dependent on the mean response equals 11% and (b) a model of single cell dose response curves, I next constructed the response distributions of each percentile for each dosage as the gamma distribution with the standard deviation taken from (a) and the mean taken from dose-response curve of single percentile (b). I applied this strategy for every single cell dose curve, so for every percentile. Next, I quantified the overlaps and averaged over all percentiles for IFN-γ (Figure 5.11E) and OSM (Figure 5.11F). Finally, I could calculate the matrices of discrimination probabilities, similar to Figure 5.4E, F. The matrices, presented as pie-chart, again show the probabilities that a cell stimulated with one dose (rows) will generate a response that is most likely for the other doses (columns). The diagonal elements of constructed matrices show fractions very close to 1, for both cytokines, indicating that when the heterogeneity comes exclusively from molecular noise, and not from cellular phenotype differences, the doses can be highly accurately discriminated. In this scenario the discrimination is much more reliable compared to the estimation performed under the assumption that the whole observed cell-to-cell variability results from molecular noise (Figure 5.4E, F), and implies that single cell is much more precise than predicted based on the cell-to-cell heterogeneity.

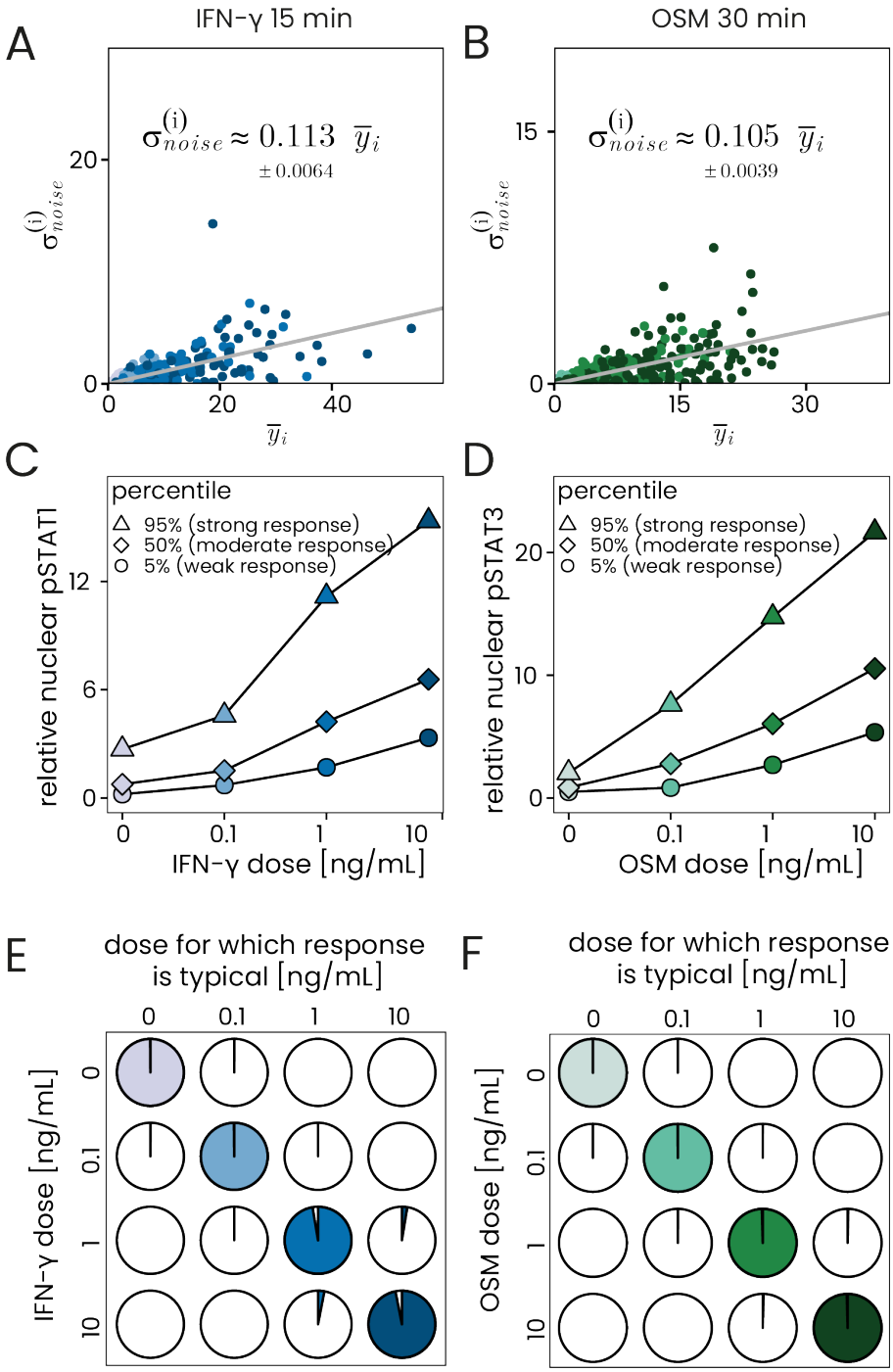


*Figure 5.11.Molecular noise is linearly dependent on the response level and is low enough to enable almost perfect dose discrimination*

(A) Inter-nuclear standard deviation, $\sigma^{(i)}_{noise}$, is plotted against inter-nuclear response, $\overline{y}_i$ of each syncytium, $i$, for IFN-γ responses in MEF-derived bi-nuclear syncytia. The fitted regression line is presented in gray, with the indicated formula and regression error. All doses at 15 minutes post-stimulation were considered jointly. (B) The same as A, but for OSM at 30 min after stimulation in BJ-derived bi-nuclear syncytia. (C) Three different percentiles of the response distribution, corresponding to weak, moderate and strong responses for each dose from A. (D) The same as C, but for OSM at 30 min after stimulation. (E) Quantification of the overlaps between IFN-γ response distributions constructed by averaging every percentile from 1 to 99 as in C, with the noise strength taken from the regression in A. (F) The same as E, but for OSM responses.

### 5.2.9. The low inter-nuclear variability does not result from equilibration of nuclear pSTATs

In the bi-nuclear experiments the inter-nuclear variability was relatively low compared to inter-syncytial variability. Contrary to the considering such inter-nuclear variability as molecular noise, this phenomenon can be explained by the fast equilibration of the pSTATs level between the nuclei. Such equilibration can be an effect of the physical connection between nuclei or fast nuclear export of pSTATs from one nucleus and subsequent import into the second nucleus, leading to the similar level of pSTATs in each of the nuclei, without the influence of the molecular noise. This interpretation, if found true, would definitely compromise the conclusions presented in the dissertation. As mentioned earlier, the nuclei physically connected were excluded from the analysis based on the whole-cell staining during syncytia preparation (Figure 5.7). However, to verify whether the considering the inter-nuclear variability as molecular noise is justified it needs to be shown, that there is no fast nuclear export of pSTATs with subsequent fast import to the other nucleus. Firstly, such process of fast export-import of pSTATs seems to be in contrast to the current view of the pSTATs shuttling, which postulate, based on experiments, that both pSTAT1 and pSTAT3 abundantly translocate to the nucleus, but exit in majority only after dephosphorylation in the form of STATs, with limited, if any occurring, export of the pSTATs molecules (Herrmann et al., 2007; Meyer et al., 2003; Reich and Liu, 2006). Secondly, I addressed experimentally the issue of presumably fast export and import of pSTAT molecules by performing the same molecular noise quantification but in very early time points after stimulation. If the low noise contribution is an effect of the inter-nuclear equilibration by the fast export-import rate, then the noise contribution should be lower in early time points. The non-phosphorylated STATs were shown to exit the nucleus already after a couple of minutes after the nuclear entry (Cimica et al., 2011; Herrmann et al., 2007; Pranada et al., 2004). In addition, the mobility of pSTATs molecules is much lower than STATs due to the DNA-binding ability of pSTATs (Haspel and Darnell, 1999; McBride and Reich, 2003; Meyer et al., 2003). Therefore, as fast as after 5 min after stimulation the putative equilibration process should influence the noise quantification in much lower degree than in 15 or 30 min after stimulation. However, when bi-nuclear syncytia were stimulated with 10 ng/mL of either IFN- γ or OSM, the $\rho_{noise}$ already after 5 min reached the value occurring also in 15 min for IFN-γ (Figure 5.12A) or both 15 and

30 for OSM (Figure 5.12A). Therefore, the fast exit of the activated pSTATs molecules with fast import to the other nucleus, without the step of the dephosphorylation, does not influence the noise quantification, confirming the correctness of the used assumptions.

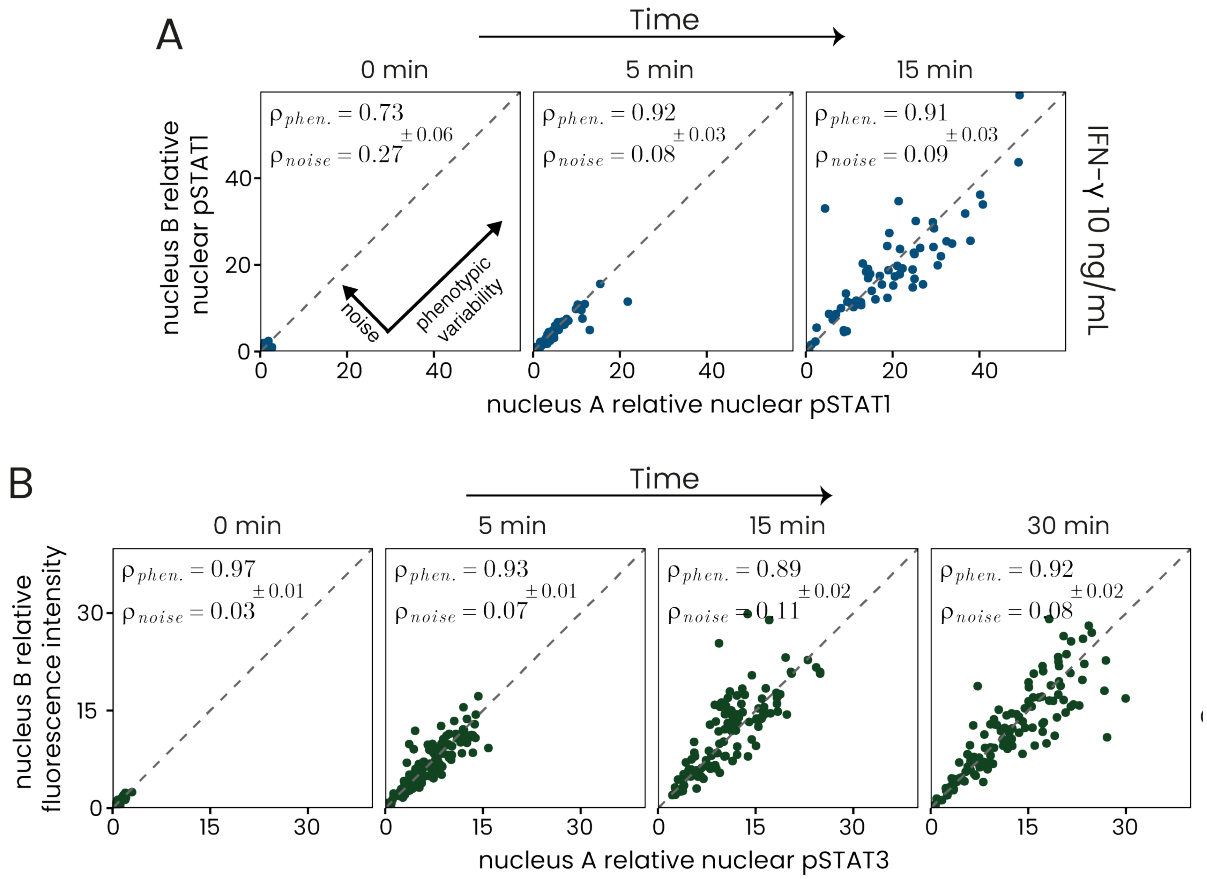


*Figure 5.12. Inter-nuclear variability of pSTATs in the syncytial nuclei is equally low at early time points after stimulation and at the time of maximal response*

(A) IFN-γ responses in MEF-derived bi-nuclear syncytia at 0-, 5- and 15-minutes post-stimulation with 10 ng/mL. Corresponds to Figure 5.9D. (B) The same as A, but for OSM responses at 0-, 5-, 15- and 30-min post stimulation with 10 ng/mL in BJ-derived bi-nuclear syncytia. Corresponds to Figure 5.9D and E. Sum of two biological replicates is shown in A and B presenting at least 65 syncytia for each dose.

### 5.2.10. Channel capacity of a single cell considerably exceeds the binary sensing precision

The information theory with its channel capacity measure allows for quantification of the ability to resolve stimulation doses by a population of single cells (see Literature review 2.5). For the single cell populations stimulated with IFN-γ and OSM, the channel capacity reached up to around 1 bit, allowing only for nearly binary discrimination of a presence or absence of a stimulant. However, the information theory assumes that all the observed cell-to-cell

heterogeneity decreases the signaling fidelity. Therefore, in the hypothetical situation where there is no molecular noise at all and the cell-to-cell heterogeneity of responses is caused solely by differences in cellular phenotypes, the channel capacity would still indicate the significant information loss and low signaling fidelity. In this situation, however, all the single cells considered individually have perfectly recognized the dose and responded precisely, each cell in its own way. Therefore, to overcome this limitation in the information theory interpretation I estimated the channel capacity for a hypothetical single cell with the molecular noise as the only source of variation. The molecular noise for each single cell was derived from bi-nuclear syncytia experiments and equals 11% of the response. Similarly to the overlap quantification, the single cell dose response curves were estimated using percentile strategy (see Results 5.2.8). With these assumptions, and simulating the single cell response distribution as gamma distribution with the mean obtained from percentile calculation and standard deviation equals 11% of the response, the single cell channel capacity reached 1.95 bits for IFN-γ and 2 bits for OSM. Such high channel capacity values indicate, that nearly all 4 doses could be precisely discriminated by individual single cells, compared to binary discrimination of presence or absence of a stimulant in a heterogeneous population of single cells. Therefore, a single cell is very reliable in signal sensing, but different cells have different sensitivities and characteristics of dose-response curves, creating the final cell-to-cell heterogeneity of a population.

## 5.3. Nuclear state and the cytokine response

In the syncytium, the molecular content of the two nuclei is different, as they originate from two different cells, which is reflected in the dye staining pattern (Figure 5.7). Therefore, the nuclear protein levels can also be different for each nucleus as well as the nuclear shape or the arrangement of the nucleopores and many other features, jointly considered as the nuclear state. The different nuclear states can potentially contribute to the differences in responses between the two nuclei and therefore also quantifies as the molecular noise in the heterogeneity decomposition analysis.

### 5.3.1. Nuclear state contributes substantially to the response variability in long times after cytokine stimulation

To test the hypothesis that the nuclear state contributes to the differences between nuclei of the bi-nuclear syncytium, I would need to find the stimulation condition where the influence of the nuclear state on the pSTAT levels is strong. In such a condition, if the hypothesis is true, the responses between two nuclei in bi-nuclear syncytia will differ substantially. One of such presumable conditions is the long time after stimulation- at that time the pSTAT levels decrease due to the dephosphorylation and nuclear export processes. Such processes are dependent on the nuclear content. Therefore, to test whether nuclear differences can start manifesting at the time of the signal decrease I performed heterogeneity decomposition for late time points after stimulation. For simplicity, I used only the highest cytokine doses, 10 ng/mL. Indeed, in syncytia stimulated with 10 ng/mL of IFN-γ and measured after 30 min, the signal of two nuclei started to differ more than in earlier time points, with $\rho_{noise}$ increasing to the value of 0.47 (Figure 5.13A), compared to $\rho_{noise} = 0.09$ present at 15 min. At 90 min after beginning of stimulation, the signal from two nuclei differed even more, with almost all points lying far from the plot diagonal, indicating substantial differences between two nuclei signals. On the other hand, for OSM stimulation with 10 ng/mL, at no time point the nuclei differed substantially and both 30, 60 and 90 min since the beginning of stimulation had similar $\rho_{phen.}$ values ranging from 0.09 to 0.04 (Figure 5.13B). In conclusion, the nuclear state can indeed influence the decomposition of bi-nuclear syncytia heterogeneity, but it is probably cell-specific or signaling pathway-dependent. For time points after IFN-γ stimulation reaching 30 min and longer, the nuclear state starts to override the molecular noise diverging the signal in the two nuclei.

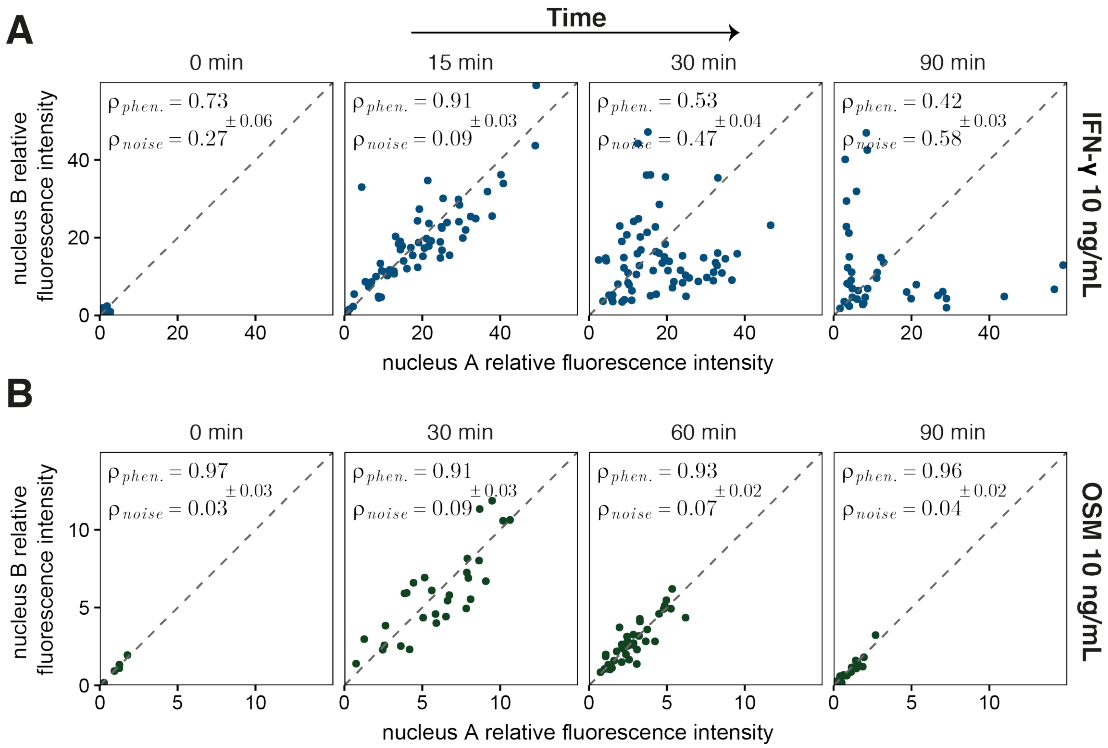


*Figure 5.13. Inter-nuclear variability of pSTAT levels in syncytial nuclei increases in long time points for IFN-γ but not for OSM*

(A) IFN-γ responses in bi-nuclear syncytia at long time points, 0-, 15-, 30- and 90-minutes post-stimulation with 10 ng/mL. Corresponds to Figure 5.9D. A time point of 15 min replicated from Figure 5.9D, 10 ng/mL for comparison. (B) The same as A, but for OSM responses at 0-, 30-, 60- and 90-min post stimulation with 10 ng/mL. Corresponds to Figure 5.9D and E. Sum of two biological replicates is shown in A presenting at least 62 syncytia for each non-zero time point. One biological replicate is shown in B presenting at least 19 syncytia for each non-zero time point.

Then, I asked what specific characteristics of the nuclear state could contribute to the increased differences between syncytial nuclei after IFN-γ stimulation in MEFs. As the IFN-γ-stimulated response starts to drop at 30 min, the increased nuclear differences indeed could be related to dephosphorylation of pSTAT1. The dephosphorylation rate largely depends on the nuclear level of the TC45 phosphatase (see Literature review 2.10)(Böhmer and Friedrich, 2014). Therefore, it is possible, that both nuclei differ in terms of the level of TC45, which does not manifest in early time points as the dephosphorylation is then relatively slow or overridden by the fast nuclear import. At the late time points however, the dephosphorylation starts to dominate over the import. To verify this, I used the vanadate (in the form of sodium orthovanadate, $Na_2VO_4$), the well-known non-specific inhibitor of phosphatases, used previously in STAT1 nuclear shuttling studies (Haspel and Darnell, 1999; Meyer et al., 2003). The phosphatase inhibition should diminish the differences of nuclear states in bi-nuclear syncytia observed in late time points after stimulation. To confirm the vanadate effectiveness

and analyze its effect on the response dynamics I treated the single cells with vanadate for 1 h and next stimulated with IFN-γ. The vanadate caused much higher nuclear pSTAT1 level in all time points in single cells after IFN-γ stimulation compared to cells with no vanadate treatment (Figure 5.14). In addition, the nuclear pSTAT1 level after vanadate treatment reached the maximum around 30 min and remained constant at least until 90 min, compared to significant signal loss at 90 min in control cells. Therefore, the vanadate treatment indeed inhibits the dephosphorylation process leading to long-lasting response with higher maximum level of nuclear pSTAT1.

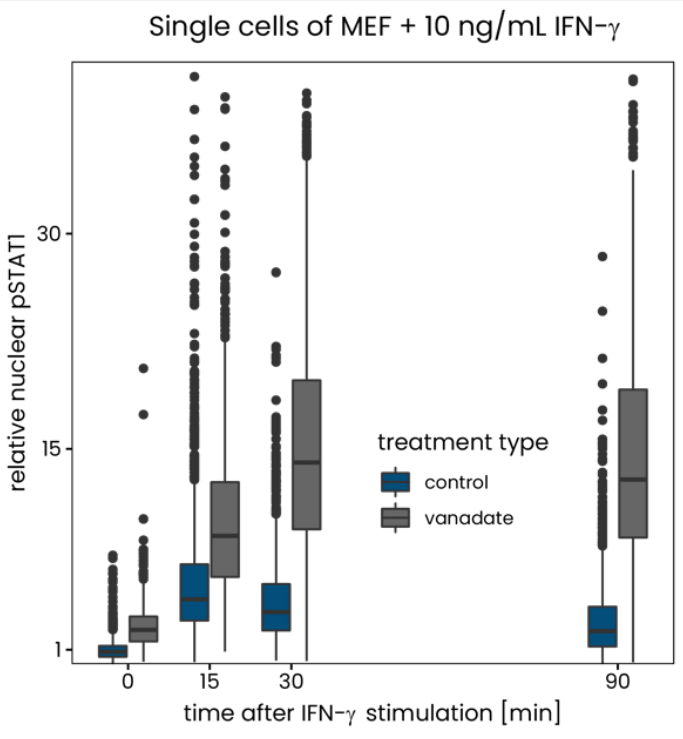


*Figure 5.14. Inhibition of phosphatases increase the response to IFN-γ and changes its dynamics*

MEF single cells were either treated with 1 mM vanadate for 1 h (gray) or left untreated (blue). After that time, all cells were stimulated with 10 ng/mL IFN-γ for 5 min and the cellular response was measured at the indicated time points. At least 1000 cells (N>1000) were analyzed for each condition. P-value < 0.0001 for each of the time point between control and vanadate-treatment cells (two-tail t test on log-transformed values and K-S test)

Then, I used the same vanadate treatment for bi-nuclear syncytia and performed heterogeneity decomposition to quantitively analyze the effect of nuclear state. Instead of using $\rho_{noise}$ notation, I will now call the same measure as fractional contribution of both the molecular noise and nuclear state, or $\rho_{noi.+nuc.}$. Inhibition of phosphatases did not influence the $\rho_{noi.+nuc.}$ at the time of 15 min (0.06+- 0.02 after vanadate treatment vs 0.07+- 0.04 in control syncytia). However, at the time of 30 min, the vanadate indeed decreased the variability between two nuclei, as the $\rho_{noi.+nuc.} = 0.02 \pm 0.01$ was much lower compared to $\rho_{noi.+nuc.} = 0.23 \pm 0.08$ of syncytia with no vanadate treatment. This shows that phosphatases indeed can influence the decomposition of heterogeneity sources in syncytia at

long time points after IFN-γ stimulation, while having no impact at the short time points. In addition, as at the time of 90 min, $\rho_{noi.+nuc.}$ after vanadate treatment increased to 0.17, indicating that the inhibition of phosphatases was not permanent, or that other components of nuclear state or molecular noise dominated the response level at this time. All these indicate that the nuclear state, and especially dephosphorylation process, indeed contributes substantially to the response in long times after IFN- γ stimulation.

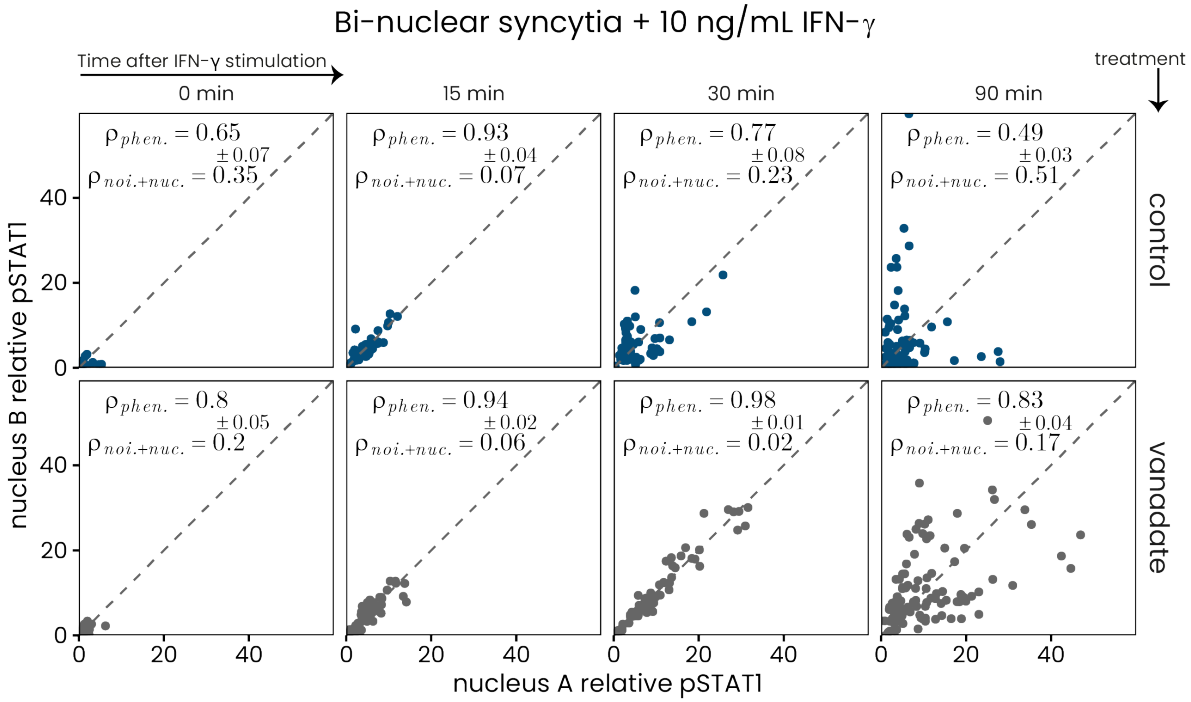


*Figure 5.15. Inhibition of dephosphorylation in bi-nuclear syncytia makes the nuclei to respond more similarly*

MEF-derived bi-nuclear syncytia were either treated with vanadate for 1 h (gray) or left untreated (blue). After that time, all syncytia were stimulated with 10 ng/mL IFN-γ for 5 min and the cellular response was measured at the indicated time points in each nucleus. The decomposition of heterogeneity onto $\rho_{phen.}$ and $\rho_{noi.+nuc.}$ was done similarly as in Figure 5.9D. At least 50 syncytia (N>50) were analyzed for each non-zero time point. Sum of all two biological replicates performed is shown.

## 5.4. Measurement error of immunocytofluorescence

One of the components of the measured level of nuclear pSTAT, $S_{measured}$, besides the true pSTAT value, $S_{true}$, is the measurement error, what can be presented by the formula:

$$S_{measured} = S_{true} + \varepsilon, \quad (5\text{-}8)$$

where $\varepsilon$ is the measurement error, which can be either positive or negative in value. Quantification of the measurement error is challenging, as it is statistically independent for each measurement. At the same time, the quantification of a measurement error can be useful in the estimation of precision of the experimental methodology. The measurement error, $\varepsilon$, of the immunofluorescence method comes from multiple factors: non-specific antibody binding, illumination differences due to scattering of non-homogeneous medium, background fluorescence of a cell as well as non-optimal marking of a cell on microscopic images. All these factors influence the final outcome in a random, or uncontrolled, way for each investigated nucleus. One of the ways to approximate the measurement error of immunofluorescence method is to measure multiple times exactly the same entities, e.g., cellular nuclei of the true value $S_{true}$. If the measurements were taken enough times, the average of the measured levels would correspond to the true value, while standard deviation of measurements, $\sigma$, would correspond to the measurement error, $\varepsilon$. In the simplest model, the error $\varepsilon$ follows a normal distribution with mean 0 and standard deviation, $\sigma$, derived from the multiple measurements of the same true value:

$$\varepsilon \sim N(0,\ \sigma), \quad (5\text{-}9)$$

However, $\sigma$ can be different depending on the $S_{true}$. For example, variability of the measurement error can be higher for the higher values of $S_{true}$. To account for that, $\sigma$ needs to be related to $S_{true}$. The simplest assumption is that the relationship would be linear and would follow the formula:

$$\sigma = \alpha S_{true}, \quad (5\text{-}10)$$

where $\alpha$ is the slope of the linear regression with the intercept = 0. Finally, rewriting Eq. 5-8 in terms of the above assumptions gives us:

$$S_{measured} = S_{true} + \alpha S_{true} \cdot \varepsilon_N, \quad (5\text{-}11)$$

where $\varepsilon_N$ follows a normal distribution with the mean 0 and standard deviation 1:

$$\varepsilon_N \sim N(0,1) \quad (5\text{-}12)$$

Therefore, according to the presented model, the slope coefficient of the linear regression $\sigma \sim \alpha S_{true}$, would approximate the level of measurement error. For obvious reasons, it is hard to measure the protein level multiple times in the same cells or nuclei. Fortunately, the bi-nuclear syncytia provide a possibility to approximate two nuclei with identical levels of pSTATs. According to Figure 5.7, the bi-nuclear syncytia can have two states: either with separate nuclei or merged nuclei. Such a binary distinction suggests that in syncytia with merged nuclei, there could be a physical connection between nuclei that causes the equilibration of the levels of nuclear proteins. Therefore, bi-nuclear syncytia with two merged nuclei can be a model of two nuclei with identical levels of pSTAT proteins.

### 5.4.1. Bi-nuclear syncytia with merged nucleoplasm can approximate the contribution of technical errors

To assess the measurement error of immunofluorescence, I quantified the nuclear pSTAT1 level in MEF-derived syncytia stimulated with IFN-γ and pSTAT3 level in BJ-derived syncytia stimulated with OSM, in syncytia with merged nucleoplasm. I analyzed images from various previous bi-nuclear stimulation experiments, with doses varying from 0 to 10 ng/mL and time points ranging from 5 to 90 min. In addition, to decrease the possibility of misidentification, the threshold for merged vs unmerged nuclei discrimination was set to avoid syncytia with partially merged nucleoplasm (Figure 5.16A). The obtained data allowed for comparison between pSTAT protein levels in two nuclei with the same pSTAT content. The decomposition of total heterogeneity applies here, although with different meanings. Namely, $\rho_{phen.}$ stays the same and corresponds to the variance caused by differences between syncytia, while $\rho_{noise}$ should be considered as fractional contribution of measurement error, $\rho_{error}$. With these assumptions, the $\rho_{error}$ for both cell types equaled 0.03 +- 0.01, while $\rho_{phen.}$ reached 0.97+-0.01 (Figure 5.16B, D). This indicates that bi-nuclear syncytia with merged nuclei have indeed very similar nuclear levels of pSTAT proteins in both nuclei and that only a small

fraction of total variability is caused by measurement error. However, the quantity of $\rho_{error}$ does not explain what is the level of noise compared to true measured value. To assess this, I performed the more detailed measurement error quantification according to the Eq. 5-8.

### 5.4.2. Measurement errors have a minor contribution to the immunocytofluorescence signal

As mentioned earlier and showed in the Eq. 5-11, the slope coefficient $\alpha$ can be considered as the measure of the contribution of measurement error to the final observed level of nuclear pSTAT proteins. If $\alpha$, expressed in %, reached the 100%, it would mean that the observable fluorescence signal is far from the true level. However, if $\alpha$ reached 0%, then all of the measured signals exactly equal the true value, according to the proposed model. To get $\alpha$, I calculated the slope of linear regression obtained by relating inter-nuclear standard deviation, $\sigma_{error}^{(i)}$, with inter-nuclear mean, $\bar{y}_i$ for all of syncytia with merged nucleoplasm, i (Figure 5.16D, E). The $\alpha$ reached around 9% of true signal for IFN-γ stimulated MEF-derived syncytia and 11% of OSM-stimulated BJ-derived syncytia, indicating that only a small fraction of a fluorescent signal can be considered as the measurement error. These results point out that the contribution of the molecular noise calculated using bi-nuclear syncytia is probably overestimated, and at least some part of the molecular noise-driven variability can be attributed to measurement error. In other words, the actual contribution of molecular noise may be lower than estimated by the introduced reasoning. However, the comparison between molecular noise and measurement error requires more in-depth investigation.

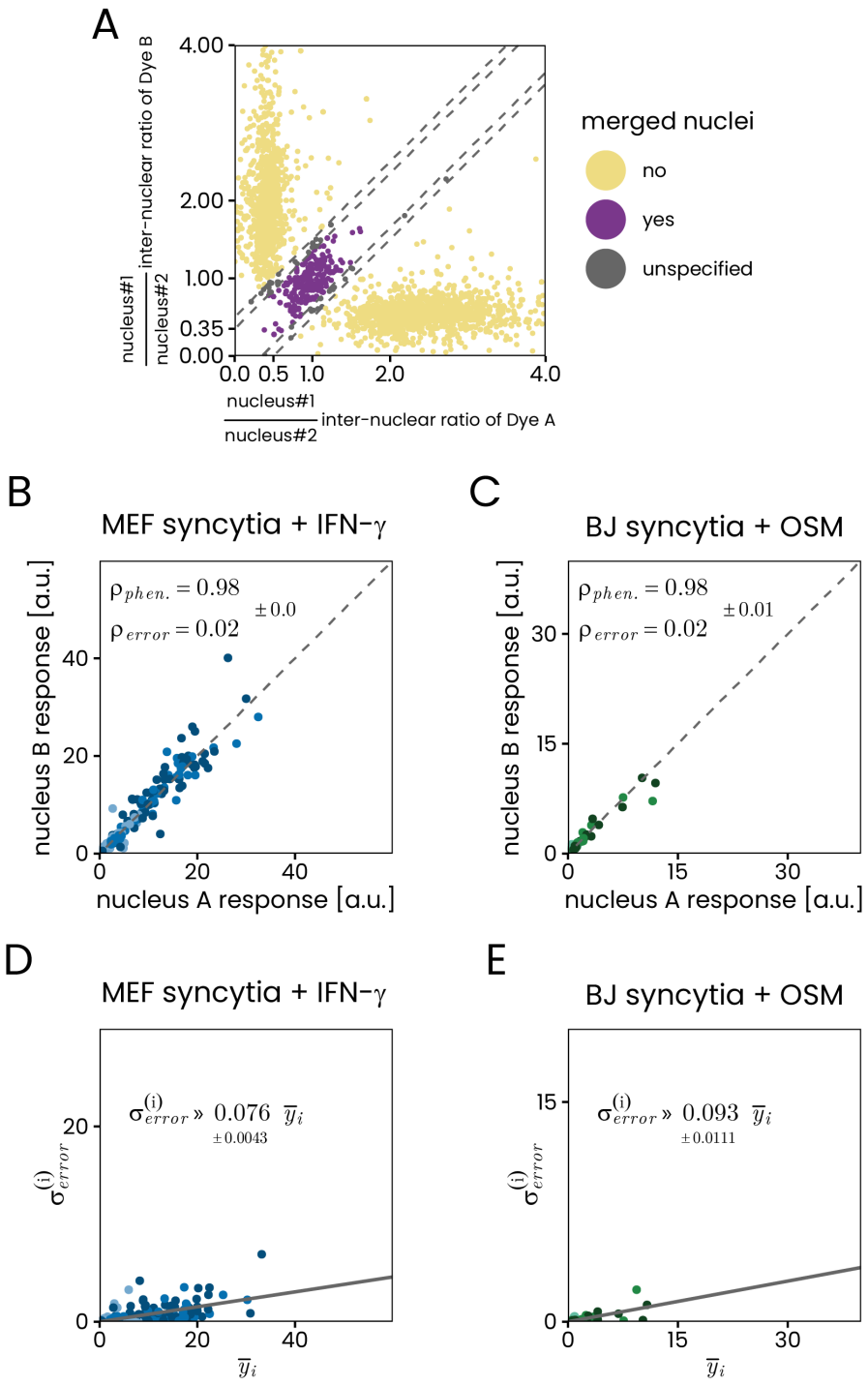


*Figure 5.16 Measurement errors have a minor contribution to the immunocytofluorescence signal*

(A) Discrimination between merged and non-merged nuclei in bi-nuclear syncytia based on non-specific protein staining. Corresponds to Figure 5.7. In addition to the previously introduced threshold, a more stricken threshold was applied, to remove from the analysis syncytia with partially merged nucleoplasm (grey). (B) IFN-γ responses in bi-nuclear syncytia with merged nucleoplasm at various time points after stimulation and various doses used (colors). Corresponds to Figure 5.9D. Instead of $\rho_{noise}$, $\rho_{error}$ is presented. (C) Same as B, but for BJ syncytia. (D) Inter-nuclear standard deviation, $\sigma^{(i)}_{error}$, is plotted against inter-nuclear response, $\overline{y}_i$ of each syncytium, $i$, for IFN-γ responses. The fitted regression line is presented in gray, with the indicated formula and regression error. All doses and time points post-stimulation were considered jointly. (E) Same as D but for BJ syncytia.

## 5.5. Levels of STATs and receptors in cytokine responses

The bi-nuclear syncytia experiments (see Results 5.2) showed that the cellular phenotype is a dominant factor of the observed cell-to-cell heterogeneity in cytokine responses. To assess what are the key components of the cellular phenotype influencing the IFN-γ and OSM responses, I measured the whole-cell levels of STATs and receptors together with cellular responses in the same cell, using flow cytometry. Precisely, for IFN-γ in MEFs, I measured both STAT1, pSTAT1 and the component of the IFN-γ receptor complex, IFNGR1. For OSM in BJ cells, I measured both STAT3, pSTAT3 and the component of the OSM receptor complex, OSMR.

### 5.5.1. Flow cytometry is suitable for measuring low-abundant proteins

The flow cytometry enables the measurement of cellular protein levels with higher sensitivity over the fluorescence microscopy, meaning the higher ability to detect even lowly-abundant proteins (Basiji et al., 2007). While STAT and pSTAT proteins occur in high abundance, the cytokine receptors generally are present in low copy number in a cell. Therefore, I chose flow cytometry to be able to measure the receptor level more precisely than using microscopy. To increase the signal of receptors even further, I permeabilized cells prior immunostaining, to detect the intracellular and membrane fraction of receptors. Flow cytometry measurements showed significant differences in signals between positive staining and negative staining for whole-cell receptors (Figure 5.17A, B) as well as STAT (Figure 5.17C, D) and pSTAT proteins (Figure 5.17E, F). Next, to avoid the false positive correlation arising from fluorescence leakage (see materials and methods), I set up the compensation using single-stained samples, obtaining no increase in signals in non-specific fluorescent channels (Figure 5.18). Therefore, these results point to the flow cytometry as suitable for measuring the level of both STATs, pSTATs and receptors of IFN-γ and OSM signaling pathways.

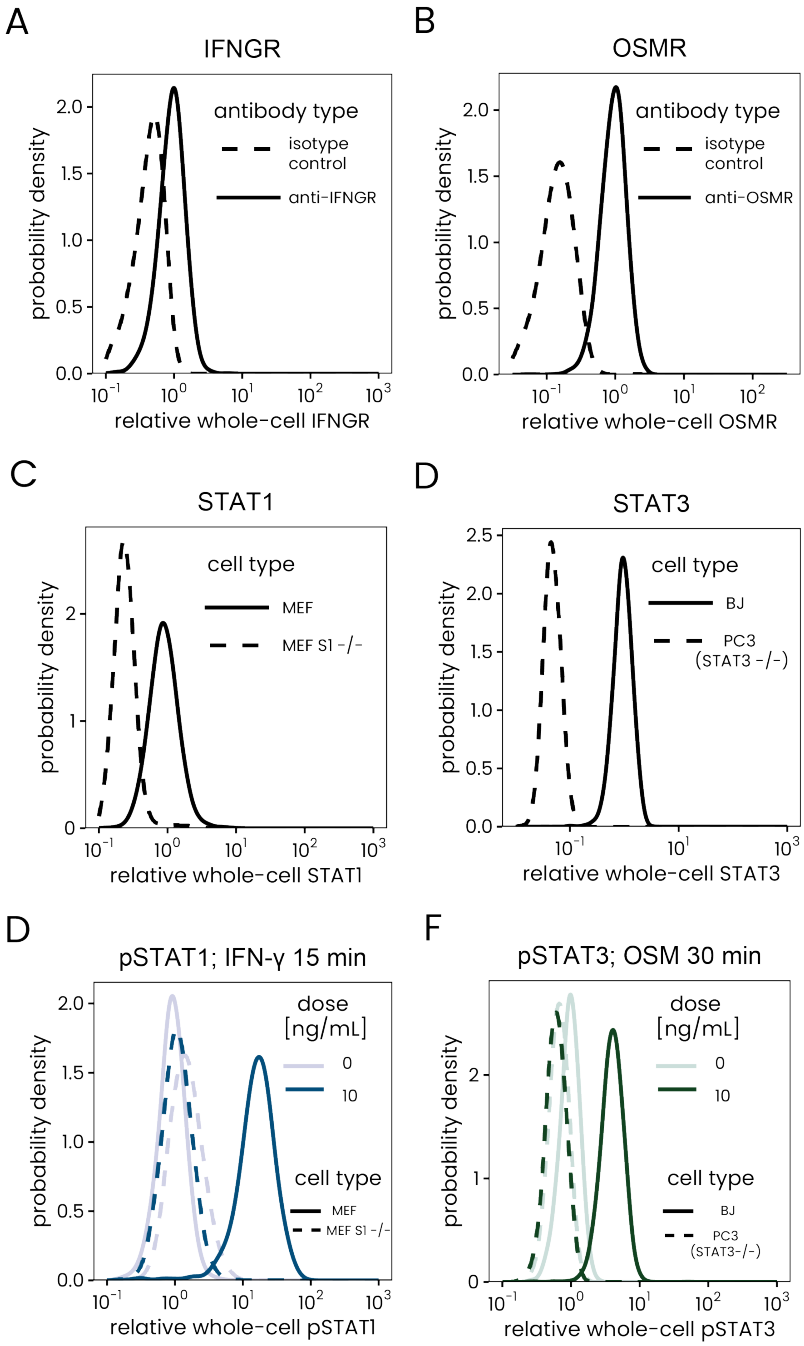


*Figure 5.17. Positive and negative staining of IFN-γ and OSM signaling pathway components measured intracellularly on the flow cytometer.*

(A) Whole-cell IFNGR measured on MEF cells with anti-IFNGR antibody (solid line) or isotype control (dashed line). (B) Whole-cell OSMR measured on BJ cells with anti-OSMR antibody (solid line) or isotype control (dashed line). (C) Whole-cell STAT1 measured on MEF cells (solid line) or in MEF S1 -/- (dashed line). (D) Whole-cell STAT3 measured on BJ cells (solid line) or PC3 cell line, considered as STAT3 -/- (dashed line). (E) Whole-cell pSTAT1 measured at 15 min after IFN-γ stimulation with either 0 ng/mL (light blue) or 10 ng/mL (dark blue) on MEF cells (solid line) or MEF S1 -/- cells (dashed line). (F) Whole-cell pSTAT3 measured at 30 min after OSM stimulation with either 0 ng/mL (light green) or 10 ng/mL (dark green) on BJ cells (solid line) or PC3 cells (dashed line). A representative of two biological replicates is shown. At least 1600 cells (N>1600) are presented in each probability density curve. P-value < 0.0001 for each of the protein between positive and negative staining control (two-tail t test on log-transformed values and K-S test).

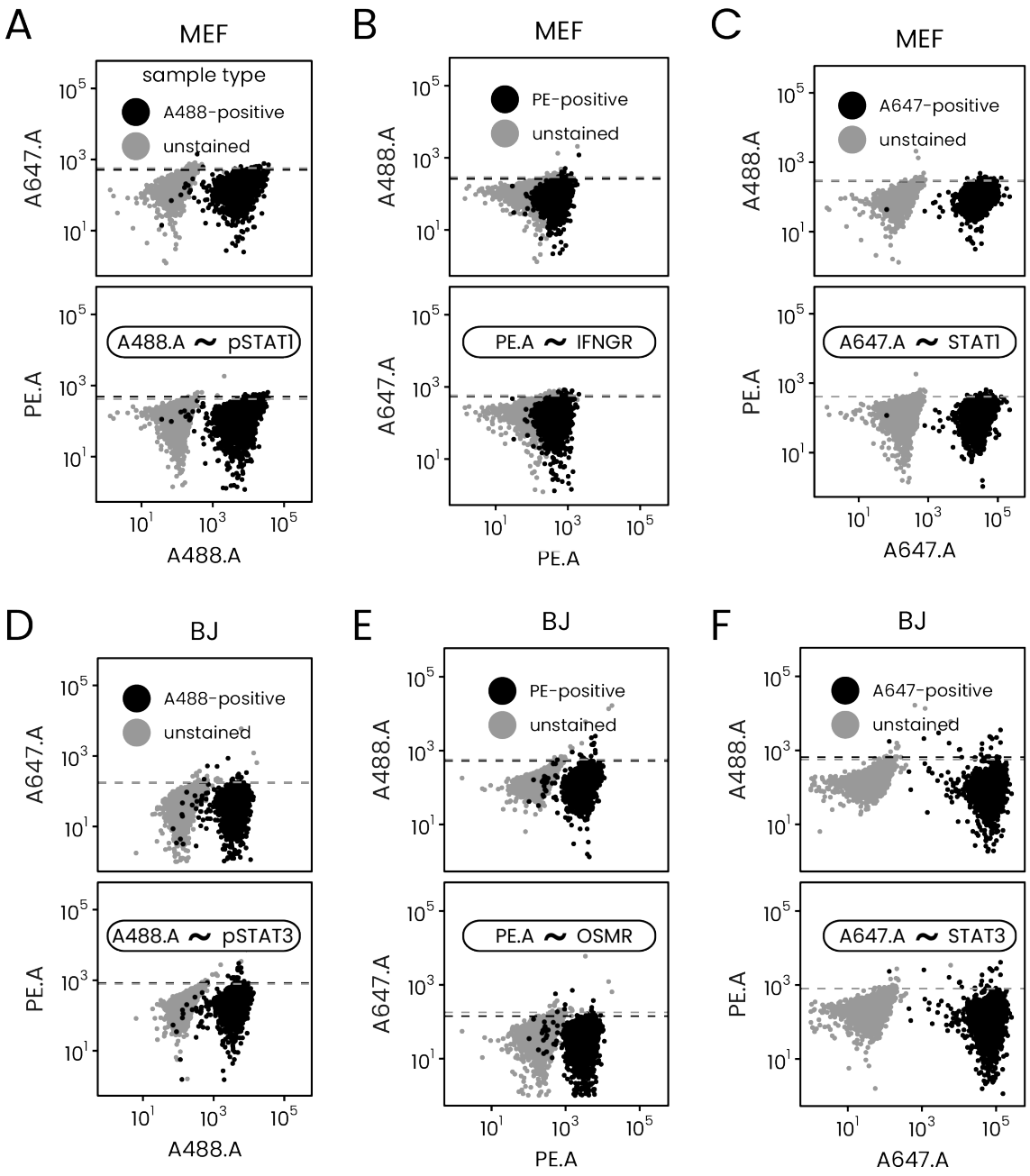


*Figure 5.18. Proper compensation assures no fluorescence leakage to non-specific channels in flow cytometry*

(A) – (C) Compensation for MEF cells; (D) – (E) Compensation for BJ cells. Each panel consists of two subpanels. Each subpanel presents the signal of either positive signal-sample (black) or unstained sample (grey) as scatter of positive signal-channel (x axis) vs non-specific channels (y axis on subpanels). The inset presents the name of the fluorescent channel and the stained protein. A488.A – Alexa Fluor 488 corresponding to pSTATs; PE.A – phycoerythrin corresponding to receptors; A647.A – Alexa Fluo 647 corresponding to STATs. Dashed lines for positive signal sample (black) or unstained sample (grey) present 99.5 percentile of the population signal. Note that those lines cover each other indicating their almost identical coordinates. At least 3700 cells (N>3700) are presented in each condition

### 5.5.2. STAT proteins are moderate predictors of the cytokine response, while receptors are weak.

Having established the staining method of STAT, pSTAT and receptor using flow cytometry, I proceeded with the co-staining experiments of cells stimulated with 10 ng/mL IFN- γ and 10 ng/mL OSM. I considered the pSTAT whole-cell total level as cellular responses, and the whole-cell total levels of STATs and receptors as the predictors of the response, all measured at 15 min for IFN-γ in MEF cells or 30 min for OSM in BJ cells after the beginning of the stimulation. The single-cell level of the response exhibits moderate correlation with the level of the STATs for both IFN-γ (Figure 5.19A) and OSM (Figure 5.19B), as cells with high responses tend to have higher levels of STAT proteins. In addition, the measurement showed low dependency between receptor levels and the response, as dark points corresponding to cells with high receptor levels are randomly spread throughout the point cloud. To analyze the data more quantitively, I utilized the linear regression with $R^2$ coefficient indicating the percentage of the response variance that can be explained by the levels of either STAT, receptor or both (Figure 5.19 insets). Specifically, for IFN-γ stimulated MEFs, the STAT1 level explained 37% of the response variance, while for BJ and OSM stimulation, the STAT3 level explained 50% of the response variance. The receptor levels showed low $R^2$ for both IFN-γ ($R^2$ = 16%) and OSM ($R^2$ = 19%) treatments. In addition, the multiple linear regression, correlating both STATs and receptors with the response, did not much increase the $R^2$ values neither for IFN-γ nor OSM, indicating the redundancy of both predictor values, STAT and receptors. In non-stimulated cells, the correlations were lower and both STAT and receptors contributed equally to the response variance explained (Figure 5.19C, D). To exclude the possibility that the obtained correlations resulted from STAT or receptor levels being responsive to cytokine stimulation, I validated that neither STAT nor receptor levels change after stimulation (Figure 5.20). Therefore, the whole-cell level of STATs is a moderately predictor of the response, indicating that indeed the cellular phenotype, with more features investigated, can at least partially determine the final response of the IFN-γ and OSM response.

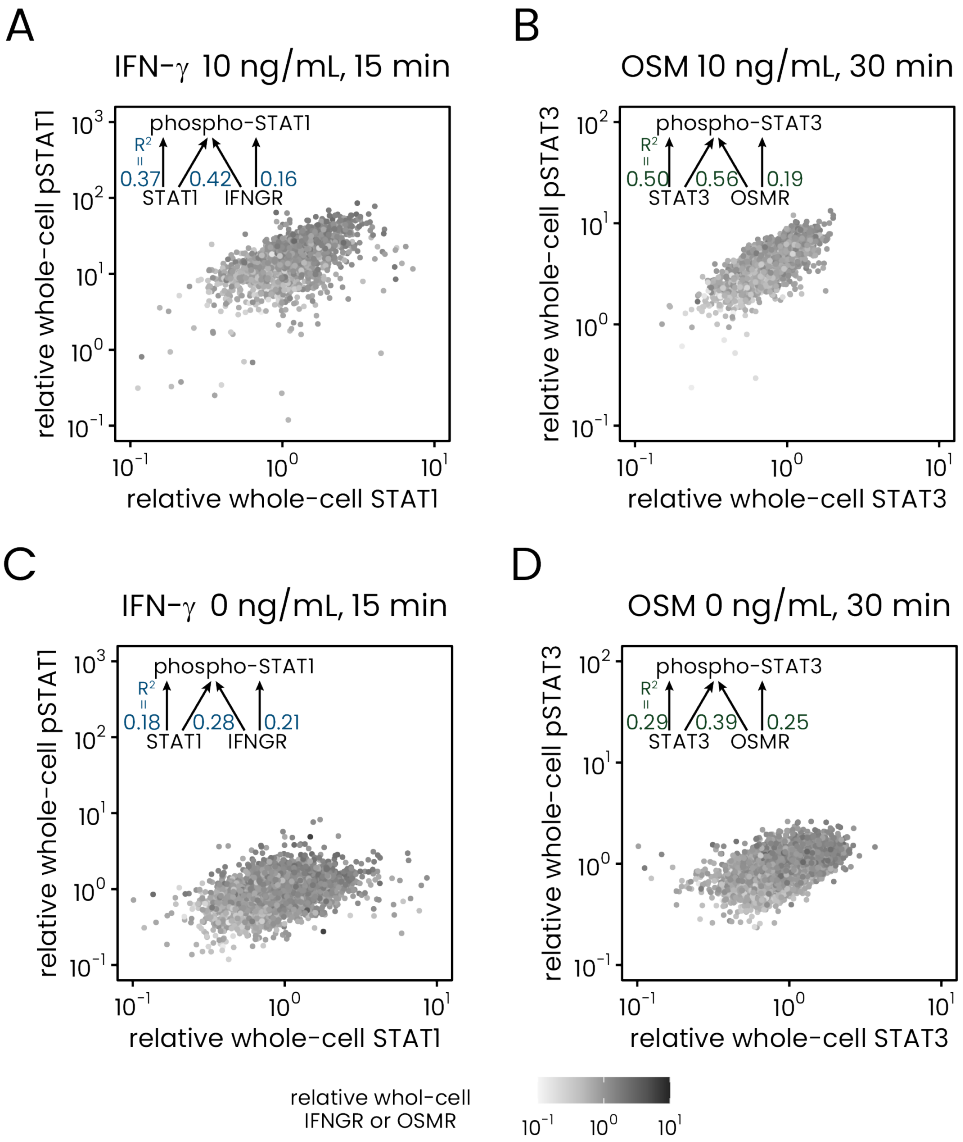


*Figure 5.19. Whole-cell level of signaling components measured intracellularly can partially predict the response to IFN-γ and OSM*

(A) Measurements of whole-cell pSTAT1 (y-axis) at 15 minutes after stimulation with 10 ng/mL of IFN-γ plotted against whole-cell STAT1 (x-axis) as measured with flow cytometry. Each point corresponds to a single cell with the shade intensity encoding the whole-cell level of the receptor component, IFNGR. The inset presents $R^2$ for a fraction of pSTAT1 variance explained by whole-cell STAT1 level, IFNGR level and the two factors jointly, as indicated by the arrows. (B) The same as in (A) but for OSM signaling: whole-cell pSTAT3 (y-axis) at 30 minutes after 10ng/ml of OSM plotted against whole-cell STAT3 (x-axis) as measured with flow cytometry. Each point corresponds to a single cell with the shade intensity encoding the whole-cell level of the receptor component, OSMR. The inset presents $R^2$ for a fraction of pSTAT3 variance explained by whole-cell STAT3 level, OSMR level and the two factors jointly, as indicated by the arrows. (C) The same as in (A) but for non-stimulated cells. (D) The same as in (C) but for non-stimulated cells.
Technical details: Measurements are expressed as the relative fluorescence. For each protein and each cell, the raw flow cytometry readout was divided by the mean fluorescence of non-stimulated cells. At least 1900 cells were measured for each condition (N≥1900). A representative of two biological replicates is shown.

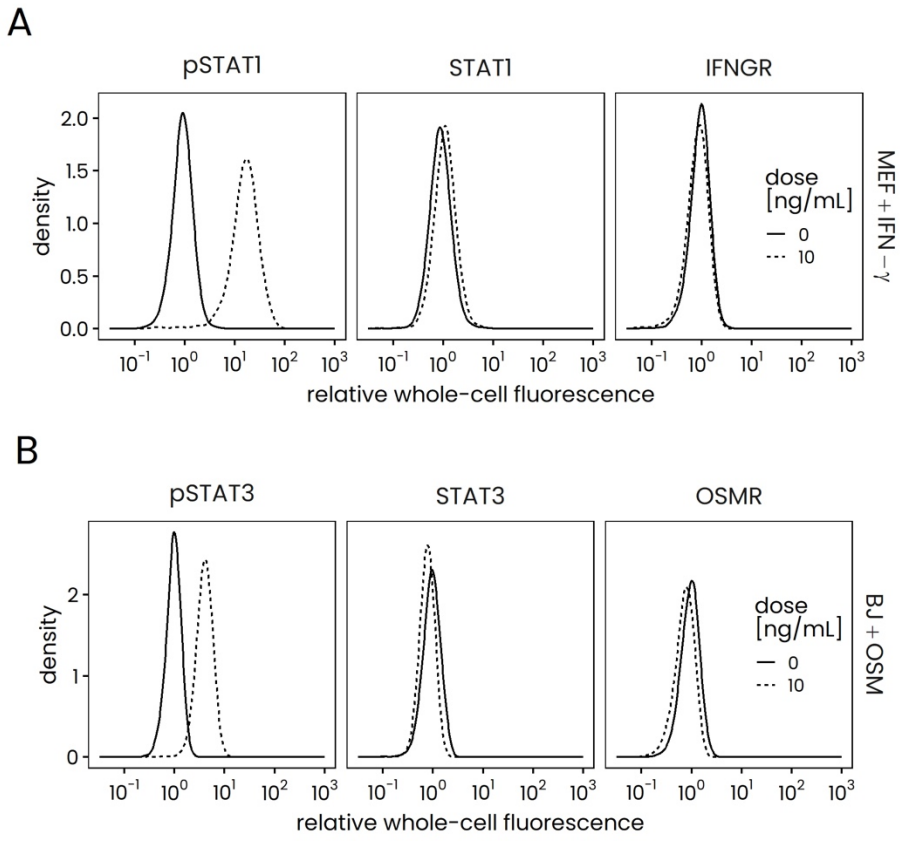


*Figure 5.20. Cytokine stimulation does not change total effector or receptor levels.*

(A) Whole-cell levels of pSTAT1 (left panel), STAT1 (middle panel) or IFNGR (right panel), as measured with flow cytometry, without stimulation (solid line) or at 15 min after 10 ng/mL IFN-γ stimulation (dashed line). (B) Whole-cell levels of pSTAT3 (left panel), STAT3 (middle panel) and OSMR (right panel), as measured with flow cytometry, at 30 min after 10 ng/mL OSM stimulation (dashed line) or without stimulation (solid line). At least 1970 cells per condition were measured (N≥1970). The small differences in distribution means in STATs and receptors were statistically important in hypothesis testing ($p < 0.0001$ for two tailed t-test on log-transformed values and K-S test) probably due to the high number of observations. However, the differences are of minor practical importance as the stimulation level explains at most 7.5% of total variance of both STAT and receptors according to $R^2$ of linear regression. In comparison, for pSTAT levels the stimulation variable explains at least 64% of the total variance.

## 5.6. The cytokine response throughout the cell cycle

The measurements of signaling pathway components indicate that cellular state can indeed be a moderate predictor of the response to cytokine stimulation. However, measuring levels of both STAT and receptors did not explain the whole response variance, indicating that there can be other factors influencing the response. One of the master cellular processes, cell cycle, could change the sensitivity of cells to the cytokine sensing or make the signaling cascade act at different speed, causing the change in the final response level. For example, cells before the DNA replication could respond at different levels than cells after the DNA replication. The chromatin condensation level is different at each of the cell cycle phase, which can influence the pSTAT molecules retention in the nucleus (Meyer et al., 2003). Also, throughout the cell cycle the volume of the cell increases at a different rate than the cell surface, pointing out the possible changed sensitivity in cells at the beginning of the cell cycle compared to cells before mitosis. To investigate this hypothesis, I combined the cell cycle phase measurement together with response measurement after cytokine stimulation on the single cell level.

### 5.6.1. Histogram of the cell cycle can be obtained using microscopy measurements

Throughout the cell cycle, the DNA replicates in phase S, leading to doubling the DNA level from phase G1 to G2 and mitosis. Therefore, one of the easiest ways to distinguish cells in the different cell cycle phases is to measure DNA content on a single cell level. Some cells will have around twice the level of DNA content (G2/M cells) as the other cells (G1 cells), with some fraction between (S cells). The DNA measurements for cell cycle staging is widely used in flow cytometry, and is based on the thresholding of the DNA content histogram. To identify the cell cycle phase of each single cell, I used a similar methodology of DNA measurement, but using fluorescent microscopy (Roukos et al., 2015). The usage of microscope, instead of flow cytometry, enables the spatial recognition of fluorescence signal and therefore allows for measuring of the cellular response to cytokine as the mean nuclear level of pSTAT instead of less biologically relevant whole-cell total level. To stage the cell cycle in single cells I fluorescently stained the DNA as usually for immunofluorescent experiments, but for image acquisition I used the epifluorescent mode (Figure 5.21A, B) instead of confocal. This ensured

the collection of the DNA signal from the whole nucleus, not only from one focal plane. The histograms of DNA content in a population of both MEF (Figure 5.21C) and BJ (Figure 5.21D) cells showed proper peaks for G1 and G2/M phases, corresponding to cells before and after DNA replication. The thresholds for each of those two phases were adjusted manually.

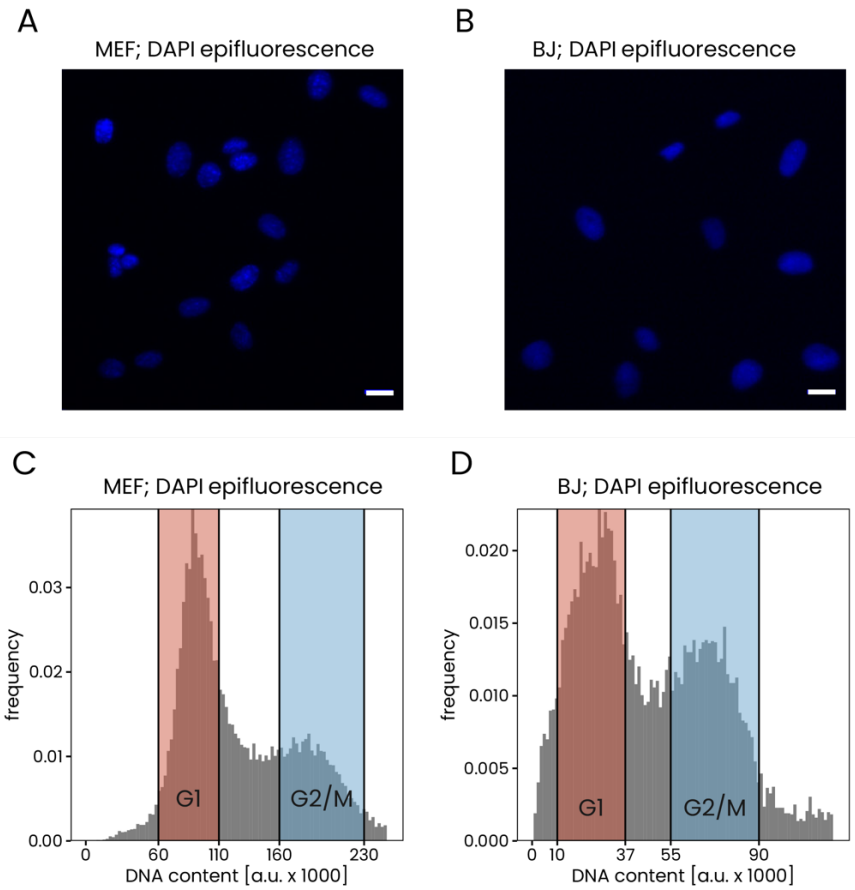


*Figure 5.21 DNA content histogram obtained during microscope image acquisition shows peaks for G1 and G2/M cell cycle phases.*

(A) Representative microscopic images of nuclei of MEF nuclei stained with DAPI and visualized in epifluorescence mode. (B) Same as A but for BJ nuclei. (C) DNA content histogram of MEF nuclei. Cells with nuclei in the red region were classified as G1 cells and classified as G2/M cells if found in the blue region. Threshold adjusted manually. (D) Same as C but for BJ cells. Scale bars 20 um. At least 13000 cells are presented in each histogram.

To validate the correctness of the cell cycle phases identification, I next combined the DNA measurement with immunofluorescence of the cyclin B protein, known to be upregulated in G2/M phases. Indeed, the level of cyclin B, measured as the mean relative fluorescence of the cellular area, was higher in cells of G2/M phases compared to G1 cells (4-fold increase for MEF cells and 3-fold increase for BJ cells), proving the correctness of the cell cycle discrimination with this method.

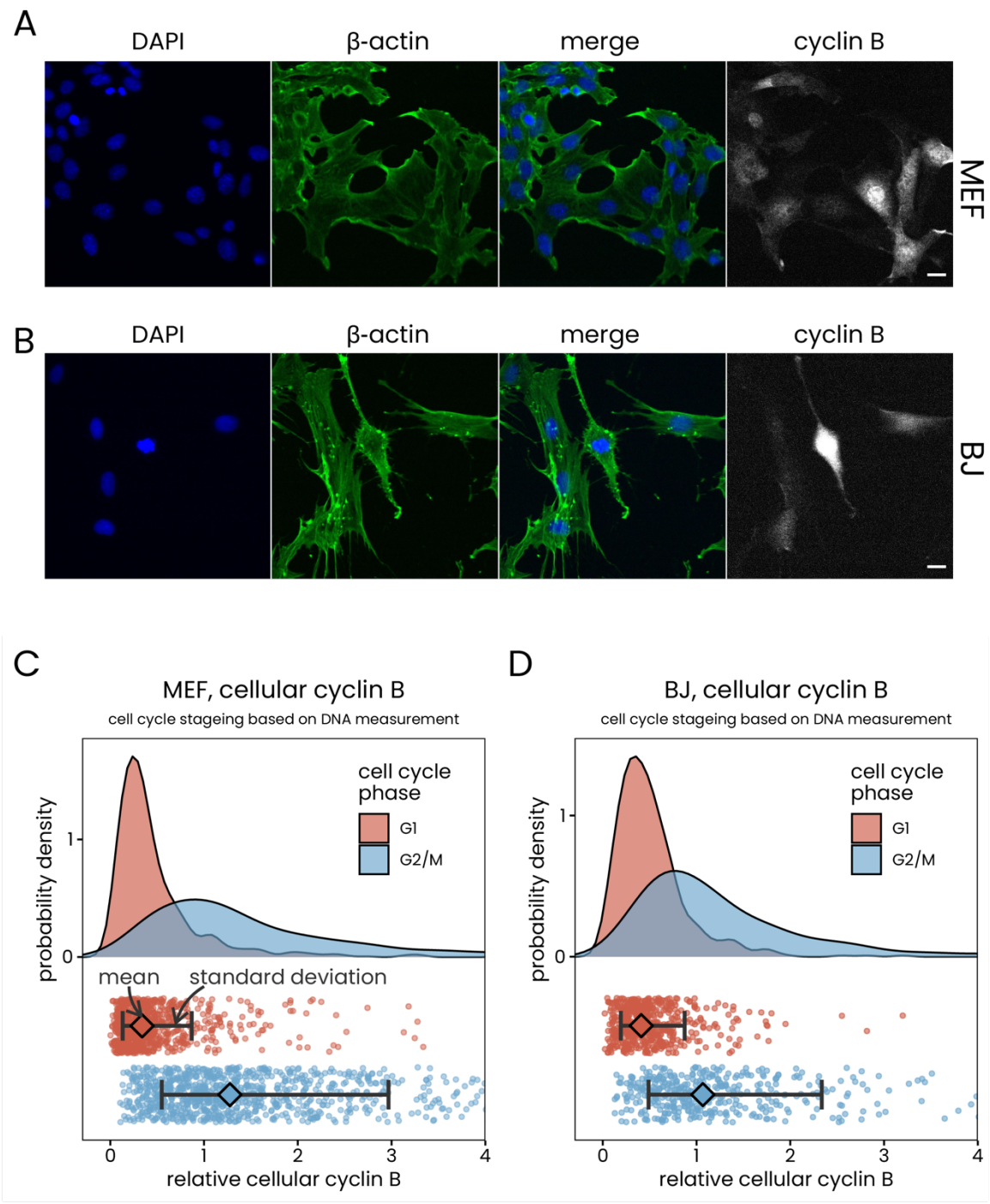


*Figure 5.22 The microscopic staging of the cell cycle phases is sensitive to cyclin B increasing level in G2/M phase.*

(A) Representative microscopic images of nuclei of MEF cells with nuclei stained with DAPI, the cellular body immunostained against B-actin and immunostained against cyclin B. DAPI channel was visualized in epifluorescence mode while B-actin and cyclin B in confocal mode. (B) Same as A but for BJ cells. (C) MEF cells were staged according to the cell cycle phase and probability density of cyclin B cellular intensity was plotted for G1 cells (red) and G2/M cells (blue). In addition, below the density plots, the jitter plot with the mean (red or blue squares) and standard deviation of the data is presented, assuming log-normality of the data. The cyclin B value was normalized to the mean level of the whole population ("relative"). (D) Same as C but for BJ cells. For C and D: $p<0.0001$, two-tailed t-test (log-transformed data) and K-S test. Scale bars 20 um. At least 416 cells were analyzed in each density plot. A representative of two biological replicates is shown. The cell cycle phase explains 28% of total variance in BJ cells and 35% in MEF cells according to $R^2$ of linear regression on log-transformed data.

### 5.6.2. Cell cycle phases show similar levels of the cytokine responses

Next, to investigate whether cells before DNA replication (G1 cells) respond differently to cells after DNA replication (G2/M cells), I stimulated MEF cells with IFN-γ (Figure 5.23A) and BJ cells with OSM (Figure 5.23B) with the dose of 10 ng/mL and analyzed their nuclear pSTAT levels together with cell cycle phase discrimination. Surprisingly, data shows no big differences between G1 and G2/M cells in terms of responses to cytokines of MEF (Figure 5.23 C) and BJ cells (Figure 5.23D), pointing that the cellular response is robust to progression in the cell cycle. This can be due to the fact that one of the main predictors of the response, STAT levels, presumably also did not differ throughout the cell cycle as well. Indeed, simultaneous measurements of mean cellular level of STAT1 in MEF cells (Figure 5.23E) and STAT3 in BJ cells (Figure 5.23F) also showed no substantial differences between G1 and G2/M phases, indicating that the cell probably keeps the constant concentration of STATs during the progression in the cell cycle, assuring the similar responses in all cell cycle phases.

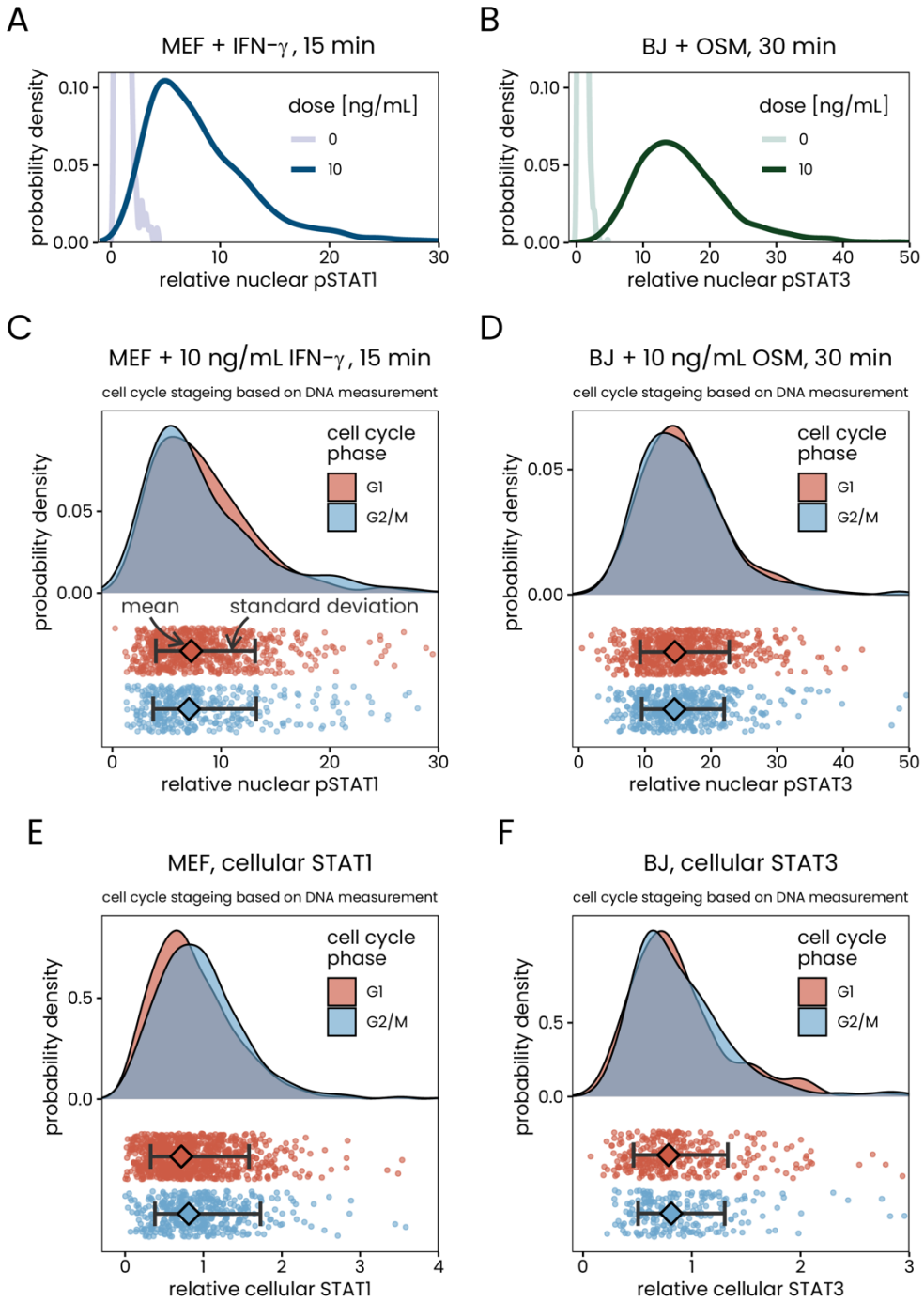


*Figure 5.23. Cellular response to cytokines is robust to cell cycle progression*

(A) The quantification of nuclear pSTAT1 level in nuclei of MEF cells stimulated with 10 ng/mL of IFN-γ for 5 min or left unstimulated and immunostained after 15 since the beginning of stimulation. The pSTAT1 value was normalized to the mean level of the untreated cells ("relative"). (B) Same as A, but for BJ cells stimulated with 10 ng/mL OSM and immunstained against pSTAT3 after 30 min. (C) MEF cells stimulated with 10 ng/mL of IFN-γ were staged according to the cell cycle phases and probability density of pSTAT1 nuclear intensity was plotted for G1 cells (red) and G2/M cells (blue). In addition, below the density plots, the jitter plot with the mean (red or blue square) and standard deviation of the data is presented, assuming log-normality of the data. (D) Same as C but for BJ cells. (E) Same as C, but for cellular STAT1 level in non-stimulated MEF cells. (F) Same as D but for cellular STAT3 level in non-stimulated BJ cells. At least 223 cells (N>223) were analyzed in each density plot. A representative of two biological replicates is shown. Statistical difference occurred only for E ($p<0.001$ for both two-tailed t-test for log-transformed data and K-S test), however, the difference in means is of minor importance as the cell cycle phases explain 0.5% of total variance of STAT1 level according to $R^2$ of linear regression on log-transformed data. For STAT3 and pSTATs levels $p > 0.1$ and the cell cycle phases explained at most 0.1% of total variance.

# 6. Discussion

Cellular responses to external stimuli are often characterized by high cell-to-cell heterogeneity, despite the same genetic background of the cells and the same culturing conditions. While it is nowadays getting clearer and well known that such heterogeneity of cellular communication is an inevitable trait of all populations of cells, very little is known about the causes of the observed high cell-to-cell heterogeneity of cellular responses to extracellular signals. It was debated, for example, to what extent the response is predetermined (influence of cellular phenotype) or stochastic (influence of molecular noise) (Koseska and Bastiaens, 2017; Madsen and Vanhaesebroeck, 2019; Wollman, 2018). My study involving IFN-γ and OSM on mice and human fibroblasts showed that the majority of the cell-to-cell heterogeneity of responses to cytokines is induced by the variability in molecular phenotypes of single cells, and not by molecular noise or measurement error, indicating high signaling precision of individual cells (Topolewski et al., 2022). I also found that among various traits of cellular phenotype, the levels of response-related proteins can partially predict the strength of the response, while the cell cycle has no influence on the response strength prediction.

## 6.1. Precision of a single cell

The precision of a cell seems to be crucial in multicellular organisms like mammals in which a great number of cells need to coordinate their activities through cell-to-cell communication so that the whole organism survives, properly develops, fights threats and adjusts to the environment. The precision of a cell in signal sensing and processing has been recently studied in terms of information theory which quantifies how much information about the stimulation doses can be encoded in the responses (Uda, 2020). The analysis of multiple signaling pathways ranging from NF-κB (Cheong et al., 2011), through TRAIL (Suderman et al., 2017), GnRH (Garner et al., 2016), Erk and $Ca^{2+}$ (Selimkhanov et al., 2014) show that a single cell barely distinguishes between absence and presence of the high dose of the stimulant, due to high heterogeneity between cells in their responses. To explain how a multicellular organism can function with such variability, the sources of observed heterogeneity of cellular reactions should first be revealed. In my study, as biological models, I used IFN-γ and OSM, two

cytokines vastly involved in immune response via JAK-STAT signaling pathway, with IFN-γ utilizing STAT1 while OSM utilizing STAT3 as main effector proteins. Using immunofluorescence, confocal imaging and single cell image analysis I confirmed that after cytokine stimulation, each STAT protein is tyrosine phosphorylated and translocated to the nucleus. However, in terms of information theory dose discrimination, pSTAT nuclear levels showed much greater ability to decode the stimulation doses compared to STAT nuclear levels. This can be explained by the higher basal level of STATs in the nucleus than the basal level of pSTAT. Precisely, both STAT1 and STAT3 constantly shuttle between cytoplasm and nucleus even without any stimulation (Cimica et al., 2011; McBride and Reich, 2003; Reich, 2013). After the stimulation, not all of STAT molecules in the nucleus have been moved to the nucleus due to stimulation, as some of them are nucleus-translocated before the stimulation, limiting the dose discrimination ability. On the other hand, pSTAT molecules before an external stimulation are present in the nucleus only marginally, as phosphorylation of pSTAT molecules is done mainly during JAK kinase activation and only low amount is detected experimentally without any stimulation (Bachmann et al., 2014; Gough et al., 2014; Majoros et al., 2016). After the stimulation almost all pSTAT molecules in the nucleus are related to the stimulation, assuring proper dose discrimination. Similar phenomena were found also in other signaling pathways, utilizing response dynamics during live cell imaging. For example, accounting for fold change instead of absolute values of nuclear transcription factors ensured higher information transfer of NF-κB (Lee et al., 2014; Zhang et al., 2017) as well as TGF-β (Frick et al., 2017). This can be explained by minimizing the influence of already existing molecules in the nucleus. Therefore, when considering the optimal measurement output for the best dose discriminability after stimulation, one should choose the one with the low enough basal level before the stimulation, assuring that the majority of the response is strictly related to the stimulation itself and not to, e.g., non-specific stimulation. Such output for the IFN-γ and OSM signaling pathways studied here were pSTAT levels in the nucleus, and not STAT levels. The tyrosine-phosphorylated forms of STATs were also considered as more cytokine response-related in other works, for example, investigating the heterogeneity of cytokine responses in cancer cells (Gough et al., 2014) or relating multiple signaling pathways during innate immunity (Czerkies et al., 2018).

The precision of a cell to sense the external signal is limited by the influence of molecular noise, that is the stochasticity of the biochemical reactions. My study using bi-nuclear syncytia with two nuclei and one shared cytoplasm showed that molecular noise contributes less than 10% of the cell-to-cell variance of signaling responses, indicating that the single cell is very precise in signal sensing and processing. The remaining variability, ~90%, can be attributed to differences in the molecular content of the cells, i.e., cellular phenotype. The presented quantification invites to revisit the view of stochastic effects in biochemical signaling and indicates that signaling in single mammalian cells can operate not far from the deterministic regime. The presented results are in line with some recent studies that measured repeated signaling responses in the same cell over time. Specifically, those studies attempted to assess the contribution of molecular noise and cellular phenotype into the total observable variability. The electric pulse study performed such decomposition by comparing the variance of responses to the same dose in each individual cell vs variance of the cellular responses of all cells (Wada et al., 2020). The decomposition revealed that the majority, that is 83%, of total variance was attributed to cellular phenotype variability. This indicates that in the biological model used, that is myotubes stimulated with electric pulse, the observed heterogeneity of $Ca^{2+}$ responses is caused mainly by differences in cellular states in the population. Similar decomposition values were obtained in a study utilizing live cell imaging of ERK signaling, which quantified the intrinsic-to-extrinsic noise ratio in the quasistationary time regime after the stimulation (Selimkhanov et al., 2014). The intrinsic noise was estimated as the mean variation between successive ERK measurements of the individual cells, while the total variance was estimated as the variance of the single cell trajectory around the average of the all trajectories. The resulting calculations showed that the intrinsic noise, or molecular noise, constitutes around 2%, while the cellular phenotype 98% of the total variance. However, fluctuations in a quasi-steady state do not have to properly reflect the fluctuation in the initial phase of the response, where most of the signaling-related reaction occurs. All the described variability decomposition proportions are very close to the one obtained in this dissertation, using bi-nuclear syncytia. Nevertheless, some other heterogeneity decomposition showed different quantities. For example, when ERK signaling pathway was repetitive stimulated by the light in the optogenetic system, measured using live-cell imaging (Toettcher et al., 2013) and analyzed quantitively (Selimkhanov et al., 2014), the molecular noise was accounted for the ~ 47% of the total variance. The difference can be attributed to the complexity of the

optogenetic system, composed of multiple genetically engineered proteins which all enabled the clever control of stimulation, but at the same time it bore the potential of not controlling the all-possible variables in the system. The bi-nuclear syncytia system is free of this disadvantage as the response of two nuclei are easy to compare, analyze and conclude. Furthermore, it allows for extending the heterogeneity decomposition to other cell signaling pathways, like growth factors, hormones, and other cytokines, which often operate in a too long regime for repetitive stimulation. This approach also allows for live imaging, giving the possibility of analyzing the stochasticity in a time-dependent manner. In addition, the analysis of non-specific staining in bi-nuclear syncytia as well as heterogeneity decomposition in early time points after the stimulation showed, that two nuclei are probably independent on each other, ruling out one of the drawbacks of repetitive stimulation which is the dependency of the subsequent measurements. On the other hand, unfortunately, bi-nuclear syncytia offer the possibility to analyze only two nuclei in the same cytoplasmic environment, compared to multiple repetitive stimulation of the same cell. However, further expanding this biological model can lead to creation of multiple-nuclei syncytia, allowing for more representative response measurements. Nevertheless, it is crucial to mention some drawbacks of the used bi-nuclear syncytia biological model. Many of the signaling pathways do not involve nuclear accumulation of the transcription factors, for example during $Ca^{2+}$ signaling, which regulates the entry and exit of $Ca^{2+}$ from various cellular compartments (Clapham, 2007). For such signaling pathways, the bi-nuclear syncytium would not be a suitable approximation of two identical cells, as they do not utilize nuclei as the main effector place. In addition, if the movement of the pSTAT molecules were chaotic, for example utilizing extremely fast diffusion, then all the pSTAT molecules quickly after the stimulation would be evenly distributed in the cytoplasm. In that situation, if any randomness of the signaling pathways occurs, then only the randomness related to nuclear import would be reflected in differences between two nuclei. Although the directional movement of pSTAT molecules is yet to be confirmed, some studies showed the involvement of cytoskeleton in the STAT1 and STAT3 signaling and nuclear transport (Guo et al., 2018; Supasai et al., 2017), the similar behavior of some transcription factors like p53 (Campbell and Hope, 2003) or NF-κB after specific stimulation (Fazal et al., 2007). The involvement of cytoskeleton in STAT signaling suggests the more complex and directional movement of pSTAT1 and pSTAT3 molecules than simple diffusion, which all would enable to consider the bi-nuclear syncytia as a valuable model of

investigation of the molecular noise. If the movement of pSTAT molecules are directional and at the time of stimulation no substantial number of those molecules mix in the cytoplasm, then any stochasticity occurring near one nucleus would manifest in the signal of that nucleus. The same is true for the second nucleus as well, enabling the simulating the two-identical cells setup and the proper estimation of molecular noise. Apart from that, it would be of great interest to confirm experimentally in more detail the usefulness of the bi-nuclear syncytia system in the studying the sources of cell-to-cell heterogeneity of cellular responses.

Taking together, the decomposition of the cytokine response heterogeneity can be successfully determined using bi-nuclear syncytia under some assumptions. Also, the bi-nuclear syncytia together with other studies on the information transmission point that the single cell is very precise in signal sensing, and operates close to deterministic manner. Such conclusion can be a foundation on the further research, where little space will be left for the stochasticity, uncertainty or unpredictability of the cellular responses to external stimulation, allowing for finding the full determinants of the too-high or too-low signaling outcomes in cancer cells or in patient-derived cells with some signaling-related diseases.

In addition to the quantification of the sources of the cell-to-cell variability, the data presented in this dissertation delivers several other interesting observations. These include the linear relation of noise to the level of the response. Precisely, the inter-nuclear standard deviation of bi-nuclear syncytia equals ~11% of the response. This measurement can be further employed by theoretical models to examine signaling fidelity in more detail and to find the limit of dose discriminability of single cells. Specifically, if we assume that the only variability of the response in a single cell is the molecular noise constituting 11% of the response, and that a single cell has a dose response curve estimated as a specific percentile of the whole population, then the dose discriminability reaches almost optimal values, easily recognizing around 4 doses of a stimulant. Even higher dose decoding could be obtained if more doses were analyzed or assuming a continuous stimulation. All these results are in great contrast to calculations of dose discriminability done previously (see Literature review 2.5). At the same time, a conclusion that a single cell can reliably distinguish between multiple stimulant doses has already occurred in the literature multiple times, especially in repetitive stimulation research (see Literature review 2.8.4). These apparent discrepancies do not come from the

weakness of experimental design of the former studies, but rather show the weaknesses of the information theory reasoning. Traditionally, the cellular phenotype variability has been considered as the extrinsic noise, which in the information theory reasoning causes a loss of information about the input signal along the signaling relay. Therefore, information theory applied to a population of single cells leads to low information flow, as single cells show a great variability of cellular phenotypes and low molecular noise contribution. The same low information flow would be obtained from the population of largely stochastic responses (Nienałtowski et al., 2021; Topolewski and Komorowski, 2021). However, those two scenarios differ substantially- in the first, with phenotypic variability as the main source of response variability, the single cell is very precise, while in the second scenario, where the molecular noise is predominant, the single cell is mainly random and not reliable in terms of the response to the stimulation. I proposed in this dissertation, that information loss by the signaling apparatus of the single-cell result only from the molecular noise. Therefore, instead of applying information theory to a population of single cells, one should utilize for example the FRA analysis together with quantification of the overlaps between distributions specific to different doses. Such an approach allows for the conclusion that some fraction of cells responded typically or atypically to given doses, giving more precise and biologically relevant information than information theory.

The decomposition of total response variability into molecular noise and phenotypic variability in the bi-nuclear syncytia has certain shortcomings that should be accounted for. Primarily, the decomposition does not take into account the experimental measurement error. Measurement noise as being statistically roughly independent for each nucleus quantifies in the above as molecular noise. Secondly, in the syncytium, the molecular content of the two nuclei is different, as these originate from two different cells. Different nuclear content can potentially contribute to the differences in responses between the two nuclei and therefore also quantifies in the above as molecular noise. Therefore, within the proposed methodology the contribution of the molecular noise can be overestimated, as it encompasses other factors. Although the activity of phosphatases investigated here did not influence the decomposition substantially at early time points since the stimulation, it does not exclude the possibility that other factors of nuclear phenotypes are quantified as the molecular noise at early time points. For example, STAT proteins enter the nucleus via nuclear

por complexes (NPCs) (Jerke et al., 2009; Liu et al., 2005), structures anchored in the nuclear membrane (Tran and Wente, 2006). The differences in levels of NPCs between two nuclei in the syncytium can influence the response independently on each nucleus, which is not related to the molecular noise. Similarly, the shape of the nucleus can also matter as well as its size, as the morphology of the fibroblast nucleus can vary (Skinner and Johnson, 2017). All those components need more insight during investigating their role as variability sources. Nevertheless, if such a role was confirmed, it would only indicate that the influence of molecular noise was overestimated using bi-nuclear syncytia, proving that a single cell is even more precise than estimated in this dissertation. In addition to the nuclear phenotype, measurement error is an inevitable trait of all measurements. In fluorescence microscopy, the error can come from the specimen itself, from the microscope or from the detector (Wolf et al., 2013). For example, the number of photons measured during microscopy image acquisition has an intrinsic uncertainty called photon noise. On the other hand, the antibody binding to a specific target is also subjected to some stochasticity, as the antibody binding occurs on a molecule level independently for each measuring entity, for example a cell. However, those stochastic and in principle independent events are less prominent and they less influence the uncertainty of the measurement in samples with high abundance of targets and therefore with high signals. For example, the photon noise scales with the square root of detected photons, therefore should be negligible in measurements where more photons are collected (Waters, 2009). Similarly, the error related to antibody binding will be minimized if the optimized time of incubation is applied, giving enough high signal. In addition to all of that, the measurement error can be also caused by differences in image analysis, especially if it is manual or semi-automated. I presented the measurement error quantification based on the bi-nuclear syncytia with the two nuclei with merged nucleoplasm. It showed that the measurement error has a minor, but not negligible contribution to the strength of the measured signal, reaching ~10% of the measured signal. However, this quantity is probably influenced by the semi-automated image analysis applied during the data analysis, overestimating the true error of the stochastic events on the particle- or molecule level. Nevertheless, it also indicates that the contribution of molecular noise also could have been overestimated due to measurement error. However, subtracting the contribution of the measurement error from the contribution of the molecular noise is not straightforward. This is because of different models and assumptions used, which make the direct comparison

difficult. However, the obtained data suggest, that the molecular error causes the molecular noise to be overestimated in the used setup. This in turn indicates that a single cell actually can operate in a deterministic, or close to deterministic regime in signal sensing, at least in IFN-γ and OSM signaling, with this claim being of great novelty.

Among questions inspired by the presented data, the issue of phenotypic variability appears to be particularly puzzling. In light of the current understanding of stochasticity in gene expression, the molecular content of the cell is partly shaped by random processes (Hagai et al., 2018; Symmons and Raj, 2016). It is not clear, however, whether or how cells account for variability in their molecular content when interpreting outcomes of signaling processes. Conceivably, in some cases, different signaling outcomes to the same input signal are interpreted in the same way in different cells. This could be achieved, for instance, by mechanisms that ensure robustness to copy number variability of signaling components, e.g., via counterbalancing correlations or bi-directional enzymes (Hart et al., 2011; Shinar et al., 2007). For example, it has been shown that cells do not sense the number of active G-protein-coupled receptors (GPCRs) receptors but their fraction (Bush et al., 2016). This ensures the robustness of signaling to the variability in the copy number of receptors. In other instances, different signaling outcomes to the same input signal could be interpreted differently in different cells. The latter seems to be the case for the two cytokines considered here, as individual cells differ significantly in their sensitivity to these stimuli. Different sensitivities could contribute to the mechanism of inflammation control or in a wider context, could constitute a bet-hedging strategy against the unpredictability of future environmental states(Carey et al., 2018; Kussell and Leibler, 2005). Clearly, the role of different cellular identities is not fully understood. Nevertheless, the high precision of a single cell opens up the possibility to find the determinants of the response. With such determinants, one would be able to specifically downregulate the highly activated signaling pathway, characteristics of many diseases, for example cancers and autoimmune diseases. It is only the identification of such determinants, which separates us from the treatment success. Fortunately, for IFN-γ and OSM signaling pathways, some of the determinants have been found throughout in the studies presented in this dissertation.

## 6.2. Determinants of the cytokine stimulated response

Molecular content of the cell is composed of distinct components, which can be often experimentally quantified. Therefore, the factors that impact differences in cellular responses can be in principle determined with dedicated experiments. Finding response determinants would provide valuable understanding into how signaling pathways function. I investigated three such presumably determinants: phosphatase level, the cell cycle, and the level of intracellular signaling proteins, with phosphatase activity and the level of intracellular STAT proteins being considerable predictors of the response.

I showed that the activity of phosphatases was at least partially responsible for differences in pSTAT levels among two nuclei of bi-nuclear syncytia after a long time since the stimulation with IFN-γ. The usage of a non-specific phosphatase inhibitor, $Na_2VO_4$, or vanadate, diminished those differences, proving that it could be the main source of single cell differences in their responses at late time points. The differences did not decrease to the base level, probably due to lack of specificity in the inhibitor activity, although the vanadate inhibitor was shown to be highly specific for phosphatases regulating JAK-STAT signaling pathways (Baron and Davignon, 2008; Haspel and Darnell, 1999). However, there is also a possibility that the inhibitor was indeed specific and blocked the majority of active phosphatase, but other factors at the very late time points differed between nuclei, or the stochasticity of the biochemical reactions indeed took over the signaling process. For example, some putative binding partners of STAT molecules could be activated in late time points after stimulation, which would decrease the ability to detect the STAT1 molecules by immunostaining. On the other hand, at the late time points, the pSTAT import process could be of lower intensity and therefore subjected to more stochastic fluctuations leading to differences between two nuclei even when the phosphatase activity level was equalized by the inhibition. Nevertheless, more studies are needed to prove which of the mentioned factors matter. However, the dephosphorylation process influences the response late after the stimulation and therefore influences the temporal dynamics of the response, which could greatly impact the cell decision. For example, it was shown that IFN-α and IFN-β, two examples of type I IFNs, have different temporal dynamics of the response. Precisely, IFN-α causes a cellular response of shorter duration than IFN-β, which in turn leads to lower expression of the long response

genes (“tunable genes”) compared to IFN-α (Schneider et al., 2014; Schreiber and Piehler, 2015). Such differences could also occur between single cells having long- or short-lasting responses, with different genes activated after the same stimulation of IFN-γ. Those differently activated genes can contribute to a broader sensitivity rate of a cellular population to various threats, e.g., different bacterial pathogenicity or replication rate (Lane et al., 2019). In addition, the inefficient dephosphorylation of mutated pSTAT1 was found in chronic mucocutaneous candidiasis disease (CMCD) (Liu et al., 2011), implying that the impaired dephosphorylation of pSTAT1 molecules could be a disease-causing agent and it is to be determined whether this can be controlled pharmacologically. Further studies regarding phosphatase process in JAK-STAT cellular signaling is needed to prove a direct correlation of the phosphatase activity with the dynamics of pSTAT nuclear level, especially for late time points, which could presumably change the further specific gene expression.

The next analyzed component of the cellular phenotype was the level of the intracellular levels of whole-cell STAT molecules and receptors. STAT levels were found to be moderate predictors of the response, while receptors showed weak predictability. The small prediction power of receptors could be an effect of measuring of intracellular receptors, which is less biologically relevant than membrane receptors. However, this type of experimental setup was necessary to increase the fluorescent signal above the noise level. More accurate measuring of the receptor level by the usage of the fluorescently labeled receptor proteins could increase the predictor power. Similarly, instead of focusing on the receptors, one could use the immunostaining against the intracellular cytokine itself, which should present biologically more relevant measure of the receptor activity, due to the internalization of such molecules in a complex with receptors (Anderson et al., 1983; Blanchard et al., 2001; Blouin and Lamaze, 2013; Zanin et al., 2021). Nevertheless, all those approaches either use more sophisticated fluorescent systems (Chmiest et al., 2016; Wilmes et al., 2015) and are of great risk due to the complexity of experimental design or low number of presumably cytokine molecules found in the cell. In contrast, STAT levels were properly measured as intracellular proteins and they showed higher response prediction ability. Similar conclusions correlating the cellular response with the level of intracellular proteins was drawn in previous studies on $Ca^{2+}$ signaling (Yao et al., 2016) and heat shock response (Guilbert et al., 2020). Such correlations of the response with the level of other proteins can have profound implications, e.g., in

medicine. Recently it was found that the cellular level of STAT1 is a good prognostic factor for overall survival in specific tumors (Zhang et al., 2020). The JAK-STAT signaling pathway is often dysregulated in cancer cells (Brooks and Putoczki, 2020). It is therefore promising to find other predictors of the JAK-STAT activity, to either inhibit/stimulate as a treatment or to use those factors as predictors of the current treatment or the expected overall survival. In summary, total whole cell measurement of STAT levels showed at least moderate prediction power, providing a good starting point for investigation of other cellular phenotype features, for example the cell cycle.

The last feature of the cellular phenotype which was assumed to be a predictor of the cellular response to IFN-γ and OSM was the cell cycle progression. However, I showed that the cell cycle progression did not contribute to differences in pSTAT levels between single cells. After comparing the distribution of the IFN-γ or OSM response in cells being before DNA duplication (G1 cells) to being after DNA duplication (G2/M cells), no evident differences were observed neither in the shape of the distribution nor in the means. This is non-obvious, if not surprising, observation because it means that despite substantial cell-to-cell heterogeneity of IFN-γ and OSM responses at the single cell level the signaling process is robust to the cell cycle. This is probably assured by keeping the similar concentration of the signaling proteins in a cell throughout the cell cycle, which I indirectly showed to be true for STAT molecules. This result of similar STAT abundance throughout the cell cycle phases is in contradiction with the work of Gao et al. (Gao et al., 2015), which analyzed the cellular localization of the STAT1 molecules in different cell cycle phases. They showed that the STAT1 abundance is substantially higher in the G1 cells compared to G2 cells. Although there is a non-debatable achievement of this study in the cellular localization and clustering of STAT1 molecules, I see some inaccuracies in the data presentation of this publication. Precisely, the authors considered the total number of STAT1 molecules per cell as the measure of the STAT1 abundance. Such measures, however, could indeed be increased in G2/M cells as they are simply bigger in size than G1 cells (Ginzberg et al., 2015, 2018). However, cell volume to some extent correlates with protein abundance (Cookson et al., 2009; Lin and Amir, 2018), causing the bigger in size G2/M cells to have similar concentration of the protein as G1 cells, which inevitably causes the higher number of molecules per cell in G2/M cells. Therefore, the cellular concentration seems to be a better measure to analyze whether the STAT1 changes throughout the cell cycle, as used in

my study. In addition, Gao et al. analyzed only 20 cells in total, which may be too small to draw robust conclusions, compared to more than 500 used in my study. In total, although STAT1 can indeed form different forms of clusters in different cell cycle phases, it seems unlikely that the mean cellular level or concentration changes throughout the cell cycle progression. In addition to that, the stimulation by IFN-γ and OSM is well known for their inhibition of the cell cycle progression, however this activity is observed after long continuous stimulation exceeding 24h (Kano et al., 1997; Klausen et al., 2000), therefore has no direct effect on quick responses analyzed in this dissertation. To summarize, I showed the robustness of the JAK-STAT signaling to cell cycle progression, which suggests that cell-to-cell heterogeneity may play a relevant biological role or have not been evolutionary eliminated for some important, and so-far rather obscure, reasons. For example, the cell cycle progression involves changes in multiple master features of a cell, for example cellular shape, gene expression, relaxation of the chromatin or cytoskeleton rearrangement (Poon, 2016). If the multicellular organism evolved to operate with cells responding uniformly, then any big deviation in the cell cycle progression and therefore in master cellular features could lead to frequent and unexpected outlier response. Such an unexpected response of a group of cells could easily move the naive organism out of the homeostasis. Therefore, multicellular organisms probably evolved to diminish the influence of the outlier responses by being used to it. Nevertheless, the cell cycle progression is regulated with multiple steps of feedback loops, protein interactions and posttranslational modifications, all having their own signaling pathways, with the input often being of intracellular nature. It would be of great interest to investigate the precision of such signaling pathways in terms of cell cycle regulation with respect to internal input- cell fate decision regime. For example, it was shown in unicellular yeasts, that the single cell decision to proliferate or to arrest in the cell cycle is greatly predicted by the single value of the concentration of the Whi5 protein in the nucleus. Such studies for multicellular organism, although very challenging and requiring the usage of intracellular input markers (Hansen and O'Shea, 2015; Ruiz et al., 2018), would show how much precise is the single in complex system with such great orchestrate of regulatory components to decide about its proliferation fate.

In summary, the presented work shows that outwardly identical cells represent different cellular phenotype features, with each cell sensing extracellular information differently. Therefore, it will be meaningful to study the structure and role of these phenotypes in more

detail, in contrast to a scenario in which differences between cells in cellular signaling have a stochastic, less palpable origin. Specifically, it appears that intracellular signaling pathway components could to some degree predict the responses of individual cells. Overall, my study appears to be indicative for further studies aiming to establish key determinants of single cell responses.

# 7. Summary and conclusions

The presented studies allowed for the revealing of sources of the cell-to-cell heterogeneity of cellular responses to IFN-γ in mouse fibroblasts and OSM in human fibroblasts and showed that:

I. Phenotypic variability accounts for ~90% of the cell-to-cell heterogeneity in IFN-γ and OSM signaling responses, while molecular noise accounts for up to ~10%.
II. Measurement errors have a minor contribution to the observed level of immunofluorescence signals, reaching ~10% of the true signal.
III. Nuclear state at late time points contributes to the cell-to-cell heterogeneity of signaling responses to the IFN-γ stimulation, while in OSM signaling responses it has no effect.
IV. Intracellular levels of STAT proteins moderately predict the signaling responses to IFN-γ and OSM stimulation, while the intracellular level of receptors are weak predictors of such responses.
V. Cells before and after DNA replication show a similar level of signaling responses to the IFN-γ and OSM stimulation, presumably due to lack of differences between STAT levels.

# 8. References


1. Abbas, A., Lichtman, A., and Pillai, S. (2017). Cellular and Molecular Immunology 9th Edition (Elsevier).
2. Aggarwal, B.B., Kunnumakkara, A.B., Harikumar, K.B., Gupta, S.R., Tharakan, S.T., Koca, C., Dey, S., and Sung, B. (2009). Signal Transducer and Activator of Transcription-3, Inflammation, and Cancer. Annals of the New York Academy of Sciences *1171*, 59–76.
3. Altschuler, S.J., and Wu, L.F. (2010). Cellular Heterogeneity: Do Differences Make a Difference? Cell *141*, 559–563.
4. Anderson, P., Yip, Y.K., and Vilcek, J. (1983). Human interferon-gamma is internalized and degraded by cultured fibroblasts. J Biol Chem *258*, 6497–6502.
5. Antebi, Y.E., Nandagopal, N., and Elowitz, M.B. (2017). An operational view of intercellular signaling pathways. Curr Opin Syst Biology *1*, 16–24.
6. Auguste, P., Guillet, C., Fourcin, M., Olivier, C., Veziers, J., Pouplard-Barthelaix, A., and Gascan, H. (1997). Signaling of Type II Oncostatin M Receptor*. J Biol Chem *272*, 15760–15764.
7. Bachmann, S.B., Frommel, S.C., Camicia, R., Winkler, H.C., Santoro, R., and Hassa, P.O. (2014). DTX3L and ARTD9 inhibit IRF1 expression and mediate in cooperation with ARTD8 survival and proliferation of metastatic prostate cancer cells. Mol Cancer *13*, 125–125.
8. Balaguer, P., and Ibeas, A. (2021). Optimal averaging time for improving observer accuracy of stochastic dynamical systems. Isa T *108*, 207–219.
9. Bar-Even, A., Paulsson, J., Maheshri, N., Carmi, M., O'Shea, E., Pilpel, Y., and Barkai, N. (2006). Noise in protein expression scales with natural protein abundance. Nat Genet *38*, 636–643.
10. Baron, M., and Davignon, J.-L. (2008). Inhibition of IFN-gamma-induced STAT1 tyrosine phosphorylation by human CMV is mediated by SHP2. Journal of Immunology (Baltimore, Md. : 1950) *181*, 5530–5536.
11. Barteneva, N.S., and Vorobjev, I.A. (2018). Heterogeneity of Metazoan Cells and Beyond: To Integrative Analysis of Cellular Populations at Single-Cell Level. (Springer New York), pp. 3–23.
12. Basiji, D.A., Ortyn, W.E., Liang, L., Venkatachalam, V., and Morrissey, P. (2007). Cellular Image Analysis and Imaging by Flow Cytometry. Clin Lab Med *27*, 653–670.
13. Begitt, A., Cavey, J., Droescher, M., and Vinkemeier, U. (2018). On the role of STAT1 and STAT6 ADP-ribosylation in the regulation of macrophage activation. Nat Commun *9*, 2144.

14. Benary, M., Bohn, S., Lüthen, M., Nolis, I.K., Blüthgen, N., and Loewer, A. (2020). Disentangling Pro-mitotic Signaling during Cell Cycle Progression using Time-Resolved Single-Cell Imaging. CellReports *31*, 107514.

15. Berridge, M.J. (2014). Module 12: Signalling Defects and Disease. Cell Signal Biology *6*, csb0001012.

16. Blanchard, F., Wang, Y., Kinzie, E., Duplomb, L., Godard, A., and Baumann, H. (2001). Oncostatin M Regulates the Synthesis and Turnover of gp130, Leukemia Inhibitory Factor Receptor α, and Oncostatin M Receptor β by Distinct Mechanisms*. J Biol Chem *276*, 47038–47045.

17. Blouin, C.M., and Lamaze, C. (2013). Interferon Gamma Receptor: The Beginning of the Journey. Front Immunol *4*, 267.

18. Böhmer, F.-D., and Friedrich, K. (2014). Protein tyrosine phosphatases as wardens of STAT signaling. Jak-Stat *3*, e28087.

19. Brasier, A.R., Tian, B., Jamaluddin, M., Kalita, M.K., Garofalo, R.P., and Lu, M. (2011). RelA Ser276 Phosphorylation-Coupled Lys310 Acetylation Controls Transcriptional Elongation of Inflammatory Cytokines in Respiratory Syncytial Virus Infection. J Virol *85*, 11752–11769.

20. Brooks, A.J., and Putoczki, T. (2020). JAK-STAT Signalling Pathway in Cancer. Cancers *12*, 1971.

21. Bush, A., Vasen, G., Constantinou, A., Dunayevich, P., Patop, I.L., Blaustein, M., and Colman-Lerner, A. (2016). Yeast GPCR signaling reflects the fraction of occupied receptors, not the number. Mol Syst Biol *12*, 898.

22. Cadart, C., Monnier, S., Grilli, J., Sáez, P.J., Srivastava, N., Attia, R., Terriac, E., Baum, B., Cosentino-Lagomarsino, M., and Piel, M. (2018). Size control in mammalian cells involves modulation of both growth rate and cell cycle duration. Nature Communications 1–15.

23. Caffarel, M.M., and Coleman, N. (2014). Oncostatin M receptor is a novel therapeutic target in cervical squamous cell carcinoma. J Pathology *232*, 386–390.

24. Campbell, E.M., and Hope, T.J. (2003). Role of the cytoskeleton in nuclear import. Adv Drug Deliver Rev *55*, 761–771.

25. Carey, J.N., Mettert, E.L., Roggiani, M., Myers, K.S., Kiley, P.J., and Goulian, M. (2018). Regulated Stochasticity in a Bacterial Signaling Network Permits Tolerance to a Rapid Environmental Change. Cell *173*, 196-207.e14.

26. Carpenter, A.E., Jones, T.R., Lamprecht, M.R., Clarke, C., Kang, I.H., Friman, O., Guertin, D.A., Chang, J.H., Lindquist, R.A., Moffat, J., et al. (2006). CellProfiler: image analysis software for identifying and quantifying cell phenotypes. Genome Biol *7*, R100.

27. Chang, A.Y., and Marshall, W.F. (2017). Organelles – understanding noise and heterogeneity in cell biology at an intermediate scale. J Cell Sci *130*, 819–826.

28. Chang, H.H., Hemberg, M., Barahona, M., Ingber, D.E., and Huang, S. (2008). Transcriptome-wide noise controls lineage choice in mammalian progenitor cells. Nature *453*, 544–547.

29. Cheong, R., Rhee, A., Wang, C.J., Nemenman, I., and Levchenko, A. (2011). Information Transduction Capacity of Noisy Biochemical Signaling Networks. Science *334*, 354–358.

30. Chmiest, D., Sharma, N., Zanin, N., Lesegno, C.V. de, Shafaq-Zadah, M., Sibut, V., Dingli, F., Hupé, P., Wilmes, S., Piehler, J., et al. (2016). Spatiotemporal control of interferon-induced JAK/STAT signalling and gene transcription by the retromer complex. Nat Commun *7*, 13476.

31. Cimica, V., Chen, H.-C., Iyer, J.K., and Reich, N.C. (2011). Dynamics of the STAT3 Transcription Factor: Nuclear Import Dependent on Ran and Importin-β1. Plos One *6*, e20188.

32. Clapham, D.E. (2007). Calcium Signaling. Cell *131*, 1047–1058.

33. Clevers, H., and Nusse, R. (2012). Wnt/β-Catenin Signaling and Disease. Cell *149*, 1192–1205.

34. Cohen, A.A., Kalisky, T., Mayo, A., Geva-Zatorsky, N., Danon, T., Issaeva, I., Kopito, R.B., Perzov, N., Milo, R., Sigal, A., et al. (2009). Protein Dynamics in Individual Human Cells: Experiment and Theory. Plos One *4*, e4901.

35. Colman-Lerner, A., Gordon, A., Serra, E., Chin, T., Resnekov, O., Endy, D., Pesce, C.G., and Brent, R. (2005). Regulated cell-to-cell variation in a cell-fate decision system. Nature *437*, 699–706.

36. Consortium, T.M.E., Yue, F., Cheng, Y., Breschi, A., Vierstra, J., Wu, W., Ryba, T., Sandstrom, R., Ma, Z., Davis, C., et al. (2014). A comparative encyclopedia of DNA elements in the mouse genome. Nature *515*, 355–364.

37. Cookson, N.A., Cookson, S.W., Tsimring, L.S., and Hasty, J. (2009). Cell cycle-dependent variations in protein concentration. Nucleic Acids Research *38*, 2676–2681.

38. Cover, T.M., and Thomas, J.A. (2012). Elements of Information Theory. Wiley.

39. Czerkies, M., Korwek, Z., Prus, W., Kochańczyk, M., Jaruszewicz-Błońska, J., Tudelska, K., Błoński, S., Kimmel, M., Brasier, A.R., and Lipniacki, T. (2018). Cell fate in antiviral response arises in the crosstalk of IRF, NF-κB and JAK/STAT pathways. Nat Commun *9*, 493.

40. Deb, D.K., Sassano, A., Lekmine, F., Majchrzak, B., Verma, A., Kambhampati, S., Uddin, S., Rahman, A., Fish, E.N., and Platanias, L.C. (2003). Activation of Protein Kinase Cδ by IFN-γ. J Immunol *171*, 267–273.

41. Decker, T., and Kovarik, P. (2000). Serine phosphorylation of STATs. Oncogene *19*, 2628–2637.

42. Eling, N., Morgan, M.D., and Marioni, J.C. (2019). Challenges in measuring and understanding biological noise. Nature Reviews Genetics 1–13.

43. Elowitz, M.B., Levine, A.J., Siggia, E.D., and Swain, P.S. (2002). Stochastic gene expression in a single cell. Science *297*, 1183–1186.

44. Facchetti, G., Knapp, B., Chang, F., and Howard, M. (2019). Reassessment of the Basis of Cell Size Control Based on Analysis of Cell-to-Cell Variability. Biophys J *117*, 1728–1738.

45. Fallahi-Sichani, M., Honarnejad, S., Heiser, L.M., Gray, J.W., and Sorger, P.K. (2013). Metrics other than potency reveal systematic variation in responses to cancer drugs. Nat Chem Biol *9*, 708–714.

46. Fang, H., Disteche, C.M., and Berletch, J.B. (2019). X Inactivation and Escape: Epigenetic and Structural Features. Frontiers Cell Dev Biology *7*, 219.

47. Fazal, F., Minhajuddin, M., Bijli, K.M., McGrath, J.L., and Rahman, A. (2007). Evidence for Actin Cytoskeleton-dependent and -independent Pathways for RelA/p65 Nuclear Translocation in Endothelial Cells*. J Biol Chem *282*, 3940–3950.

48. Foreman, R., and Wollman, R. (2020). Mammalian gene expression variability is explained by underlying cell state. Molecular Systems Biology *16*, 6436–13.

49. Frick, C.L., Yarka, C., Nunns, H., and Goentoro, L. (2017). Sensing relative signal in the Tgf-β/Smad pathway. Proc National Acad Sci *114*, E2975–E2982.

50. Fuentealba, L.C., Eivers, E., Geissert, D., Taelman, V., and Robertis, E.M.D. (2008). Asymmetric mitosis: Unequal segregation of proteins destined for degradation. Proc National Acad Sci *105*, 7732–7737.

51. Fuller, D., Chen, W., Adler, M., Groisman, A., Levine, H., Rappel, W.-J., and Loomis, W.F. (2010). External and internal constraints on eukaryotic chemotaxis. Proc National Acad Sci *107*, 9656–9659.

52. Gao, J., Wang, F., Liu, Y., Cai, M., Xu, H., Jiang, J., and Wang, H. (2015). Revealing the cellular localization of STAT1 during the cell cycle by super-resolution imaging. Nature Publishing Group *5*, 1415–1418.

53. Garner, K.L., Perrett, R.M., Voliotis, M., Bowsher, C., Pope, G.R., Pham, T., Caunt, C.J., Tsaneva-Atanasova, K., and McArdle, C.A. (2016). Information Transfer in Gonadotropin-releasing Hormone (GnRH) Signaling: extracellular signal-regulated kinase (ERK)-mediated feedback loops control hormone sensing. J Biol Chem *291*, 2246–2259.

54. Ginzberg, M.B., Kafri, R., and Kirschner, M. (2015). On being the right (cell) size. Science *348*, 1245075–1245075.

55. Ginzberg, M.B., Chang, N., D'Souza, H., Patel, N., Kafri, R., and Kirschner, M.W. (2018). Cell size sensing in animal cells coordinates anabolic growth rates and cell cycle progression to maintain cell size uniformity. Elife *7*, e26957.

56. Gough, A.H., Chen, N., Shun, T.Y., Lezon, T.R., Boltz, R.C., Reese, C.E., Wagner, J., Vernetti, L.A., Grandis, J.R., Lee, A.V., et al. (2014). Identifying and Quantifying Heterogeneity in High Content Analysis: Application of Heterogeneity Indices to Drug Discovery. PLoS ONE *9*, e102678-16.

57. Granados, A.A., Pietsch, J.M.J., Cepeda-Humerez, S.A., Farquhar, I.L., Tkačik, G., and Swain, P.S. (2018). Distributed and dynamic intracellular organization of extracellular information. Proc National Acad Sci *115*, 201716659.

58. Gregory, T.R. (2001). Coincidence, coevolution, or causation? DNA content, cellsize, and the C-value enigma. Biol Rev *76*, 65–101.

59. Gross, S.M., Dane, M.A., Bucher, E., and Heiser, L.M. (2019). Individual Cells Can Resolve Variations in Stimulus Intensity along the IGF-PI3K-AKT Signaling Axis. Cell Systems *9*, 580-588.e4.

60. Guilbert, M., Anquez, F., Pruvost, A., Thommen, Q., and Courtade, E. (2020). Protein level variability determines phenotypic heterogeneity in proteotoxic stress response. The FEBS Journal *287*, 5345–5361.

61. Guo, H., Kuang, S., Song, Q., Liu, M., Sun, X., and Yu, Q. (2018). Cucurbitacin I inhibits STAT3, but enhances STAT1 signaling in human cancer cells in vitro through disrupting actin filaments. Acta Pharmacol Sin *39*, 425–437.

62. Guruharsha, K.G., Kankel, M.W., and Artavanis-Tsakonas, S. (2012). The Notch signalling system: recent insights into the complexity of a conserved pathway. Nat Rev Genet *13*, 654–666.

63. Hagai, T., Chen, X., Miragaia, R.J., Rostom, R., Gomes, T., Kunowska, N., Henriksson, J., Park, J.-E., Proserpio, V., Donati, G., et al. (2018). Gene expression variability across cells and species shapes innate immunity. Nature 1–24.

64. Hansen, A.S., and O'Shea, E.K. (2015). Limits on information transduction through amplitude and frequency regulation of transcription factor activity.

65. Harper, P.S. (2011). Mary Lyon and the hypothesis of random X chromosome inactivation. Hum Genet *130*, 169–174.

66. Hart, Y., Madar, D., Yuan, J., Bren, A., Mayo, A.E., Rabinowitz, J.D., and Alon, U. (2011). Robust Control of Nitrogen Assimilation by a Bifunctional Enzyme in E. coli. Mol Cell *41*, 117–127.

67. Haspel, R.L., and Darnell, J.E. (1999). A nuclear protein tyrosine phosphatase is required for the inactivation of Stat1. Proc National Acad Sci *96*, 10188–10193.

68. Hermanns, H.M. (2015). Oncostatin M and interleukin-31: Cytokines, receptors, signal transduction and physiology. Cytokine Growth F R *26*, 545–558.

69. Hermanns, H.M., Radtke, S., Haan, C., Leur, H.S.-V. de, Tavernier, J., Heinrich, P.C., and Behrmann, I. (1999). Contributions of leukemia inhibitory factor receptor and oncostatin M receptor to signal transduction in heterodimeric complexes with glycoprotein 130. J Immunol Baltim Md 1950 *163*, 6651–6658.

70. Herrmann, A., Vogt, M., Mönnigmann, M., Clahsen, T., Sommer, U., Haan, S., Poli, V., Heinrich, P.C., and Müller-Newen, G. (2007). Nucleocytoplasmic shuttling of persistently activated STAT3. J Cell Sci *120*, 3249–3261.

71. Hintzen, C., Evers, C., Lippok, B.E., Volkmer, R., Heinrich, P.C., Radtke, S., and Hermanns, H.M. (2008a). Box 2 Region of the Oncostatin M Receptor Determines Specificity for Recruitment of Janus Kinases and STAT5 Activation*. J Biol Chem *283*, 19465–19477.

72. Hintzen, C., Haan, C., Tuckermann, J.P., Heinrich, P.C., and Hermanns, H.M. (2008b). Oncostatin M-Induced and Constitutive Activation of the JAK2/STAT5/CIS Pathway Suppresses CCL1, but Not CCL7 and CCL8, Chemokine Expression. J Immunol *181*, 7341–7349.

73. Ho, H.H., and Ivashkiv, L.B. (2006). Role of STAT3 in Type I Interferon Responses NEGATIVE REGULATION OF STAT1-DEPENDENT INFLAMMATORY GENE ACTIVATION*. J Biol Chem *281*, 14111–14118.

74. Hoeve, J. ten, Ibarra-Sanchez, M. de J., Fu, Y., Zhu, W., Tremblay, M., David, M., and Shuai, K. (2002). Identification of a Nuclear Stat1 Protein Tyrosine Phosphatase. Mol Cell Biol *22*, 5662–5668.

75. Housden, B.E., and Perrimon, N. (2014). Spatial and temporal organization of signaling pathways. Trends Biochem Sci *39*, 457–464.

76. Huang, S. (2009). Non-genetic heterogeneity of cells in development: more than just noise. Development *136*, 3853–3862.

77. Huh, D., and Paulsson, J. (2011). Random partitioning of molecules at cell division. Proc National Acad Sci *108*, 15004–15009.

78. Iwata, H., Goettsch, C., Sharma, A., Ricchiuto, P., Goh, W.W.B., Halu, A., Yamada, I., Yoshida, H., Hara, T., Wei, M., et al. (2016). PARP9 and PARP14 cross-regulate macrophage activation via STAT1 ADP-ribosylation. Nat Commun *7*, 12849.

79. Jerke, U., Tkachuk, S., Kiyan, J., Stepanova, V., Kusch, A., Hinz, M., Dietz, R., Haller, H., Fuhrman, B., and Dumler, I. (2009). Stat1 Nuclear Translocation by Nucleolin upon Monocyte Differentiation. Plos One *4*, e8302.

80. Jetka, T., Nienałtowski, K., Winarski, T., Błoński, S., and Komorowski, M. (2019). Information-theoretic analysis of multivariate single-cell signaling responses. PLoS Computational Biology *15*, e1007132-23.

81. Kano, A., Watanabe, Y., Takeda, N., Aizawa, S., and Akaike, T. (1997). Analysis of IFN- -Induced Cell Cycle Arrest and Cell Death in Hepatocytes. J Biochem *121*, 677–683.

82. Keren, K., Pincus, Z., Allen, G.M., Barnhart, E.L., Marriott, G., Mogilner, A., and Theriot, J.A. (2008). Mechanism of shape determination in motile cells. Nature *453*, 475–480.

83. Keshelava, A., Solis, G.P., Hersch, M., Koval, A., Kryuchkov, M., Bergmann, S., and Katanaev, V.L. (2018). High capacity in G protein-coupled receptor signaling. Nat Commun *9*, 876.

84. Kholodenko, B.N. (2006). Cell-signalling dynamics in time and space. Nat Rev Mol Cell Bio *7*, 165–176.

85. Kim, M.S., Louwagie, J., Carvalho, B., Droste, J.S.T. sive, Park, H.L., Chae, Y.K., Yamashita, K., Liu, J., Ostrow, K.L., Ling, S., et al. (2009). Promoter DNA Methylation of Oncostatin M receptor-β as a Novel Diagnostic and Therapeutic Marker in Colon Cancer. Plos One *4*, e6555.

86. Klausen, P., Pedersen, L., Jurlander, J., and Baumann, H. (2000). Oncostatin M and Interleukin 6 inhibit cell cycle progression by prevention of p27kip1 degradation in HepG2 cells. Oncogene *19*, 3675–3683.

87. Ko, M.S., Nakauchi, H., and Takahashi, N. (1990). The dose dependence of glucocorticoid-inducible gene expression results from changes in the number of transcriptionally active templates. Embo J *9*, 2835–2842.

88. Komorowski, M., and Tawfik, D.S. (2019). The Limited Information Capacity of Cross-Reactive Sensors Drives the Evolutionary Expansion of Signaling. Cell Syst *8*, 76-85.e6.

89. Koseska, A., and Bastiaens, P.I. (2017). Cell signaling as a cognitive process. Embo J *36*, 568–582.

90. Krämer, O.H., Baus, D., Knauer, S.K., Stein, S., Jäger, E., Stauber, R.H., Grez, M., Pfitzner, E., and Heinzel, T. (2006). Acetylation of Stat1 modulates NF-κB activity. Gene Dev *20*, 473–485.

91. Kumar, S., Saradhi, M., Chaturvedi, N.K., and Tyagi, R.K. (2006). Intracellular localization and nucleocytoplasmic trafficking of steroid receptors: An overview. Mol Cell Endocrinol *246*, 147–156.

92. Kussell, E., and Leibler, S. (2005). Phenotypic Diversity, Population Growth, and Information in Fluctuating Environments. Science *309*, 2075–2078.

93. Lacreusette, A., Nguyen, J.-M., Pandolfino, M.-C., Khammari, A., Dreno, B., Jacques, Y., Godard, A., and Blanchard, F. (2007). Loss of oncostatin M receptor β in metastatic melanoma cells. Oncogene *26*, 881–892.

94. Lane, K., Andres-Terre, M., Kudo, T., Monack, D.M., and Covert, M.W. (2019). Escalating Threat Levels of Bacterial Infection Can Be Discriminated by Distinct MAPK and NF-κB Signaling Dynamics in Single Host Cells. Cell Systems *8*, 183-196.e4.

95. Lee, E.-Y., Schultz, K.L.W., and Griffin, D.E. (2013). Mice Deficient in Interferon-Gamma or Interferon-Gamma Receptor 1 Have Distinct Inflammatory Responses to Acute Viral Encephalomyelitis. Plos One *8*, e76412.

96. Lee, R.E.C., Walker, S.R., Savery, K., Frank, D.A., and Gaudet, S. (2014). Fold Change of Nuclear NF-κB Determines TNF-Induced Transcription in Single Cells. Mol Cell *53*, 867–879.

97. Lees, J.R. (2015). Interferon gamma in autoimmunity: A complicated player on a complex stage. Cytokine *74*, 18–26.

98. Lin, J., and Amir, A. (2018). Homeostasis of protein and mRNA concentrations in growing cells. Nature Communications 1–11.

99. Liu, L., McBride, K.M., and Reich, N.C. (2005). STAT3 nuclear import is independent of tyrosine phosphorylation and mediated by importin-α3. P Natl Acad Sci Usa *102*, 8150–8155.

100. Liu, L., Okada, S., Kong, X.-F., Kreins, A.Y., Cypowyj, S., Abhyankar, A., Toubiana, J., Itan, Y., Audry, M., Nitschke, P., et al. (2011). Gain-of-function human STAT1 mutations

impair IL-17 immunity and underlie chronic mucocutaneous candidiasis. J Exp Medicine *208*, 1635–1648.

101. Lyon, M.F. (1961). Gene Action in the X-chromosome of the Mouse (Mus musculus L.). Nature *190*, 372–373.

102. MacLeod, M.K., and Anderton, S.M. (2015). Antigen-based immunotherapy (AIT) for autoimmune and allergic disease. Curr Opin Pharmacol *23*, 11–16.

103. Madsen, R.R., and Vanhaesebroeck, B. (2019). Cracking the context-specific PI3K signaling code. Sci Signal *13*, eaay2940.

104. Majoros, A., Platanitis, E., Szappanos, D., Cheon, H., Vogl, C., Shukla, P., Stark, G.R., Sexl, V., Schreiber, R., Schindler, C., et al. (2016). Response to interferons and antibacterial innate immunity in the absence of tyrosine-phosphorylated STAT1. Embo Rep *17*, 367–382.

105. Majoros, A., Platanitis, E., Kernbauer-Hölzl, E., Rosebrock, F., Müller, M., and Decker, T. (2017). Canonical and Non-Canonical Aspects of JAK–STAT Signaling: Lessons from Interferons for Cytokine Responses. Front Immunol *8*, 29.

106. Masjedi, A., Hajizadeh, F., Dargani, F.B., Beyzai, B., Aksoun, M., Hojjat-Farsangi, M., Zekiy, A., and Jadidi-Niaragh, F. (2020). Oncostatin M: A mysterious cytokine in cancers. Int Immunopharmacol *90*, 107158.

107. Mazzarello, P. (1999). A unifying concept: the history of cell theory. Nat Cell Biol *1*, E13–E15.

108. McBride, K.M., and Reich, N.C. (2003). The Ins and Outs of STAT1 Nuclear Transport. Sci Stke *2003*, re13–re13.

109. Meyer, T., Begitt, A., Lödige, I., Rossum, M. van, and Vinkemeier, U. (2002). Constitutive and IFN-γ-induced nuclear import of STAT1 proceed through independent pathways. Embo J *21*, 344–354.

110. Meyer, T., Marg, A., Lemke, P., Wiesner, B., and Vinkemeier, U. (2003). DNA binding controls inactivation and nuclear accumulation of the transcription factor Stat1. Gene Dev *17*, 1992–2005.

111. Miyawaki, A., Iizuka, Y., Sugino, H., and Watanabe, Y. (2019). IL-11 prevents IFN-γ-induced hepatocyte death through selective downregulation of IFN-γ/STAT1 signaling and ROS scavenging. Plos One *14*, e0211123.

112. Mojic, M., Takeda, K., and Hayakawa, Y. (2018). The Dark Side of IFN-γ: Its Role in Promoting Cancer Immunoevasion. Int J Mol Sci *19*, 89.

113. Mora-Garcia, P., and Sakamoto, K.M. (1999). Cell Signaling Defects and Human Disease. Mol Genet Metab *66*, 143–171.

114. Morris, R., Kershaw, N.J., and Babon, J.J. (2018). The molecular details of cytokine signaling via the JAK/STAT pathway. Protein Sci *27*, 1984–2009.

115. Murphy, S.P., Tayade, C., Ashkar, A.A., Hatta, K., Zhang, J., and Croy, B.A. (2009). Interferon Gamma in Successful Pregnancies1. Biol Reprod *80*, 848–859.

116. Murray, P.J. (2007). The JAK-STAT Signaling Pathway: Input and Output Integration. J Immunol *178*, 2623–2629.

117. Nagahama, K.Y., Togo, S., Holz, O., Magnussen, H., Liu, X., Seyama, K., Takahashi, K., and Rennard, S.I. (2013). Oncostatin M Modulates Fibroblast Function via Signal Transducers and Activators of Transcription Proteins–3. Am J Resp Cell Mol *49*, 130715131937002.

118. Nagel, M.A., James, S.F., Traktinskiy, I., Wyborny, A., Choe, A., Rempel, A., Baird, N.L., and Gilden, D. (2014). Inhibition of Phosphorylated-STAT1 Nuclear Translocation and Antiviral Protein Expression in Human Brain Vascular Adventitial Fibroblasts Infected with Varicella-Zoster Virus. J Virol *88*, 11634–11637.

119. Nair, A., Chauhan, P., Saha, B., and Kubatzky, K.F. (2019). Conceptual Evolution of Cell Signaling. Int J Mol Sci *20*, 3292.

120. Nandagopal, N., Santat, L.A., LeBon, L., Sprinzak, D., Bronner, M.E., and Elowitz, M.B. (2018). Dynamic Ligand Discrimination in the Notch Signaling Pathway. Cell *172*, 869-880.e19.

121. Nature journal advices, https://www.nature.com/nature-portfolio/for-authors/write.

122. Nesterova, T.B., Popova, B.C., Cobb, B.S., Norton, S., Senner, C.E., Tang, Y.A., Spruce, T., Rodriguez, T.A., Sado, T., Merkenschlager, M., et al. (2008). Dicer regulates Xist promoter methylation in ES cells indirectly through transcriptional control of Dnmt3a. Epigenet Chromatin *1*, 2.

123. Newton, K., and Dixit, V.M. (2012). Signaling in Innate Immunity and Inflammation. Csh Perspect Biol *4*, a006049.

124. Nguyen, H., Ramana, C.V., Bayes, J., and Stark, G.R. (2001). Roles of Phosphatidylinositol 3-Kinase in Interferon-γ-dependent Phosphorylation of STAT1 on Serine 727 and Activation of Gene Expression*. J Biol Chem *276*, 33361–33368.

125. Ni, L., and Lu, J. (2018). Interferon gamma in cancer immunotherapy. Cancer Med-Us *7*, 4509–4516.

126. Nienałtowski, K., Rigby, R.E., Walczak, J., Zakrzewska, K.E., Głów, E., Rehwinkel, J., and Komorowski, M. (2021). Fractional response analysis reveals logarithmic cytokine responses in cellular populations. Nat Commun *12*, 4175.

127. Novick, A., and Weiner, M. (1957). ENZYME INDUCTION AS AN ALL-OR-NONE PHENOMENON. Proc National Acad Sci *43*, 553–566.

128. O'Hara, K.A., Kedda, M. -A., Thompson, P.J., and Knight, D.A. (2003). Oncostatin M: an interleukin-6-like cytokine relevant to airway remodelling and the pathogenesis of asthma. Clin Exp Allergy *33*, 1026–1032.

129. Okada, Y., Watanabe, T., Shoji, T., Taguchi, K., Ogo, N., and Asai, A. (2018). Visualization and quantification of dynamic STAT3 homodimerization in living cells using homoFluoppi. Sci Rep-Uk *8*, 2385.

130. Phillips, N.E., Mandic, A., Omidi, S., Naef, F., and Suter, D.M. (2019). Memory and relatedness of transcriptional activity in mammalian cell lineages. Nat Commun *10*, 1208.

131. Poon, R.Y.C. (2016). Cell Cycle Oscillators, Methods and Protocols. Methods Mol Biology *1342*, 3–19.

132. Pope, R.J., Garner, K.L., Voliotis, M., Lay, A.C., Betin, V.M., Tsaneva-Atanasova, K., Welsh, G.I., Coward, R.J., and McArdle, C.A. (2020). An information theoretic approach to insulin sensing by human kidney podocytes. Molecular and Cellular Endocrinology *518*, 110976–10.

133. Pranada, A.L., Metz, S., Herrmann, A., Heinrich, P.C., and Müller-Newen, G. (2004). Real Time Analysis of STAT3 Nucleocytoplasmic Shuttling*. J Biol Chem *279*, 15114–15123.

134. Preuße, K., Tveriakhina, L., Schuster-Gossler, K., Gaspar, C., Rosa, A.I., Henrique, D., Gossler, A., and Stauber, M. (2015). Context-Dependent Functional Divergence of the Notch Ligands DLL1 and DLL4 In Vivo. Plos Genet *11*, e1005328.

135. Purvis, J.E., and Lahav, G. (2013). Encoding and Decoding Cellular Information through Signaling Dynamics. Cell *152*, 945–956.

136. Qing, Y., and Stark, G.R. (2004). Alternative Activation of STAT1 and STAT3 in Response to Interferon-γ*. J Biol Chem *279*, 41679–41685.

137. Raj, A., and Oudenaarden, A. van (2008). Nature, Nurture, or Chance: Stochastic Gene Expression and Its Consequences. Cell *135*, 216–226.

138. Raj, A., Peskin, C.S., Tranchina, D., Vargas, D.Y., and Tyagi, S. (2006). Stochastic mRNA Synthesis in Mammalian Cells. Plos Biol *4*, e309.

139. Raser, J.M., and O'Shea, E.K. (2004). Control of Stochasticity in Eukaryotic Gene Expression. Science *304*, 1811–1814.

140. Rauch, I., Müller, M., and Decker, T. (2014). The regulation of inflammation by interferons and their STATs. Jak-Stat *2*, e23820.

141. Reich, N.C. (2013). STATs get their move on. Jak-Stat *2*, e27080.

142. Reich, N.C., and Liu, L. (2006). Tracking STAT nuclear traffic. Nature Reviews Immunology *6*, 602–612.

143. Richards, C.D. (2013). The Enigmatic Cytokine Oncostatin M and Roles in Disease. Isrn Inflamm *2013*, 1–23.

144. Rocha, V.Z., Folco, E.J., Sukhova, G., Shimizu, K., Gotsman, I., Vernon, A.H., and Libby, P. (2008). Interferon-γ, a Th1 Cytokine, Regulates Fat Inflammation. Circ Res *103*, 467–476.

145. Roukos, V., Pegoraro, G., Voss, T.C., and Misteli, T. (2015). Cell cycle staging of individual cells by fluorescence microscopy. Nature Protocols *10*, 334–348.

146. Roux, J., Hafner, M., Bandara, S., Sims, J.J., Hudson, H., Chai, D., and Sorger, P.K. (2015). Fractional killing arises from cell-to-cell variability in overcoming a caspase activity threshold. Mol Syst Biol *11*, 803.

147. Rowland, M.A., and Deeds, E.J. (2014). Crosstalk and the evolution of specificity in two-component signaling. Proc National Acad Sci *111*, 5550–5555.

148. Rowland, M.A., Greenbaum, J.M., and Deeds, E.J. (2017). Crosstalk and the evolvability of intracellular communication. Nat Commun *8*, 16009.

149. Ruiz, R., Cruz, F. de la, and Fernandez-Lopez, R. (2018). Negative feedback increases information transmission, enabling bacteria to discriminate sublethal antibiotic concentrations. Sci Adv *4*, eaat5771.

150. Sampattavanich, S., Steiert, B., Kramer, B.A., Gyori, B.M., Albeck, J.G., and Sorger, P.K. (2018). Encoding Growth Factor Identity in the Temporal Dynamics of FOXO3 under the Combinatorial Control of ERK and AKT Kinases. Cell Syst *6*, 664-678.e9.

151. Santos, S.D.M., Verveer, P.J., and Bastiaens, P.I.H. (2007). Growth factor-induced MAPK network topology shapes Erk response determining PC-12 cell fate. Nat Cell Biol *9*, 324–330.

152. Sarközi, R., Hauser, C., Noppert, S.-J., Kronbichler, A., Pirklbauer, M., Haller, V.M., Grillari, J., Grillari-Voglauer, R., Mayer, G., and Schramek, H. (2011). Oncostatin M is a novel inhibitor of TGF-β1-induced matricellular protein expression. Am J Physiol-Renal *301*, F1014–F1025.

153. Scaffidi, A.K., Mutsaers, S.E., Moodley, Y.P., McAnulty, R.J., Laurent, G.J., Thompson, P.J., and Knight, D.A. (2002). Oncostatin M stimulates proliferation, induces collagen production and inhibits apoptosis of human lung fibroblasts. Brit J Pharmacol *136*, 793–801.

154. Schneider, W.M., Chevillotte, M.D., and Rice, C.M. (2014). Interferon-Stimulated Genes: A Complex Web of Host Defenses. Annu Rev Immunol *32*, 513–545.

155. Scholtz, G., Braband, A., Tolley, L., Reimann, A., Mittmann, B., Lukhaup, C., Steuerwald, F., and Vogt, G. (2003). Parthenogenesis in an outsider crayfish. Nature *421*, 806–806.

156. Schreiber, G., and Piehler, J. (2015). The molecular basis for functional plasticity in type I interferon signaling. Trends in Immunology *36*, 139–149.

157. Sebolt-Leopold, J.S., and Herrera, R. (2004). Targeting the mitogen-activated protein kinase cascade to treat cancer. Nat Rev Cancer *4*, 937–947.

158. Selimkhanov, J., Taylor, B., Yao, J., Pilko, A., Albeck, J., Hoffmann, A., Tsimring, L., and Wollman, R. (2014). Accurate information transmission through dynamic biochemical signaling networks. Science *346*, 1370–1373.

159. Shamir, M., Bar-On, Y., Phillips, R., and Milo, R. (2016). SnapShot: Timescales in Cell Biology. Cell *164*, 1302-1302.e1.

160. Shannon, C.E. (1948). A mathematical theory of communication. Bell Syst Technical J *27*, 379–423.

161. Sharma, R.P., Rosen, C., Melbourne, J.K., Feiner, B., and Chase, K.A. (2017). Activated Phosphorylated STAT1 Levels as a Biologically Relevant Immune Signal in Schizophrenia. Neuroimmunomodulat *23*, 224–229.

162. Shinar, G., Milo, R., Martínez, M.R., and Alon, U. (2007). Input–output robustness in simple bacterial signaling systems. Proc National Acad Sci *104*, 19931–19935.

163. Shlyakhtina, Y., Moran, K.L., and Portal, M.M. (2019). Asymmetric Inheritance of Cell Fate Determinants: Focus on RNA. Non-Coding Rna *5*, 38.

164. Shtrichman, R., and Samuel, C.E. (2001). The role of gamma interferon in antimicrobial immunity. Curr Opin Microbiol *4*, 251–259.

165. Sigal, A., Milo, R., Cohen, A., Geva-Zatorsky, N., Klein, Y., Liron, Y., Rosenfeld, N., Danon, T., Perzov, N., and Alon, U. (2006). Variability and memory of protein levels in human cells. Nature *444*, 643–646.

166. Skinner, B.M., and Johnson, E.E.P. (2017). Nuclear morphologies: their diversity and functional relevance. Chromosoma *126*, 195–212.

167. Snijder, B., Sacher, R., Rämö, P., Damm, E.-M., Liberali, P., and Pelkmans, L. (2009). Population context determines cell-to-cell variability in endocytosis and virus infection. Nature *461*, 520–523.

168. Spencer, S.L., Gaudet, S., Albeck, J.G., Burke, J.M., and Sorger, P.K. (2009). Non-genetic origins of cell-to-cell variability in TRAIL-induced apoptosis. Nature Publishing Group *459*, 428–432.

169. Spiller, D.G., Wood, C.D., Rand, D.A., and White, M.R.H. (2010). Measurement of single-cell dynamics. Nature *465*, 736–745.

170. Suderman, R., Bachman, J.A., Smith, A., Sorger, P.K., and Deeds, E.J. (2017). Fundamental trade-offs between information flow in single cells and cellular populations. Proc National Acad Sci *114*, 5755–5760.

171. Supasai, S., Aimo, L., Adamo, A.M., Mackenzie, G.G., and Oteiza, P.I. (2017). Zinc deficiency affects the STAT1/3 signaling pathways in part through redox-mediated mechanisms. Redox Biol *11*, 469–481.

172. Swain, P.S., Elowitz, M.B., and Siggia, E.D. (2002). Intrinsic and extrinsic contributions to stochasticity in gene expression. Proc National Acad Sci *99*, 12795–12800.

173. Symmons, O., and Raj, A. (2016). What's Luck Got to Do with It: Single Cells, Multiple Fates, and Biological Nondeterminism. Mol Cell *62*, 788–802.

174. Takaoka, A., Tanaka, N., Mitani, Y., Miyazaki, T., Fujii, H., Sato, M., Kovarik, P., Decker, T., Schlessinger, J., and Taniguchi, T. (2013). Protein tyrosine kinase Pyk2 mediates the Jak-dependent activation of MAPK and Stat1 in IFN-γ, but not IFN-α, signaling. Embo J *18*, 2480–2488.

175. Tanaka, M., and Miyahima, A. (2003). Oncostatin M, a multifunctional cytokine. Rev Physiol Bioch P *149*, 39–52.

176. Taniguchi, K., and Karin, M. (2018). NF-κB, inflammation, immunity and cancer: coming of age. Nat Rev Immunol *18*, 309–324.

177. Tannenbaum, C.S., and Hamilton, T.A. (2000). Immune-inflammatory mechanisms in IFNγ-mediated anti-tumor activity. Semin Cancer Biol *10*, 113–123.

178. Teixeira, L.K., Fonseca, B.P., Barboza, B.A., and Viola, J.P. (2005). The role of interferon-gamma on immune and allergic responses. Memórias Instituto Oswaldo Cruz *100*, 137–144.

179. Tkačik, G., Dubuis, J.O., Petkova, M.D., and Gregor, T. (2014). Positional Information, Positional Error, and Read-Out Precision in Morphogenesis: A Mathematical Framework. Genetics *199*, genetics.114.171850.

180. Toettcher, J.E., Weiner, O.D., and Lim, W.A. (2013). Using Optogenetics to Interrogate the Dynamic Control of Signal Transmission by the Ras/Erk Module. Cell *155*, 1422–1434.

181. Topolewski, P., and Komorowski, M. (2021). Information-theoretic analyses of cellular strategies for achieving high signaling capacity — dynamics, cross-wiring and heterogeneity of cellular states. Curr Opin Syst Biology *27*, 100352.

182. Topolewski, P., Zakrzewska, K.E., Walczak, J., Nienałtowski, K., Müller-Newen, G., Singh, A., and Komorowski, M. (2022). Phenotypic variability, not noise, accounts for most of the cell-to-cell heterogeneity in IFN-γ and oncostatin M signaling responses. Sci Signal *15*.

183. Tran, E.J., and Wente, S.R. (2006). Dynamic Nuclear Pore Complexes: Life on the Edge. Cell *125*, 1041–1053.

184. Tyson, J.J., and Novak, B. (2008). Temporal Organization of the Cell Cycle. Curr Biol *18*, R759–R768.

185. Uda, S. (2020). Application of information theory in systems biology. Biophysical Rev *12*, 377–384.

186. Uhlén, M., Fagerberg, L., Hallström, B.M., Lindskog, C., Oksvold, P., Mardinoglu, A., Sivertsson, Å., Kampf, C., Sjöstedt, E., Asplund, A., et al. (2015). Tissue-based map of the human proteome. Science *347*, 1260419.

187. Uzbekov, R.E. (2004). Analysis of the Cell Cycle and a Method Employing Synchronized Cells for Study of Protein Expression at Various Stages of the Cell Cycle. Biochem Mosc *69*, 485–496.

188. Valente, G., Ozmen, L., Novelli, F., Geuna, M., Palestro, G., Forni, G., and Garotta, G. (1992). Distribution of interferon-γ receptor in human tissues. Eur J Immunol *22*, 2403–2412.

189. Vargas–Garcia, C.A., Ghusinga, K.R., and Singh, A. (2018). Cell size control and gene expression homeostasis in single-cells. Curr Opin Syst Biology *8*, 109–116.

190. Vilar, J.M.G., Guet, C.C., and Leibler, S. (2003). Modeling network dynamics. J Cell Biology *161*, 471–476.

191. Vogt, G. (2015). Stochastic developmental variation, an epigenetic source of phenotypic diversity with far-reaching biological consequences. J Biosciences *40*, 159–204.

192. Vogt, G., Huber, M., Thiemann, M., Boogaart, G. van den, Schmitz, O.J., and Schubart, C.D. (2008). Production of different phenotypes from the same genotype in the same environment by developmental variation. J Exp Biol *211*, 510–523.

193. Voliotis, M., Garner, K.L., Alobaid, H., Tsaneva-Atanasova, K., and McArdle, C.A. (2018). Gonadotropin-releasing hormone signaling: An information theoretic approach. Mol Cell Endocrinol *463*, 106–115.

194. Wada, T., Hironaka, K., Wataya, M., Fujii, M., Eto, M., Uda, S., Hoshino, D., Kunida, K., Inoue, H., Kubota, H., et al. (2020). Single-Cell Information Analysis Reveals That Skeletal Muscles Incorporate Cell-to-Cell Variability as Information Not Noise. CellReports *32*, 108051.

195. Walker, E.C., Johnson, R.W., Hu, Y., Brennan, H.J., Poulton, I.J., Zhang, J.-G., Jenkins, B.J., Smyth, G.K., Nicola, N.A., and Sims, N.A. (2016). Murine Oncostatin M Acts via Leukemia Inhibitory Factor Receptor to Phosphorylate Signal Transducer and Activator of Transcription 3 (STAT3) but Not STAT1, an Effect That Protects Bone Mass*. J Biol Chem *291*, 21703–21716.

196. Wang, L., Wang, F., and Gershwin, M.E. (2015). Human autoimmune diseases: a comprehensive update. J Intern Med *278*, 369–395.

197. Waters, J.C. (2009). Accuracy and precision in quantitative fluorescence microscopy. J Cell Biology *185*, 1135–1148.

198. West, N.R., Murphy, L.C., and Watson, P.H. (2012). Oncostatin M suppresses oestrogen receptor-α expression and is associated with poor outcome in human breast cancer. Endocr-Relat Cancer *19*, 181–195.

199. Wilmes, S., Beutel, O., Li, Z., Francois-Newton, V., Richter, C.P., Janning, D., Kroll, C., Hanhart, P., Hötte, K., You, C., et al. (2015). Receptor dimerization dynamics as a regulatory valve for plasticity of type I interferon signaling. J Cell Biology *209*, 579–593.

200. Wolf, D.E., Samarasekera, C., and Swedlow, J.R. (2013). Chapter 14 Quantitative Analysis of Digital Microscope Images. Methods Cell Biol *114*, 337–367.

201. Wollman, R. (2018). Robustness, accuracy, and cell state heterogeneity in biological systems. Curr Opin Syst Biology *8*, 46–50.

202. Yao, J., Pilko, A., and Wollman, R. (2016). Distinct cellular states determine calcium signaling response. Mol Syst Biol *12*, 894.

203. Zaidi, M.R. (2019). The Interferon-Gamma Paradox in Cancer. J Interf Cytokine Res *39*, 30–38.

204. Zaidi, M.R., and Merlino, G. (2011). The Two Faces of Interferon-γ in Cancer. Am Assoc Cancer Res *17*, 6118–6124.

205. Zanin, N., Lesegno, C.V. de, Lamaze, C., and Blouin, C.M. (2021). Interferon Receptor Trafficking and Signaling: Journey to the Cross Roads. Front Immunol *11*, 615603.

206. Zarling, J.M., Shoyab, M., Marquardt, H., Hanson, M.B., Lioubin, M.N., and Todaro, G.J. (1986). Oncostatin M: a growth regulator produced by differentiated histiocytic lymphoma cells. Proc National Acad Sci *83*, 9739–9743.

207. Zhang, J., Wang, F., Liu, F., and Xu, G. (2020). Predicting STAT1 as a prognostic marker in patients with solid cancer. Ther Adv Med Oncol *12*, 1758835920917558.

208. Zhang, Q., Gupta, S., Schipper, D.L., Kowalczyk, G.J., Mancini, A.E., Faeder, J.R., and Lee, R.E.C. (2017). NF-κB Dynamics Discriminate between TNF Doses in Single Cells. Cell Syst *5*, 638-645.e5.

209. Zimnik, S., Gaestel, M., and Niedenthal, R. (2008). Mutually exclusive STAT1 modifications identified by Ubc9/substrate dimerization-dependent SUMOylation. Nucleic Acids Res *37*, e30–e30.

# 9. Publications and financial support

Publications:

- Topolewski, P., Zakrzewska, K.E., Walczak, J., Nienałtowski, K., Müller-Newen, G., Singh, A., and Komorowski, M. (2022). Phenotypic variability, not noise, accounts for most of the cell-to-cell heterogeneity in IFN-γ and oncostatin M signaling responses. Science Signaling *15*.
- Topolewski, P., and Komorowski, M. (2021). Information-theoretic analyses of cellular strategies for achieving high signaling capacity — dynamics, cross-wiring and heterogeneity of cellular states. Current Opinion in Systems Biology 27, 100352.

Financial support

- Polish National Science Centre under grant PRELUDIUM 2019/33/N/NZ2/02691.
- Foundation for Polish Science within the First TEAM (First TEAM/2017-3/21) program co-financed by the European Union under the European Regional Development Fund.